FACULTY OF SCIENCES

STRATIGRAPHIC FORWARD MODELLING THE LATE OLIGOCENE TO MIDDLE MIOCENE EVOLUTION OF THE MALDIVES CARBONATE PLATFORM (INDIAN OCEAN)

Thomas Van der Looven
Student number: 01206796

Promotor: Prof. dr. Marc De Batist
Copromotor: Dr. Gerd Winterleitner

Jury: Prof. dr. David Van Rooij, Prof. dr. Thijs Vandenbroucke

Master's dissertation submitted in partial fulfilment of the requirements for the degree of master in geology

Academic year: 2018-2019

GHENT UNIVERSITY

KU LEUVEN

Acknowledgements

First and foremost, I wish to thank Dr. Gerd Winterleiter, supervisor of this project and co-promotor from the University of Potsdam. He provided me with many new insights, guided me through several difficulties and still gave me the complete freedom to outline my own project. He was always available to assist me when I needed advice or when I encountered a problem with the software or the hardware (and this happened a lot!).

I also want to thank my promotor from the University of Ghent, Prof. Marc de Batist, to support this international exchange and assist me with all the administrative issues. His flexibility on the administration of my Erasmus+ studies exchange, greatly encouraged me to renew the experience for my master thesis. I also wish to thank both him and Timothy Tella for their thorough reviews and helpful suggestions for the final thesis text.

Furthermore, I want to express my gratitude to Prof. Maria Mutti and the whole carbonate sedimentology research group for the engaging seminar discussions and for making me feel at home at the University of Potsdam. I truly enjoyed my two years at the University of Potsdam, where all the courses and field trips greatly inspired me for this project and further research.

Lastly, I want to thank Sofia and my parents for their unconditional support during my years of study and the last intensive 6 months of thesis-work.

Table of contents

List of Figures

The Story Of My Research

Geologists are always interested in how different rocks are distributed beneath the Earths' surface. Because drilling and coring is a very expensive business, they only have a few points available where they know exactly what is lying beneath their feet. What lies in between these control points is then estimated by constructing several possible 3D-models and choosing the most plausible. Traditionally, this modelling is done by geostatistical methods, where statistics are used to estimate what lies between the wells. Mathematical formulas however do not always produce realistic subsurface models, as they do not account for the natural processes that formed these rocks.

An alternative way of realizing a subsurface model, is by reconstructing the geological history of a basin in chronological order. Such a Stratigraphic Forward Model (SFM) simulates all geological processes that were involved in the formation of a sedimentary body over time. In practice, the software builds a 3D model by adding layers of sediments in several time steps. As such, it can reconstruct how a lake or sea is gradually filled up with sand and mud, or how coral reefs grow over several million years. To validate the completed model, the simulated 'layer cake' is matched in selected control points with available borehole data. The complexity in this modelling approach lies in the simplification of the geological processes. Multiple natural processes participate in evolution of a sedimentary basin and interact with one other. The global climate, for example, affects the ocean currents, which in turn affect the distribution of sediment particles. By simulating each individual process, geologists can estimate their relative impact and gain insight in how they interact.

For my master thesis, I chose to construct my own stratigraphic forward model on the Maldives carbonate platform from scratch. Therefore, I had to study all the possible processes that contributed to the formation of this extensively studied, submerged sedimentary body. In order to gain a complete overview of its depositional history, I had to study a great variety of geological processes. This involved reading papers that were focused on very different topics, ranging from stratigraphy to structural geology, sedimentology, biology, geophysics, mathematics, paleoclimatology, paleontology and reservoir modeling. Doing so, I genuinely felt like all of the theoretical concepts that I had studied over the years, as a bachelor and master student, finally came together into a single tangible model. This 3D stratigraphic model (figure) is a product of multiple simulated processes, but also the result of a long journey of research and development: months of data gathering, more than 300 'trial-and-error' simulations involving many nerve-racking obstacles, but also gave me great joy and satisfaction when the final model took shape.

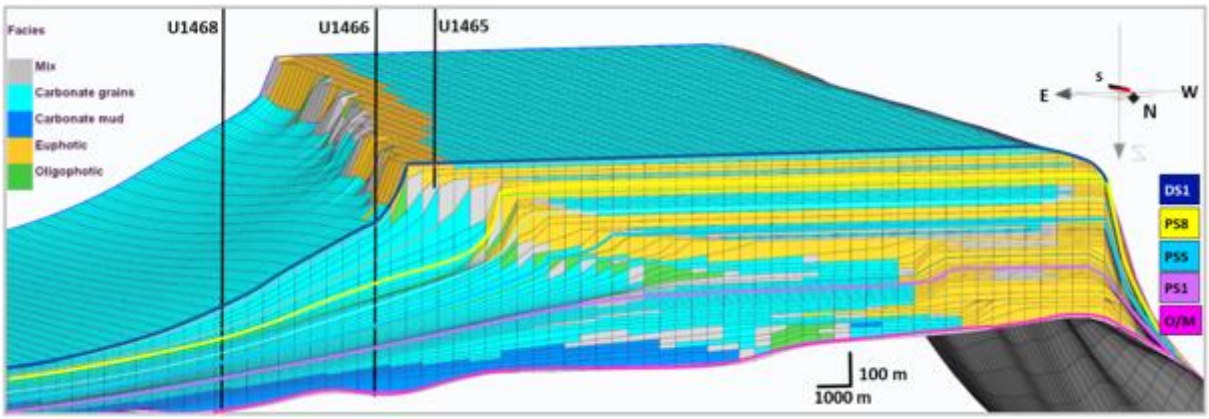

Chapter 1: Introduction

The Maldives atoll archipelago forms the top of a 3000 m thick submerged carbonate platform in the western Indian Ocean. The fascinating depositional history of the Maldives carbonate platform was extensively studied for both exploration and academic purposes, providing a large database of publications. This vast amount of available data makes it an ideal setting to study the formation and sequence stratigraphy of carbonate platforms. Although the evolution of the Maldives is fairly well understood, the contribution of different processes in the platform development remains a matter of debate. The complex web of interacting, scale-dependent controls on stratigraphy makes it difficult to assess the individual impact of each parameter on the carbonate platform architecture. Modelling depositional geometries by simulating genetic processes has therefore been of major interest to understand how carbonate platforms are constructed. Stratigraphic forward modelling (SFM) allows the quantification of each controlling factor and gaining a deeper insight in how their combined effect produces a specific stratigraphic architecture. This study uses such a 3D-stratigraphic forward modelling software, DionisosFlow, to improve our understanding of the interaction between different carbonate-producing organisms under changing environmental conditions. Once a stratigraphic model is calibrated to the ground-truth, it can be used to test several theoretical concepts about carbonate depositional mechanisms. In addition, the model forms a predictive tool for the depositional facies distribution and stratigraphic geometry, away from points of control. Facies distribution prediction with SFM is, however, still in its early days, while the exploration industry still works on these advancements. More research on how to develop such models and how to tie them to the geological reality is necessary to generate a streamlined approach.

This study aims at gaining a deeper insight in the possibilities and limitations of applying SFM to a real setting from the geological past. The comprehensively studied Maldives carbonate platform forms an excellent case study, as several conceptual models were developed for its genesis. This study will focus on a section of the platform, formed from the late Oligocene to the Middle Miocene that is exceptionally well documented by seismic and well data. Consequently, a genetic model proposed by Betzler *et al.* (2018) is tested by simulating its main driving mechanisms. The calibration procedure of the stratigraphic model aims to provide a 3D depositional facies distribution and a deeper insight in the biotic changes within the platform. Two specific hypotheses are tested, surrounding these biotic changes under changing environmental conditions. At the same time, this study provides a workflow and guideline for future modelling efforts, focused on how to incorporate theoretical concepts, calculated assumptions and multi-scale geological data in a single model. The proposed model setup could function as an analogue for similar settings of the same age window.

1.1 Carbonate sequence stratigraphy

Since the end of the 20th century, sequence stratigraphy has been widely applied to study sedimentary systems. The concepts of sequence stratigraphy are used to study these systems by defining "genetically-related" stratigraphic units in the sedimentary record, namely the depositional sequences (Pomar and Haq, 2016). Each of these successions is defined by erosional or depositional surfaces, caused by changes in relative sea level. A strong rise in sea-level, a transgression, leads to deepening of the basin with the typical formation of maximum flooding surfaces, often found in the sedimentary record as condensed sections. Strong sea-level drops on the other hand, may expose coastal environments, leaving them vulnerable to erosion and thus creating unconformities and sequence boundaries. Due to the cyclic nature of sea-level changes, these surfaces will envelop depositionally related parasequences. The stacking pattern of several parasequences can be linked to the balance between higher order sea-level changes and sedimentation rates. Three stacking geometries are differentiated: aggradation, retrogradation and progradation (figure 1). Based on their geometry, the

parasequences are grouped in systems tracts. Depending on the author, three or four systems tracts make up a sequence, representing a full sea-level cycle (Pomar and Ward, 1994; Posamentier and Allen, 1999). A sequence is accordingly defined as a succession of relatively conformable strata bounded at their upper surface and base by unconformities and their correlative conformities (Vail *et al.*, 1977), i.e. the sequence boundaries.

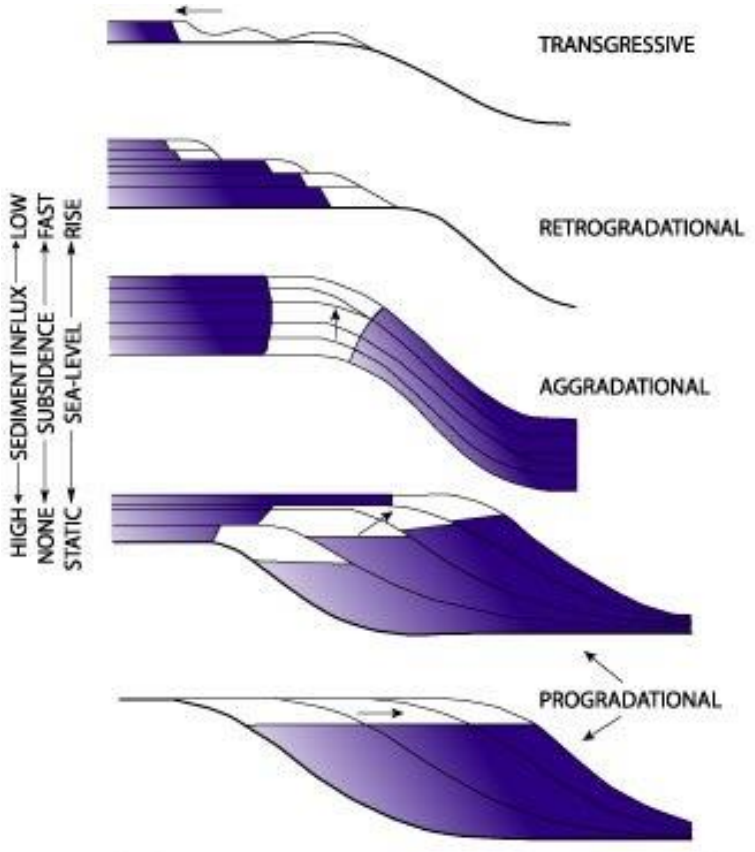

Figure 1. Depositional architectures as a function of accommodation space and sediment influx (Emery and Myers, 1996)

The initial conceptual models for sequence stratigraphic analysis (e.g. Vail *et al.*, 1977) were based on the physical behavior of sediment particles and were mainly applied to clastic systems. Hydrodynamic thresholds for sediment mobilization played an important role in these models as they affect the stratigraphic geometry. Jervey (1988) suggested accommodation space as the major control on the stacking of sequences, which he defined as “the space available for sediment accumulation”. The changes in accommodation were tfhe result of relative sea-level changes, which depend both on the global eustasy and local tectonics. Later, several authors noted that sediment influx exerted at least a co-equal control on the available accommodation space (Posamentier and Allen, 1999; Catuneanu, 2002). As comprehension of the influence of other hydrodynamic processes on the redistribution of sediment, like slope and wave effects, improved, Swift and Thorne (1991) defined the shelf equilibrium profile as a dynamic equilibrium between sediment input and hydraulic energy. According to this principle the sediments can accumulate until they reach the equilibrium profile. Above this theoretical surface the hydraulic energy is sufficient to transport the sediment and redistribute it along the shelf. The hydraulic energy depends on tidal, wave and storm energy and their associated current strengths. In clastic systems, the shelf redistribution processes follow a textural gradient, dominated by the particle size, which allows a lithofacies differentiation (Swift and Thorne, 1991). At stratigraphic scales, the shelf equilibrium profile can be seen as a physical upper boundary of sedimentary aggradation, marking the maximal accommodation space in a clastic system (Pomar and Haq, 2016).

The success of these first models, also known as the Exxon models, for predictive purposes in clastic basin analysis called for a comparable model for carbonate systems (Pomar and Haq, 2016). Carbonate systems, however do not follow the same hydrodynamic rules as their clastic counterparts. Carbonate shelves can produce a great diversity in depositional profiles, inconsistent with the shelf equilibrium profile (Pomar, 2001b). The cause for this variability lies within the biological nature of carbonate sediment production (figure 3). The sediment-producing organisms are bound to specific production loci by their ecological requirements. The *in situ* production by these carbonate factories is the first major difference compared to clastic systems, in which sediment is brought in from the hinterland. The second one is the ability of these factories to build rigid sedimentary structures, that defy the clastic hydrodynamic thresholds. These two factors led Pomar and Kendall (2008) to propose a subdivision of the accommodation, as defined by Jervey (1988), into physical and ecological accommodation. Physical accommodation would be constrained to "the space available for sedimentary fill by a lithoclastic system in a setting dominated by the character of the local hydrodynamics", equivalent to the shelf equilibrium profile (Pomar and Kendall, 2008). The ecological accommodation is the capacity of organisms to produce and to accumulate sediments above and below this hydrodynamic threshold (Pomar, 2001b, 2001a). The wide spectrum of carbonate depositional profiles is a result of the interplay between these two types of accommodation.

In contrast to clastic sediment, carbonate sediment is mostly produced *in situ* by an assemblage of organisms. Schlager (2000, 2005) distinguishes three basic modes of carbonate production: abiotic, biotically induced and biotically controlled carbonate precipitation. These modes combine into different production systems or 'carbonate factories' (figure 2):

1. Tropical shallow-water systems (T-factories) consist mainly of photoautotrophic biotically controlled producers such as green and red algae, living often in symbiosis with heterotrophic organisms like hermatypic corals, large benthic foraminifera and certain bivalves. Less represented are abiotic or biotically induced precipitation in the form of marine cements and ooids. These factories occur nowadays in warm surface waters between 30° N and S of the equator, following the 20°C surface water winter isotherms. This system's strong light dependency is responsible for the narrow production depth range with a high growth potential, making it particularly sensitive to drowning.
2. Cool-water systems (C-factories) are dominated by heterotrophic biotically controlled producers such as foraminifera, sponges, bivalves, gastropods, brachiopods, bryozoans and echinoderms. This makes them less dependent on light but all the more on a steady nutrient supply. Photo-autotrophic organisms can contribute to the community in the form of red algae and symbiotic foraminifers. Their production profile reaches greater depths than the T-factories but with lower growth rates. The C-factories only occur in cooler waters where they can outcompete the otherwise fast-growing T-factories. They can be found from the T-factory limits up to polar latitudes when provided with nutrients.
3. Mud-mound systems (M-factories) are mainly constructed by abiotic and biotically induced precipitation. The fine-grained micritic carbonate is produced by microbes that are able to survive in aphotic and poorly oxygenated, but nutrient-rich waters. Pores within this automicritic framework can be filled by marine cements. Despite their wide depth range M-factories occur rarely in shallow waters due to competition with the other factories. However, during periods of low oxygenation or after severe extinctions in the geological past, these mounds could extend into shallow waters.

Each of these factories not only possesses its own depth profile but also different accumulation rates. Accumulation rates are the ability of a carbonate factory to build up vertically until sea level. These rates are in most cases substantially lower than the growth potential, because (1) calculated accumulation rates are rarely corrected for compaction, (2) the growth potential is often limited by sea level causing the platform to prograde and (3) due to erosion and remobilization the buildup components are partially exported. Consequently, aggradation rates can only be used to quantify the lower limit of the growth potential (Bosscher and Schlager, 1993). Through geological time, the accumulation rates follow a scaled decreasing trend with increasing observed time interval (Sadler, 1981). Nevertheless, T-factories consistently have higher mean rates than their fellow factories over the various time intervals. C-factories only reach 25 % of tropical rates, while M-factories are estimated at 80-90 % (Schlager, 2005). The relationship of the carbonate factories with water depth and production rates indicates the interdependency of the accommodation space and the sediment input in carbonate systems.

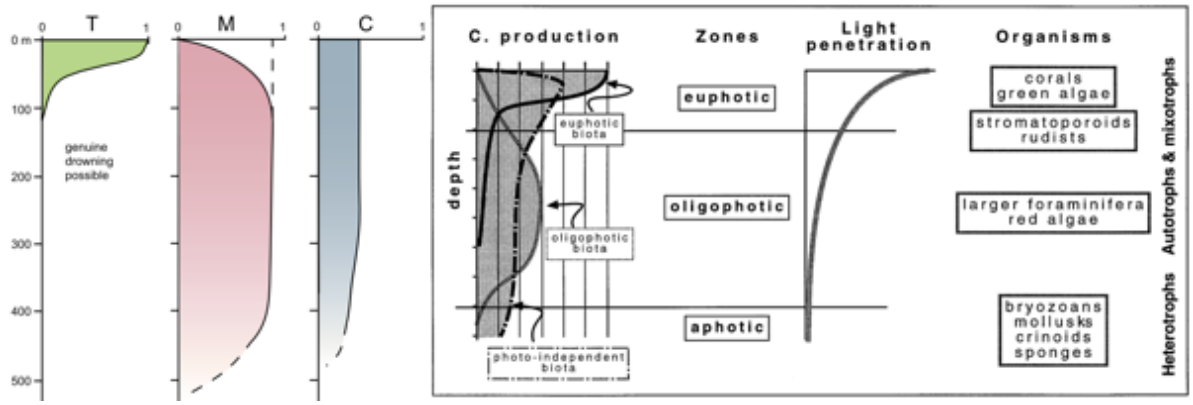

Figure 2. Left: Production rates of carbonate factories in function of depth as a fraction of the tropical standard (Schlager, 2005). Right: Carbonate production of main biota groups, divided by light dependence (Pomar, 2001b)

Next to their latitudinal distribution, each carbonate factory can be decomposed into its constructing organisms. As light is undoubtedly the most influential parameter on biotically controlled production, Pomar (2001b) groups carbonate-producing organisms into three communities based on their light dependency (figure 3): (1) euphotic communities live in shallow, well illuminated, high-energetic environments; (2) oligophotic communities in deeper, less illuminated areas below wave base and (3) photo-independent biota, which can occur over the entire water column but are dependent on nutrients. Each community composition further relies on the ecological requirements of its composing organisms, such as nutrient availability, salinity, oxygenation, water chemistry, temperature gradients, water energy and substrate. To add to the complexity of classifying carbonate producers, all these ecological requirements change over time as the biota evolve (Pomar and Kendall, 2008).

Each biotic system has its own competence for building above and below the hydrodynamic shelf equilibrium profile. This ability, defined as the ecological accommodation, depends on the type of sediments that is produced, the production loci and the sediment transport (Pomar and Kendall, 2008). Clastic sediments are sorted along a textural gradient from coarse to fine grained as they are transported down the continental margin, leading to a bimodal grain-size distribution. Sedimentary carbonate sediments on the other hand, do not follow this pattern as they are produced *in situ*. This multimodal grain-size distribution will rather reflect the size of the skeleton particles, produced in place, than be a proxy for hydrodynamic energy (Pomar and Haq, 2016). In addition, the sediment dispersal by hydrodynamics can be obstructed by processes like sediment trapping, binding and baffling, framework construction and early cementation (Pomar, 2001a). For example, coarse skeleton particles can be formed beneath the wave base and remain in place due to a lack of hydraulic energy, while fine-grained particles within the tidal zone can be bound by microbial activity (Pomar and Haq, 2016).

The impact of ecological accommodation on the depositional profile, is excellently illustrated by the large range of carbonate platform types that can develop under similar global and regional conditions (Pomar *et al.*, 2012). A carbonate platform is a general term, used for carbonate sequences with a large variation in architecture (Pomar, 2001b). Several attempts to classify these structures are based on morphological descriptions with homoclinal ramps and rimmed shelves used as end members of a wide variety in architectures (Burchette and Wright, 1992; Handford and Loucks, 1993). Pomar (2001b) argues, however, that these classifications lack the incorporation of genetic factors, linking the platform type to its ecological accommodation. A key example is the Miocene of the Mediterranean, where several platform types are associated with different ecological communities, while formed under similar global and regional circumstances (Pomar *et al.*, 2012). In this comparison, reef-rimmed platforms and open platforms possess the maximum capacity for building above the hydrodynamic boundaries associated with physical accommodation. The *in situ* growth of euphotic large-skeleton metazoans, provides a rigid framework for sediment accumulation. Distally steepened and homoclinal ramps are dominated by oligophotic and aphotic carbonate production. They are mainly composed of loose grains, with some encrusting organisms, making them prone to sediment redistribution along the shelf equilibrium profile. Intermediate geometries tend to one of these end members depending on their ecological accommodation and sediment transport from euphotic to oligophotic zone and vice versa (Pomar *et al.*, 2012).

In summary, regional and global factors will determine the intrabasinal conditions and the hydrodynamical regime and so the physical accommodation changes. Depending on the ecological requirements of the organisms, a specific biotic community will form under these intrabasinal conditions. Several biotic communities can exist next to each other and interact, forming the carbonate factory. The composition of the carbonate factory not only controls the type of carbonate production, but also the production loci and the alteration of sediment redistribution. These three components will make up the ecological accommodation which can change through time with biological evolution. The interplay of ecological and physical accommodation will determine the depositional profile of the carbonate platform.

Each component in this complex web of interdependent parameters influences the stratigraphic architecture in one way or another. Quantifying and assessing the impact of each individual control remains a challenge in carbonate sequence stratigraphy. Due to evolution, different controls can dominate in a different setting, either in the geological past or present. Many general conceptual models were formulated over decades of scientific research but still require validation in specified settings.

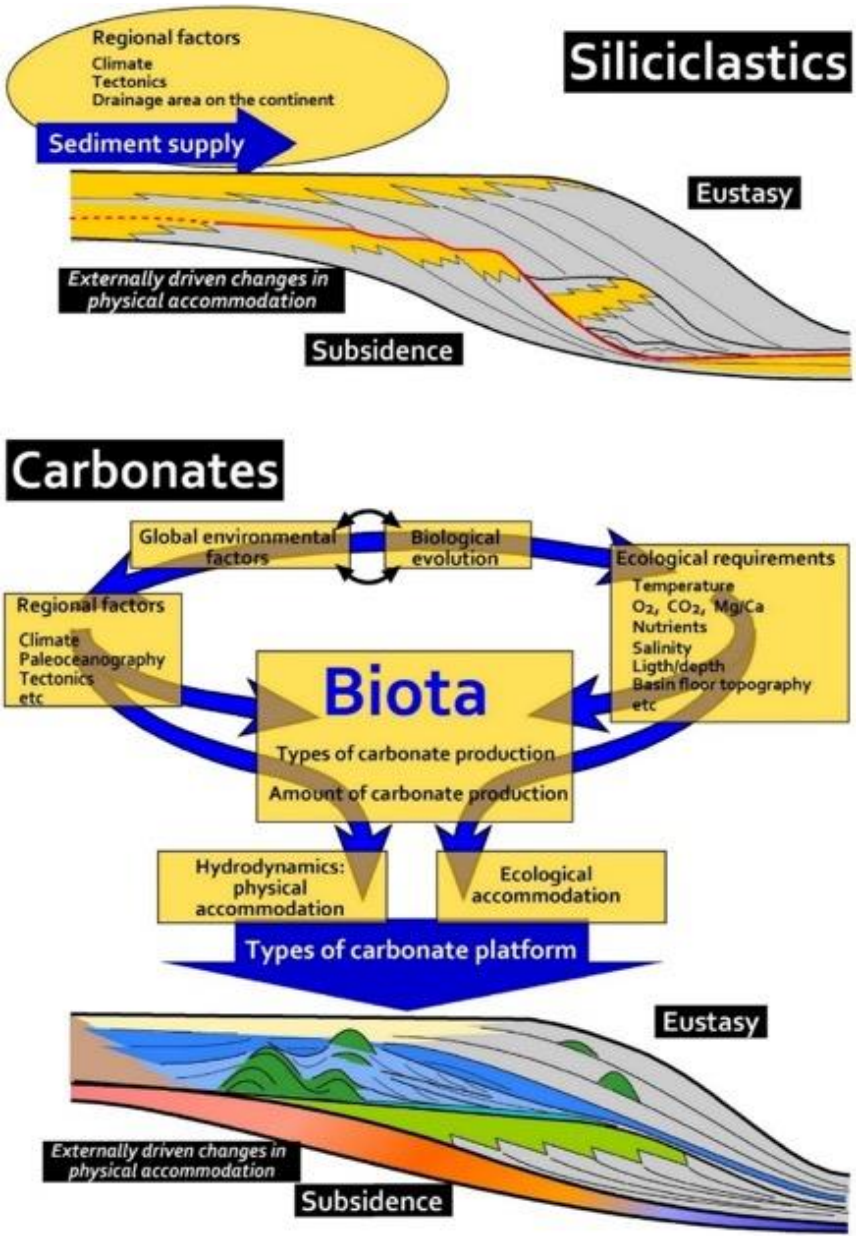

Figure 3. Sequence stratigraphic controls in clastic and carbonate system (Pomar and Haq, 2016)

1.2 Stratigraphic Forward Modelling

The general idea behind Stratigraphic Forward Modelling (SFM) is to quantify and simulate the geological processes over time to reproduce the morphology and internal architecture of sedimentary bodies (Watney *et al.*, 1999). It is a computer simulation technique that creates synthetic stratal patterns by simulating tectonic and stratigraphic processes such as subsidence and uplift, sediment supply or production, and the various processes of sediment transport and deposition (Burgess, 2012). The first stratigraphic models were developed to quantitatively test conceptual ideas on depositional mechanisms over geological time scales. If stratal geometries, predicted by a conceptual model, could be reproduced by a mathematical description of its conceptual processes, the proposed model proves to be internally consistent and the processes properly understood (Warrlich *et al.*, 2002). Moreover, such numerical modelling provides a quantitative expression of interacting processes within the defined system (Burgess, 2012). This has been proven particularly useful in systems where several stratigraphic controls interact to derive the most influential ones (Seard *et al.*, 2013; Kolodka *et al.*, 2016).

Several types of stratigraphic models were developed over the last few decades, with the most recent ones simulating three-dimensional scenarios. Some models are developed to simulate specific environments, like fluvial plains (Cojan *et al.*, 2005) or carbonate platforms (Warrlich *et al.*, 2002). Others, known as combined whole system models, can include several environments to represent a source-to-sink simulation. These models include representation of several processes, such as ocean currents, waves, slope failures, rainfall, evaporation and are applicable in both clastic and carbonate environments (Burgess, 2012). One of the most advanced programs of this kind is DionisosFlow (Granjeon and Joseph, 1999), which has become an industry standard in hydrocarbon exploration. Among 3D models, it has been proven to be the most robust in various settings, as it handles both long-term and short-term processes (Shafie and Madon, 2008).

SFM has been proven to be an effective basin modelling technique applicable to a wide spectrum of scales, both in space and time. DionisosFlow, as prime example, has been used for both modelling millennial scale stratigraphy (Csato *et al.*, 2014), and for basin evolution over ten million years (Granjeon and Joseph, 1999). Not only the duration but also the age of the basins varies from Cretaceous (Hawie *et al.*, 2015) to Miocene (Kolodka *et al.*, 2016) carbonate platforms, to the relatively recent Holocene drowning of the Tahiti reefs (Seard *et al.*, 2013). The latter was constructed on a much smaller model domain size (9.6 km^2) compared to an exploration scale model for the Lower Cretaceous of Oman (90,000 km^2) (Al-Salmi *et al.*, 2019). This wide spectrum of possibilities for a single program, creates perspectives for future research on its applicability and use for stratigraphy and facies predictions on various scales. This diversity in applications is unfortunately also reflected in the diversity in modelling approaches and workflows. Each setting requires different simplifications to represent its dominant depositional mechanisms. As SFM is still in its early days, more studies are necessary to provide analogues for future modelling attempts.

So far, the application goals of SFM have been essentially twofold, namely for experimental and predictive purposes. Firstly, the technique is often applied in an experimental way to validate theoretical concepts of physical systems. These studies test the variability in stratigraphic architecture of a pre-defined sedimentary system in response to individual parameter changes. This has been used in clastic systems to for example test model diffusion equations (Granjeon and Joseph, 1999; Granjeon, 2014) or research the theoretical stratigraphic architecture under short-term climatic cycles (Csato *et al.*, 2014). In carbonate systems, it is often used to test the impact of environmental parameters, linked to the ecologic accommodation of the system (Pomar and Kendall, 2008), on the resulting platform geometry (Williams *et al.*, 2011). Such studies of the environmental control on platform architecture have also been performed on real examples derived from the geological record. Their main objective is to derive key parameters from the complex web in the evolution of a specific basin (Kolodka *et al.*, 2016).

Secondly, SFM is used in petroleum exploration to predict the distribution of source and reservoir rocks. The quality of a hydrocarbon reservoir depends on its porosity and permeability. Carbonate reservoirs are in particular notorious for their internal complexity in these domains (Agar and Hampson, 2014). They can exhibit significant facies changes within short distances, resulting in unpredictable production behavior (Marzouk *et al.*, 1995). Their heterogeneous pore distribution is in first instance generated by the depositional system and the biotic producers. This primary porosity is post-depositionally altered by tectonism, burial and various diagenetic processes. Enhanced secondary porosity can be formed by dissolution, fracturing and faulting. Conversely, porosity can be reduced by cementation and compaction (Mazzullo, 2004). Dolomitization, a process unique to carbonate rocks, plays another important role in the alteration of the primary porosity distribution (Braithwaite *et al.*, 2004). Carbonate rocks, built up by biota with rigid frameworks are able to better preserve their

primary porosity (Pomar and Haq, 2016). Especially reef reservoirs provide, as such, a strong link between specific porosity fabrics and depositional facies (Nurmi *et al.*, 1990).

Predicting depositional facies away from points of control, like expensive wells, remains a major challenge in exploration geology. Traditionally, stochastic and semivariogram-based methods are used to interpolate inter-well rock properties in static geological models (Lucia and Fogg, 1990). These geostatistical methods partially reduce the uncertainties, inherent to geological modelling, but are prone to deviation from the depositional morphology (Warrlich *et al.*, 2008). Especially in carbonate rocks, the complex sedimentary geometries like mounds and clinoforms, prove to be difficult to grasp with traditional stochastic methods. Furthermore, these methods might fail to sufficiently capture the depositional facies heterogeneities due to a lack of accountability for geological processes (Hawie *et al.*, 2015). The texture heterogeneities in a carbonate reservoir occur on various scales, depending on their genetic processes. Thus, a combination of different scale-dependent geostatistic modelling techniques is often required to recreate the natural distribution of rock properties (Amour *et al.*, 2013).

To incorporate more genetic factors in the modelling strategy, process-based forward models were developed to predict the vertical and lateral distribution of depositional environments. Because this primary texture is controlled by processes acting in space at the time of deposition, it is possible to both conceptualize and model these depositional mechanisms (Whitaker *et al.*, 2014). Due to its forward modelling approach, SFM uses a pre-determined set of input parameters and mathematical equations to ensure an internal consistency within the model (Shafie and Madon, 2008). This rule-based approach provides a more robust extrapolation potential than certain stochastic models. Once a model is calibrated to a specific dataset it provides a rigorous mathematical consistency for prediction, based on the forward model input data and its algorithms. This requires however that all processes involved in the strata deposition are properly understood and described (Warrlich *et al.*, 2008). The deterministic approach of SFM does not necessarily make traditional stochastic modelling techniques obsolete but provides a helpful addition to improve facies distribution models and gain deeper insight in the processes behind the stratigraphic architecture (Hawie *et al.*, 2015). The results of the stratigraphic simulation can be compared to the seismic interpretation to refine the static geological model, which leads to improved dynamic reservoir modelling (Warrlich *et al.*, 2008).

An accurate stratigraphic model for prediction purposes requires a good understanding of all the processes involved in the formation of the stratigraphic body and a proper constraints on the controlling input parameters (Warrlich *et al.*, 2008). Modern analogues are often used to replace unknown conditions or reduce uncertainties on ill-defined concepts. Further testing of multiple scenarios is often required and performed through a sensitivity analysis on the model output. For such an analysis, several simulations are executed by changing one parameter at a time, while the other are kept constant. The results of these simulations are then compared to observed data, such as wells or seismic data, to assess the impact of each parameter (Seard *et al.*, 2013; Kolodka *et al.*, 2016; Busson *et al.*, 2019). Most recent innovations in SFM, allow to run automated sensitivity analyses with multiple realizations that yield quantified information on the impact of each individual parameter based on the fit with a reference case scenario (Warrlich *et al.*, 2008; Hawie *et al.*, 2015).

Chapter 2: Geological setting and evolution of the Maldives carbonate platform

2.1 The modern Maldives

The Maldives archipelago consists of a north-south orientated chain of atolls, located in the western Indian Ocean (figure 4). The atolls are organized in a double row, delineating the rims of an isolated, elongated carbonate platform. The platform contains a bank internal basin, the Inner Sea of the Maldives, that reaches depths of up to 550 m. The shallow sea is connected to the deeper Indian Ocean by channels, cutting through the platform rim and separating the atoll clusters (Betzler *et al.*, 2018). The individual atolls have a maximum elevation of 5 m above sea level which makes the Republic of Maldives, the lowest country on Earth (Gischler *et al.*, 2008). The water depths in the atoll lagoons varies between 31 and 82 m (Belopolsky and Droxler, 2003).

The Maldives' equatorial climate is characterized by the Indian monsoon system. This system generates a seasonally reversing wind system, creating strong ocean currents. During Northern Hemisphere summer, south-western winds generate eastward directed currents, the Southwest Monsoon Current. In winter, Northeast Monsoon winds take over and create westward flows in the form of the North Equatorial Current. Inter-seasonally, Indian Ocean westerlies concentrate all eastward flow into a narrow, 600 km wide band along the equator, the Equatorial Jet. These intense surface currents can reach down to 200 m of water depth with velocities up to 1.3 m/s (Tomczak and Godfrey, 2001). Within the modern atoll's channels this results in velocities up to 2 m/s, strongly influencing the depositional processes. These strong currents reshaped the seafloor of Inner Sea depositing sediment-drift bodies around the atolls (Betzler *et al.*, 2018).

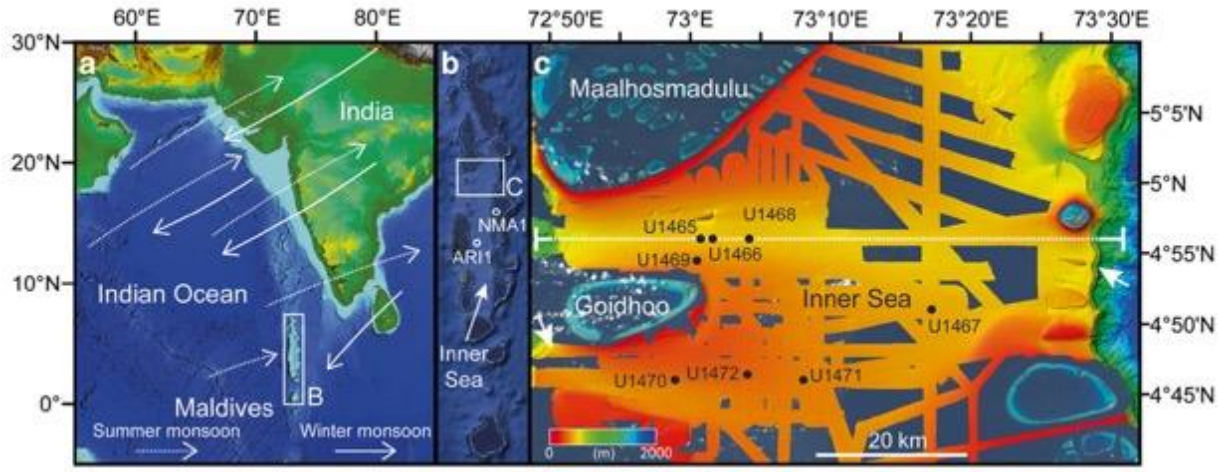

Figure 4. (a) Map of western Indian Ocean with monsoon system and (B) location of the Maldives archipelago. (b) Maldives archipelago with locations of Inner Sea, (C) study area and wells ARI-1 and NMA-1. (c) Bathymetry map of study area, similar to the model dimensions, with atoll contours, locations of IODP 359 wells and seismic line NEOMA-P65 (after Betzler et al., 2018)

2.2 Chagos-Laccadives Ridge

The Maldives carbonate platform was initially formed on top of the Chagos-Laccadives ridge. This aseismic volcanic structure stretches from the southwestern coast of India along the 73° meridian to south of the equator. Duncan and Hargraves (1990) researched the origin of this structure and linked its genesis to stationary hotspot activity, located nowadays beneath the island of Réunion. They provided geochronologic evidence that this hotspot became active with the rapid eruption of the Deccan flood basalts in Western India at the Cretaceous-Paleogene transition (65-68 Ma). While the Indian and African plate moved northwards, the remaining hotspot trail produced several volcanic

plateaus, such as the basements of the Laccadives, the Maldives (57 Ma), the Chagos bank (49 Ma) and the Mascarene plateau (45-31 Ma) (Duncan and Hargraves, 1990). This Paleocene basement served as a topographic high for the initial carbonate factories.

2.3 Maldives carbonate platform architecture

2.3.1 Previous studies and available data

The architecture of the Maldives carbonate platform has been studied for both academic and exploration purposes, providing a vast amount of publications. The available data contains interpreted seismic profiles from different surveys, giving insights in the internal and external architecture of the platform. A total of 13 wells were drilled across the platform, from which four reach the volcanic basement. In these points of control, the well descriptions provide a continuous log with information on lithology, stratigraphy and depositional environment.

In the 70's the Maldives were first investigated for hydrocarbon exploration by Elf Aquitaine, who held an exploration license for the Inner Sea basin. They acquired 6750 km of 2-D deep marine seismic profiles in the central basin and in the atoll lagoons. An accompanying exploration well (NMA-1) was drilled in the North Male atoll lagoon. The well with a total depth of 2221 m penetrated the carbonate platform from recent to Eocene deposits up until the Paleocene basement. The well encountered potential reservoirs and source rocks but no hydrocarbons. The combined data, studied by Aubert and Droxler (1996) and by Purdy and Bertram (1993), provided various insights in the evolution of the carbonate platform since the Eocene to recent times. The interpretation of the unmigrated seismic data suffered, however, from the low resolution and several seismic artefacts, due to a lack of technological advancement at the time (Belopolsky and Droxler, 2003).

During the 1980's a second wave of interest in the Maldives occurred. In the context of the Ocean Drilling Program (ODP), leg 115, three wells were drilled through the carbonate platform in 1987 (Backman *et al.*, 1988). Site 714 and 715, drilled on the platform margin, targeted the volcanic basement and were used in the study of the origin of the Chagos-Laccadives ridge (Duncan and Hargraves, 1990). Site 716 was located in the Northern part of the Inner Sea and recovered 226 m of periplatform sediment from the Pleistocene and Miocene (Backman *et al.*, 1988).

In 1989, the Royal Dutch/Shell acquired the exploration concession for the Inner Sea. Shell obtained seismic data along a rectangular grid spanning the entire Inner Sea and some inter-atoll passages over an area of 275 x 50 km. The streamer lengths did not allow to collect data within the atoll lagoons. The densely spaced (1-2 km) 2-D sections provide medium-resolution (10-25 m) data with a good penetration up to the volcanic basement. Shell drilled an additional well, ARI-1, in the Inner Sea with a total depth of 3365 m, including 50 m of basement basalts. Again, no hydrocarbons were encountered due to a lack of sealing and mature source rocks. Shell terminated the Maldives project and disclosed all seismic and well data in 1997 to Rice University in Houston, Texas. These data were studied by Belopolsky (2000) and Belopolsky and Droxler (2003, 2004a, 2004b), who provided an extensive overview of the Cenozoic evolution of the Maldives carbonate platform. They were able visualize the subsurface in great detail, thanks to the dense seismic grid. Belopolsky and Droxler (2004a) produced several time structure horizon maps throughout the carbonate platform.

In December 2007, the German research vessel R/V METEOR set out to acquire multibeam imagery, seafloor samples and seismic reflection data on the Maldives platform. This expedition M74/4 aimed at gaining a deeper understanding of the climatic and paleoceanographic effects on the Neogene evolution of the Maldives, hence the NEOMA project. The multibeam images were used to research the morphology of several drowned reef terraces in the Maldives archipelago (Betzler *et al.*, 2009, 2013; Fürstenau *et al.*, 2010). The seismic data consists of 1400 km of seismic reflection profiles, covering previously surveyed and unsurveyed areas in the northern half of the Inner Sea. The vertical resolution of this data is higher (4-6 m) than the former industrial data from Shell and Elf, but offers less penetration. Well correlation was executed with wells NMA-1, ARI-1 and ODP site 716 (Betzler *et al.*, 2009, 2013; Lüdmann *et al.*, 2013).

Building further on the results of the NEOMA project, eight new wells were drilled in the framework of the IODP Expedition 359 in 2015 (figure 6). Sedimentary cores of sites U1465, U1466, U1468, U1469, and U1470 contained a sedimentary sequence covering a transition from carbonate platform to drift sequences from Oligocene to Pleistocene ages. Sites U1467, U1471, and U1472 only recovered Miocene to Pleistocene carbonate drift sequences. Stratigraphic, geophysical and geochemical core measurements allowed to improve the age determination of the seismic stratigraphy and gain insight in the timing of Neogene climatic changes (appendix A) (Betzler *et al.*, 2016, 2018).

All this available data was used to gain a complete understanding of the driving mechanisms behind the evolution of the Maldives carbonate platform. Interpreted deep seismic profiles from Purdy and Bertram (1993), Aubert and Droxler (1996), and Belopolsky and Droxler (2003, 2004b, 2004a) were used to acquire a 3D overview of the complete internal platform architecture. Shallower interpreted sections from Betzler *et al*. (2013, 2018) provided a more detailed insight in the Neogene evolution of the platform and will form the backbone of this study. These high-resolution seismic profiles and comprehensive well data are used to directly calibrate the developed stratigraphic model. Furthermore, the conceptual genetic model, outlined by Betzler *et al*. (2018) is tested by modelling its main driving processes and reproducing the seismic stratigraphy.

2.3.2 Cenozoic evolution

The evolution of the Maldives carbonate platform can be divided into three episodes, roughly concurring with the Paleogene, the Neogene and the Quaternary. The first episode consists of the Eocene installment and growth of shallow, flat-topped carbonate banks on the Paleocene volcanic basement (figure 5). By the latest Oligocene this carbonate sequence is almost completely drowned, with exception of the marginal platform rims. After this first drowning event, a second phase of carbonate bank growth arises and continues until the late Middle Miocene. In the Late Miocene, the carbonate platform underwent a second regional-scale drowning, driven by an intensified South Asian Monsoon. The strong currents associated with this third episode, shaped the Maldives archipelago into its present configuration of separated atolls (Betzler *et al.*, 2009, 2013, 2018).

2.3.2.1 Paleogene

The sedimentation during the Paleogene is dominated by tectonic instability of the Paleocene basement (60-50 Ma). Purdy and Bertram (1993) characterized the structure of the volcanic ridge with seismic and subsidence data from well NMA-1. The N-S orientated ridge appears to be cut by an oblique *en échelon* graben system, formed due to minor crustal extension until the Oligocene. The extension was caused by the up-doming of the crust by volcanic activity along the Réunion hotspot track. Describing and mapping of the graben system was done by Purdy and Bertram (1993), Aubert and Droxler (1996) and in more detail by Belopolsky and Droxler (2004a), thanks to the higher resolution of the Shell seismic grid.

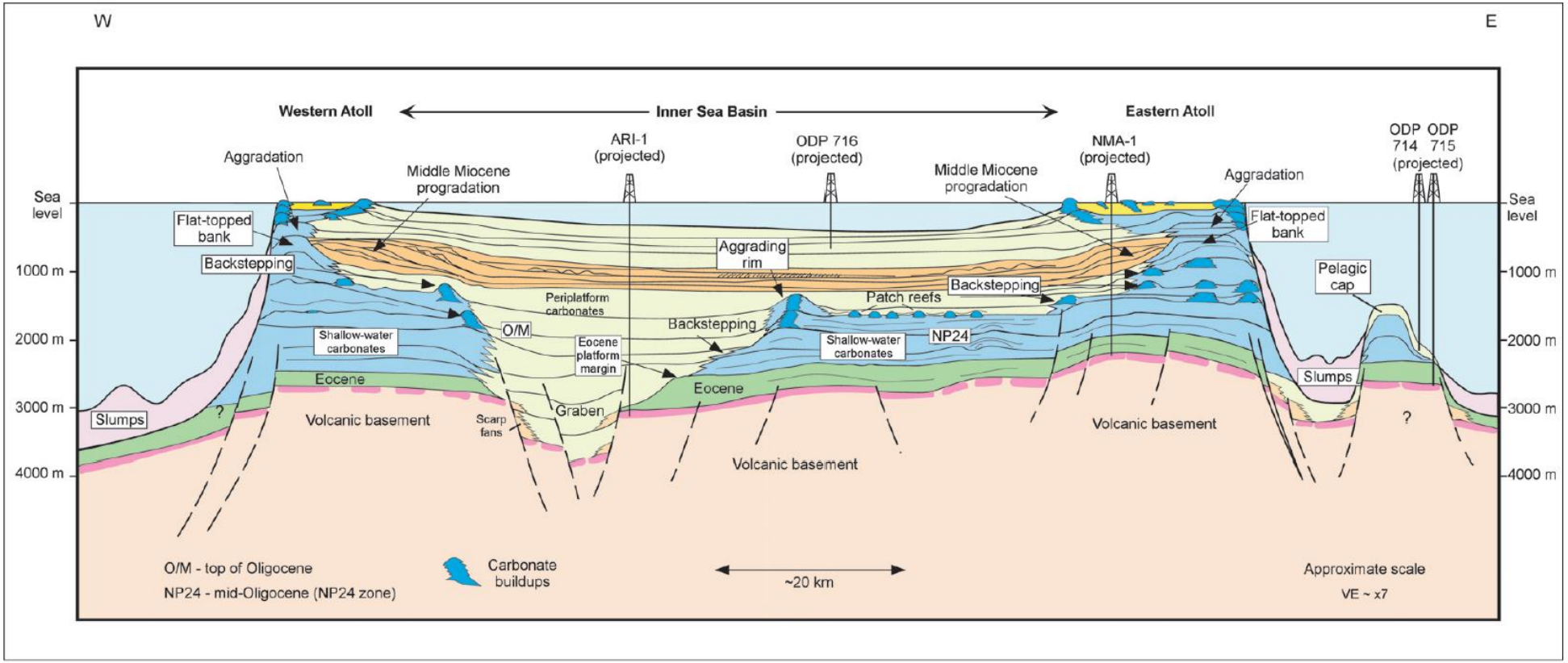

Figure 5. Schematic cross section through the Maldives carbonate platform, based on a composition of multiple seismic profiles. Well locations are projected along the transect. Note that all faults terminate before horizon O/M. (Belopolsky and Droxler, 2004a)

The *en échelon* pattern across the Chagos-Laccadives ridge is a near-surface expression of the left-lateral transform fault called the Chagos fracture zone. In the subsurface of the Maldives Inner Sea two axial grabens with a north-northwest – south-southeast orientation are present. Both consist of several normal faults cutting through basement blocks and overlying sediments. Movement along these faults continued until the early Oligocene indicating the end of the crustal extension (Purdy and Bertram, 1993). Deepening of the grabens during the Paleogene turned them into deeper seaways that were filled with sediment transported from the graben rims (Belopolsky and Droxler, 2004a).

The shoulders of the grabens formed topographic highs, allowing the wide-spread establishment of shallow, flat-topped carbonates in the early Eocene. These banks aggraded and backstepped throughout the Eocene and Oligocene due to a subsidence-induced, relative sea-level rise. The position of the grabens controlled the initial formation of the carbonate banks. The interior slope breaks remained pronounced due to the continuous activity of the faults. Consequently, the seaways keep mimicking the initial graben shape and position. Nevertheless, the deepening grabens were gradually filled by pelagic and periplatform sediments, reducing the seaway depths. The late Oligocene is characterized by the development of elevated bank margins, separating the bank interior from the open ocean (Belopolsky and Droxler, 2003, 2004a). The protected lagoon environments evolved from flat topped carbonate banks into mounded patch reefs, while the exterior marginal reef crest extended almost along the entire platform rim. This change in depositional profile can be linked to the first large-scale drowning of the platform, marking the end of the first episode of continuous platform growth (Belopolsky and Droxler, 2004a).

2.3.2.2 Neogene

The Neogene of the Maldives is characterized by tectonic stability throughout the carbonate bank with little faulting and no tectonically driven subsidence until the Late Miocene (Purdy and Bertram, 1993). Furthermore, several authors traced the late Oligocene drowning unconformity across the platform to the same depths, arguing against differential subsidence past this point (Aubert and Droxler, 1996; Belopolsky and Droxler, 2004a; Betzler *et al.*, 2009, 2013). In absence of tectonically induced subsidence during the Early and Middle Miocene (Purdy and Bertram, 1993), the depositional geometry is almost entirely controlled by changes in eustasy. Due to this sea-level controlled platform evolution, the Neogene is commonly subdivided by its sequence stratigraphy. Belopolsky and Droxler (2003, 2004a, 2004b) used the seismic reflection amplitude to correlate the stratigraphic sequences with sea-level cycles and presented a model that was fully interpreted in function of relative sea-level fluctuations.

After acquisition of new data in the NEOMA project, Betzler *et al*. (2009, 2013) suggested that there was more to the Neogene evolution than pure sea-level control. Based on the new high-resolution seismic data and detailed core information from IODP Expedition 359, a new model and stratigraphic subdivision was proposed by Betzler *et al*. (2018). Five intervals with a distinctive configuration were identified in the Neogene platform stratigraphy (figure 6). The intervals are separated by six sequence boundaries, identified as stratigraphic turning points in sedimentation patterns. Age determination of the sequence boundaries with micropaleontologic evidence provides a solid timeframe for detailed platform architecture analysis. The general trend during the Neogene sedimentation consists of a gradual infill of the Inner Sea by carbonate platform growth up until the Middle Miocene. At the latest Middle Miocene the sedimentation pattern shifted abruptly towards the deposition of sediment drifts under increasing influence of vigorous currents.

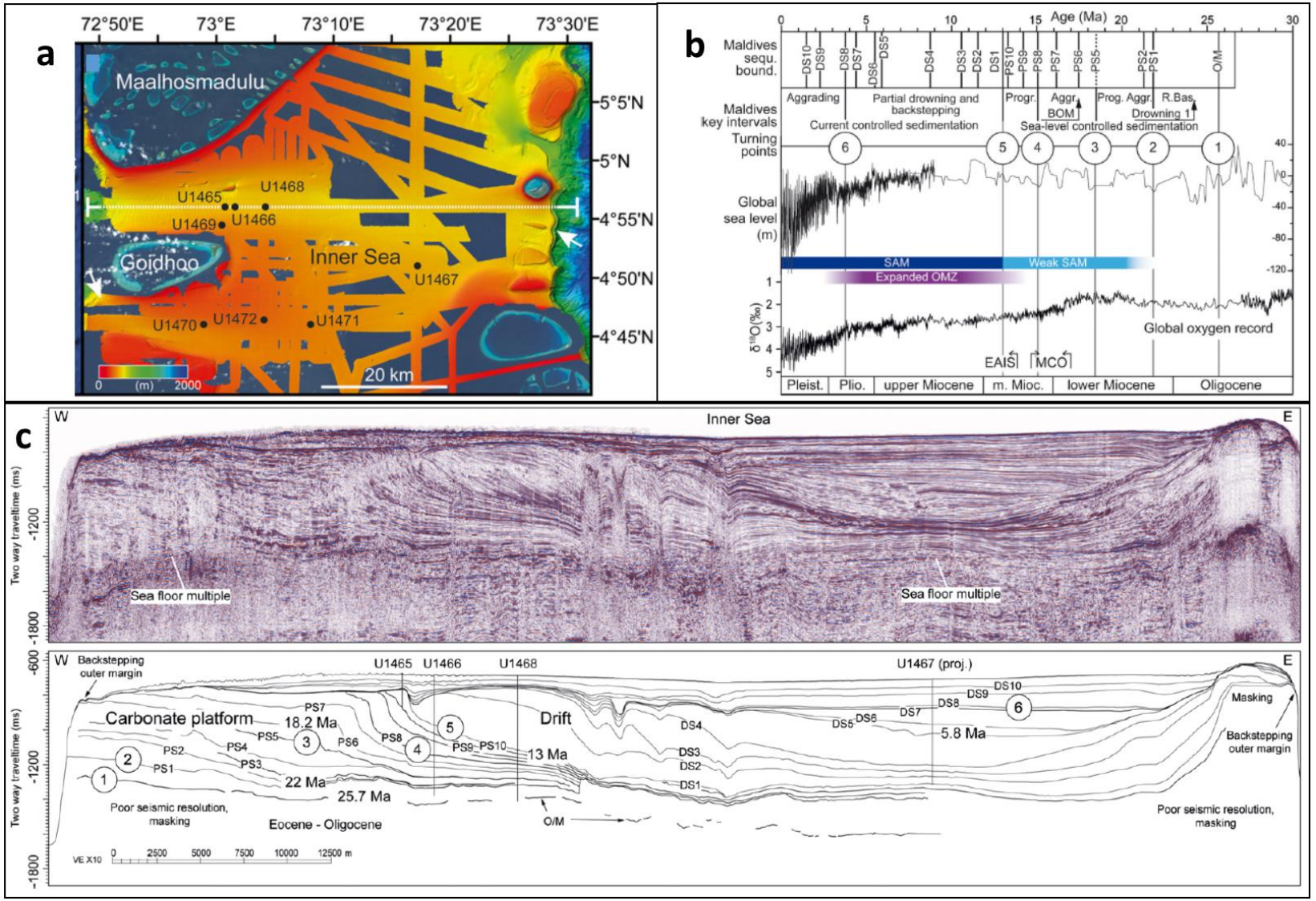

Figure 6. (a) Study area with location of (c) seismic line NEOMA-P65 and wells. Color scale represents bathymetry. (b) Evolution of Maldives carbonate platform in six stratigraphic turning points. Periods of expanded oxygen minimum zone (OMZ), Miocene Climate Optimum (MCO), weak and intensified South Asian Monsoon (SAM) are indicated. (c) Seismic line NEOMA-P65 and its interpretation into platform sequence (PS) and drift sequence (DS) boundaries. Indication of well locations along transect, interpreted horizon ages and turning points in platform evolution (after Betzler et al., 2018)

Drowning unconformity: O/M horizon (late Oligocene to Early Miocene)

A drowning unconformity from the latest Oligocene, referred to as horizon O/M, can be traced across the platform and serves as the first turning point in its evolution through the Neogene (figure 6) (Betzler *et al.*, 2018). The latest Oligocene is marked by a global sea-level rise of approximately 50 m after a sea-level lowstand (Miller *et al.*, 2005). This is confirmed by several wells that record a substantial deepening trend throughout the Maldives between 24 and 22 Ma (Betzler *et al.*, 2018). Aubert and Droxler (1996) suggested exposure and karstification of this horizon prior to the drowning. Later studies confirmed a pre-Miocene sea-level drop but found no evidence of exposure (Belopolsky and Droxler, 2004a). In any case, the late-Oligocene rimmed platform configuration reacted to the subsequent sea-level rise by backstepping to the outer margins. The platform interior developed into drowning patch reefs while the exterior rims were restricted to a narrow zone in contact with the open ocean. These marginal reef crests kept up with the sea-level rise by aggrading throughout the earliest Miocene. Belopolsky and Droxler (2004a) explain the widening of the Inner Sea by a difference in growth potential between platform interior and exterior in combination with a sea-level rise. The higher growth potential of the aggrading rims compared to the protected interior, resulted in a platform geometry, referred to as an "empty bucket" (Kendall and Schlager, 1981; Schlager, 1993). Betzler *et al.* (2018) argue that a sea-level rise of 50 m at the O/M boundary (Miller *et al.*, 2005) is insufficient to cause platform drowning and backstepping. They propose an alternative cause based on the presence of organic-rich layers in several cores in this time interval (Betzler *et al.*, 2018). These sapropel-like layers could indicate an oxygen deficiency and an increased nutrient input associated with an upwelling event. High nutrient inputs are known to reduce the growth potential of carbonate factories and might have contributed to the partial drowning of the platform (Hallock and Schlager, 1986).

Sea-level controlled platform growth (Early- to Middle Miocene)

After the reef growth was confined to a 5 km wide strip at the platform edges, these rims prograded inwards during the Miocene, gradually enclosing the Inner Sea. The general prograding trend towards the basin center can be observed across the entire platform, although it was more substantial on the western than the eastern margin (Aubert and Droxler, 1996; Belopolsky and Droxler, 2004a). This asymmetric growth of the bank margins is best explained by the dominance of easterly currents during the Early to Middle Miocene, stimulating progradation on the leeward bank edge (Betzler *et al.*, 2013).

During the Early Miocene, a shallow-water carbonate succession was established on the Oligocene drowned platform interior. This succession developed a carbonate ramp depositional profile, marking the second turning point at its base (PS1; 22 Ma) (figure 6). The carbonate ramp steepened through aggradation, forming an interior well-defined bank edge (Betzler *et al.*, 2018). The ramp-to-rimmed platform evolution was in agreement with the global sea-level rise, culminating in a highstand around 20 Ma (Miller *et al.*, 2005). The following sea-level drop forced the platform to prograde inwards and closed the cycle with a sea-level lowstand at 18.5 Ma (turning point 3; PS5) (figure 6). The consecutive episode of sea-level rise and highstand was associated with a new platform aggradation phase that ended around 15.1 Ma. Simultaneously, the outer platform margins were backstepping, away from the open Indian Ocean (Betzler *et al.*, 2018). This time interval corresponds with a warm climate period with associated high sea levels that lasted from 17 to 14.7 Ma. This period, known as the Miocene Climate Optimum (MCO), embodied global annual mean temperatures that were 3-8°C higher than pre-industrial levels and atmospheric pCO_2 values reaching around 500 ppm (Zachos *et al.*, 2001; Holbourn *et al.*, 2015). After the MCO, Earth underwent a long-term global cooling that resulted in the onset of Northern Hemisphere glaciation at 2.8 Ma (Holbourn *et al.*, 2005). The associated eustatic sea-level lowering is recorded in the stratigraphic record of the Maldives by another phase of platform progradation. The sequence boundary at 15.1 Ma marks this geometry turnover, assigned to the fourth

turning point (PS8) (figure 6). After this second progradational phase, the excellent correlation between global sea-level changes and the sequence stratigraphy of the Maldives carbonate platform ends abruptly at 13 Ma. This sequence boundary, forming the fifth turning point (DS1), marks the onset of a completely different depositional system (figure 6) (Betzler *et al.*, 2018).

Current controlled sedimentation of drift bodies (Middle Miocene to Pliocene)

The Middle- to Late Miocene platform evolution is characterized by partial drowning of the bank and development of channels. These channels cut perpendicular through the elongated bank edges, creating a connection with the open ocean. Some separated bank parts resisted the drowning and kept aggrading to present sea level, leading to the present atoll configuration. This partial bank drowning was formerly interpreted in function of changes in relative sea level (Purdy and Bertram, 1993; Aubert and Droxler, 1996; Belopolsky and Droxler, 2004a). Aubert and Droxler (1996) acknowledge that the genetic relationship between these channels and the bank drowning, remained unclear due to a lack of sedimentological and high-resolution seismic data. Betzler *et al.* (2009) proposed a new model to explain the channel origin by the establishment of the South Asian Monsoon (SAM) system.

Around the Middle- to Late Miocene transition several climate changes transpired, that turned around the sedimentation patterns in the Indian Ocean. The uplift of the Himalaya, caused an increased sediment flux into the Indian Ocean around 11 Ma (Rea, 1992; Zheng *et al.*, 2004) and a peak in Indus fan sedimentation rate between 16 and 11 Ma (Clift *et al.*, 2008). This impactful tectonic event, combined with closure of the Tethys created a seasonal atmospheric pattern with strong reversing winds. This monsoonal wind system generated vigorous ocean currents, inducing upwelling over topographic highs (Betzler *et al.*, 2016). Planktonic foraminifera from the Arabian Sea were used to date these upwelling events and provided evidence that this SAM system developed at 12.9 Ma and the summer monsoon came to its full force around 7 Ma (Kroon *et al.*, 1991; Gupta *et al.*, 2015). Additionally, the stratigraphic record combined with geochemical evidence on the IODP 359 cores suggests that the onset of drift deposition occurred within a few 100 kyrs (Betzler *et al.*, 2016).

The onset of the SAM has several negative effects on the platform growth, which eventually resulted in a stepwise partial drowning that ended during the early Pliocene (Betzler *et al.*, 2009). Nutrient influx, associated with upwelling events are known to suppress coral reef growth (Hallock and Schlager, 1986). After the MCO, Earth underwent a global cooling, provoking a long-term eustatic sea-level lowering (Holbourn *et al.*, 2005). This caused the platform to become frequently exposed, terminating the carbonate production. When these platforms were submerged again during minor sea-level cycles, the currents were too strong for the ecosystem to recover (Betzler *et al.*, 2016). Instead, the currents widened the channels in the platform rim to passages in between separated atolls. The eroded sediment was redeposited in the Inner Sea as drift fans, which were further shaped by bottom currents into contourite drifts. As these bottom currents swept away the sediment around the atolls, progradation was inhibited (Lüdmann *et al.*, 2013). A last factor, that contributed to the drowning of the platform was the expansion of the Oxygen Minimum Zone (OMZ) from the Arabian Sea into the Maldives during the Late Miocene (Betzler *et al.*, 2016).

2.3.2.3 Quaternary: Aggradation of the individual atolls (Pliocene to recent)

The stepwise drowning of the Maldives carbonate platform ended at 3.8 Ma, forming the sixth and last stratigraphic turning point (figure 6) (Betzler *et al.*, 2018). The rims of the carbonate platform were cut into a double row of dispersed individual atolls. Gradual eustatic lowering and a retraction of the OMZ allowed the individual atolls to aggrade again and keep up with sea level until present times (Betzler *et al.*, 2016).

Chapter 3: Methods

3.1 Modelling workflow

Building a stratigraphic forward model for a sedimentary body involves a procedure of simplification and conceptualization of its genetic processes. An overview of how this was tackled in this study is depicted in a workflow diagram in figure 8. The first step starts with a detailed study of the sedimentary system, focused on published literature. A realistic geological model requires namely that all sedimentary processes involved in the deposition are fully understood (Warrlich *et al.*, 2008). After understanding the genesis of the sedimentary body, the deposition mechanism must be transferred into several key parameters. A first selection of impactful stratigraphic controls is desirable, because the more uncertain parameters are included in the model, the more difficult the model calibration becomes. The selection of key parameters is then quantified and constrained by sedimentological evidence from the study area or from similar settings. This leads to a subdivision of well-constrained input parameters and parameters with variable uncertainties. Depending on the amount of uncertain parameters and the size of their respective uncertainties, it might be necessary to make assumptions, in order to facilitate the calibration process (Warrlich *et al.*, 2008). Due to the deterministic nature of stratigraphic forward modelling, all parameters need a single value assigned before a model can be produced. This result is then evaluated as a function of its plausibility after which the input parameters are altered in order to fine-tune the model. This strenuous calibration process of 'trial-and-error' can become complex, when too many uncertain parameters are involved. The model result is evaluated in function of calibration data on the modeled basin, such as wells and seismic data. Wells allow to calibrate the model at points of control in terms of lithology and thickness. Well data, such as a gamma ray logs can for example be directly compared with simulated sediment properties of the 3D model, like mud content. Facies logs can be used for indirect comparison, through a depositional facies classification of the stratigraphic grid, based on its properties. Thickness of simulated sequences can be calibrated with time markers from the wells. Extensive well data in the proposed study area is available from the IODP expedition 359, with well markers (Betzler *et al.*, 2017) and a lithological interpretation into depositional facies (Betzler *et al.*, 2018). Lastly, interpreted seismic profiles (figure 6, appendix A) were used to derive depositional morphologies. Lacking conversion to the depth domain, they were not used to tie the simulated sequences to interpreted sequence boundaries.

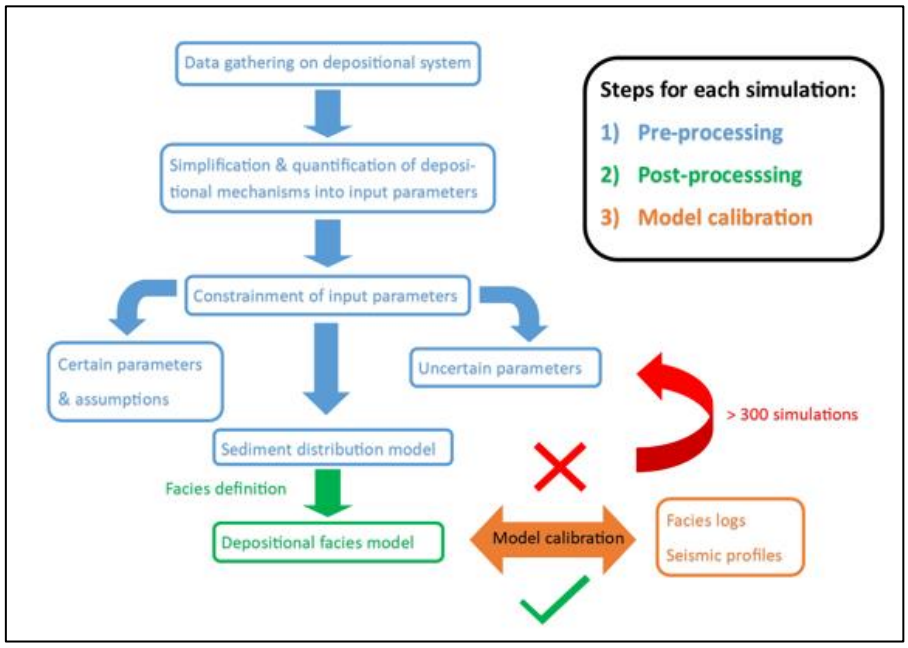

Figure 8. Modelling workflow for each simulation

3.2 DionisosFlow

This study uses the 3D numerical modelling software DionisosFlow, developed by the Institut Français du Pétrole (IFP). DionisosFlow is based on a water-driven diffusion that allows simulating sedimentary and tectonic processes in both carbonate and siliciclastic settings. It was developed to model geometry and facies of sedimentary bodies over regional spatial scales (10 to 100 km) and geological time scales (10 kyr to 100 Myr) in a sequence of time steps (Granjeon and Joseph, 1999; Granjeon, 2014).

The model construction is founded on an initial paleobathymetry at a given age, which is divided in grid cells according to the size of the model domain. From the defined initial age, the simulation creates new grid layers in a sequence of time steps, for a specified time interval. The size of the grid cells and the time step determine the simulation duration and are limited by the computing power of the hardware. For each newly created grid cell, the software considers three main stratigraphic processes, based on its position in space and time:

1. The available accommodation space for sediment infill, determined by the subsidence and eustasy level. Subsidence is computed from a set of user-defined subsidence maps. The eustatic sea level is retrieved by sampling a eustasy curve at each model time step.
2. The sediment accumulation, which can be clastic supply, basement erosion, carbonate production or evaporite precipitation. In carbonate settings the production happens *in situ* and depends on the ratio between production values for each sediment class. The production for each class is defined over time and depth and can be further restricted by ecological requirements, such as wave energy, substrate and turbidity. The defined production rates form the sum of the benthic and pelagic production over the entire water column.
3. The sediment transport, importing and exporting sediment to and from its neighboring cells. The sediment transport is calculated by diffusion equations, fit to simulate sediment transport at a regional scale (Granjeon and Joseph, 1999; Granjeon, 2014). Two types of transport can be simulated with DionisosFlow: (1) long-term transport driven by slope-action, wave energy and water discharge and (2) short-term transport like debris-flows. Long-term transport equation, used in this study, can be written as a sum of three linear equations (Seard *et al.*, 2013; Hawie *et al.*, 2015):

$$Q = K_{gravity} \times S + K_{water} \times \emptyset_{water} \times S + K_{wave} \times E_{wave} \times S$$

with Q representing the average sediment flow (km^2/kyr), S the slope, K the diffusion coefficient of each process (km^2/kyr), $\emptyset_{water}$ the water flow and E_{wave} the wave energy. The diffusion coefficients (K) of each process have to be estimated by the user for each sediment class, in function of the grain size and depositional environment, continental or marine. The sedimentation and/or erosion is calculated at each point from a mass conservation equation and defined erosion rates. After prediction of the sediment distribution by the diffusion equation, the slope stability in each cell is checked. If the slope angle exceeds the static angle of repose of the composing grain-size fractions, all sediments are moved downslope until an equilibrium is reached. Lastly, the compaction of the sediment can be calculated from burial laws and sediment load estimation (Granjeon, 2014).

Upon creation, each cell is characterized by its thickness and several depositional properties, such as bathymetry, slope, sedimentation rate, wave energy and the composing fractions of each sediment class (Seard *et al.*, 2013). Based on these properties the 3D model grid can be classified into user-defined facies.

Chapter 4: Model Design

4.1 Pre-processing: Input parameters definition

The parametrization of the depositional mechanism starts with quantifying and constraining the input parameters from literature data. Based on the available data set, the input parameters were subdivided in two categories: the basin conditions and the sediment characteristics. Overall, the basin conditions contained much less uncertainties than the sediment properties. Therefore, the quantified basin parameters, combined with some assumptions, were used as a solid framework on which various scenarios of carbonate sedimentation could be tested. After a suitable representation of the depositional mechanism was validated, several hypotheses on the stratigraphic controls were evaluated. Due to the low constraints on sediment properties, most notably production rates and transport properties, this process required more than 300 simulations. This section will discuss the data on which quantified input parameters are based and outline several concepts in carbonate production that helped to constrain the more uncertain parameters.

Each simulation ran from 25.75 Ma to 13 Ma, in 51 time steps, each 0.25 Ma in length. The total time interval, corresponds with the four first episodes of platform evolution with distinct geometry, separated by five stratigraphic turning points (figure 6) (Betzler *et al.*, 2018). This conceptual model was based on the sequence stratigraphy of the western platform margin, because its progradation/aggradation trends are more pronounced than on the eastern margin. This study will try to reconstruct these western margin trends by simulating the depositional processes that formed each sequence. The produced sequence volumes represent fully compacted sediment loads, matching with the present-day volumes. Compaction laws were not used in this study, as they greatly complicate the calibration of the model (Al-Salmi *et al.*, 2019). Moreover, compaction laws in carbonate sequences are ill-constrained due to variable cementation and lithification of each fabric (Purdy and Bertram, 1993). Properly accounting for this process would require knowledge of the lithification and pressure solution history of each interval up until the present-day sedimentary cover.

4.1.1 Basin conditions

4.1.1.1 Domain definition and initial bathymetry construction

Before any other input parameter can be tested through simulation, the software needs an initial bathymetric surface, upon which new grid layers are created. In the Maldives carbonate platform, the O/M horizon creates a strong reflection, clearly visible in seismic reflection profiles from various publications (Aubert and Droxler, 1996; Belopolsky and Droxler, 2003, 2004a, 2004b; Betzler *et al.*, 2013, 2018). This drowning unconformity forms an ideal model base surface that can be traced throughout the entire platform.

Well data from NMA-1, ARI-1 (Aubert and Droxler, 1996), ODP 716 (Belopolsky, 2000), and all wells from IODP 359 (Betzler *et al.*, 2017) were used in Petrel to construct a stratigraphic framework. All published seismic sections (Aubert and Droxler, 1996; Belopolsky, 2000; Belopolsky and Droxler, 2003, 2004a, 2004b; Betzler *et al.*, 2013, 2018; Lüdmann *et al.*, 2013) were digitized, georeferenced and fitted to the well data, in absence of a depth conversion. Based on well markers for ground-truth and seismic profiles for its morphology, the topography of the O/M horizon was approximated. Further detailed surface editing was based on the time-structure map from Belopolsky and Droxler (2004a). The entire surface was elevated to paleo-sea level, correcting for an estimated total subsidence of 1130 m (Purdy and Bertram, 1993), assuming that the Eocene shallow-water platform had not been exposed (Belopolsky and Droxler, 2004a).

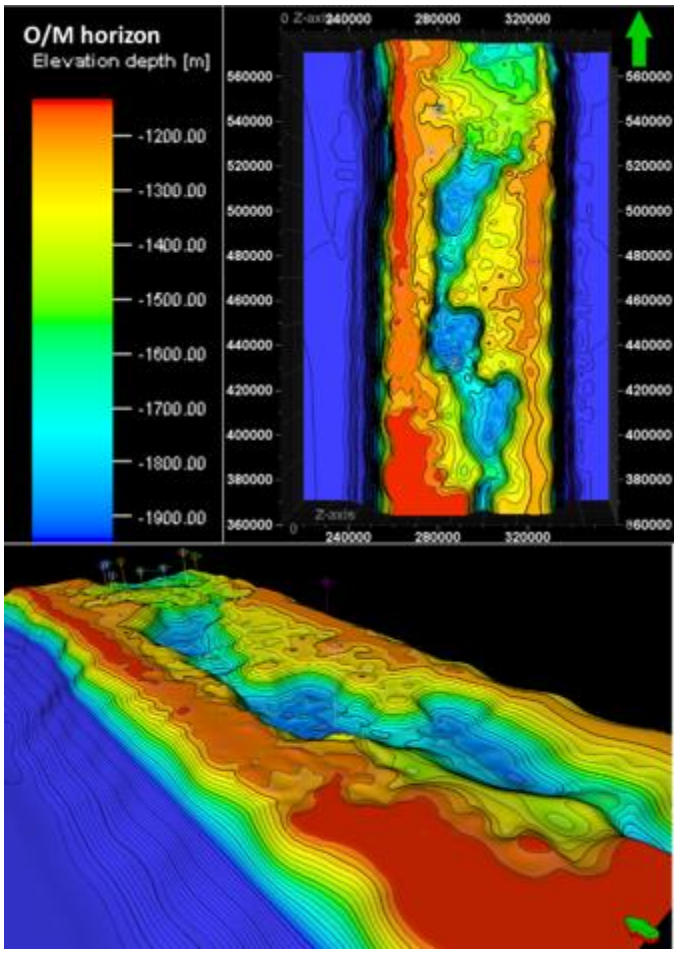

Figure 9. Top and oblique 3D view of the reconstructed O/M horizon across the entire Maldives carbonate platform. The elevated outer rims consist of Paleogene shallow carbonates sequences. The inner seaways mimic the graben morphology, while being filled up largely with periplatform sediments.

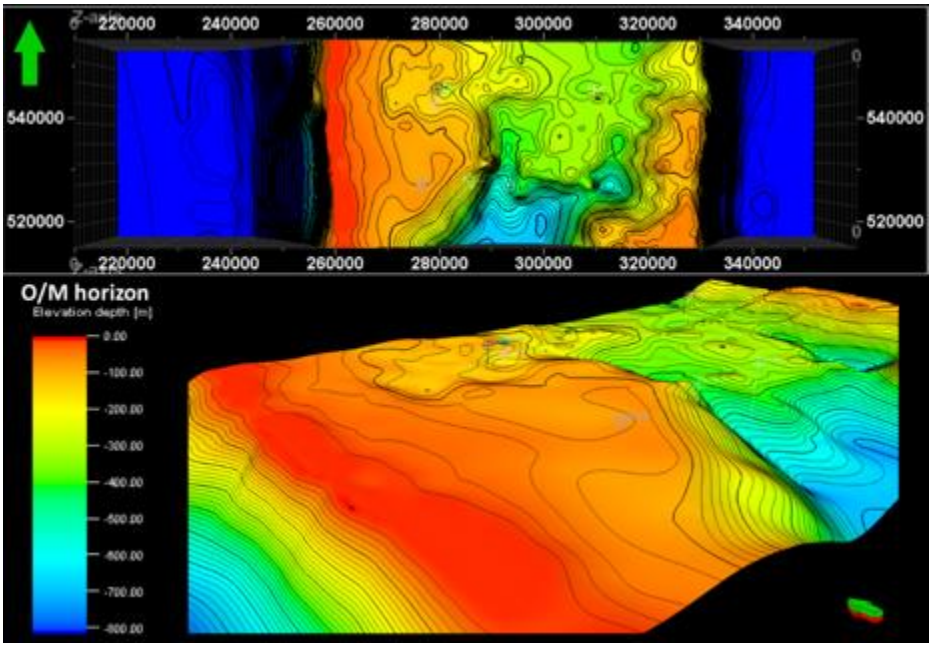

Figure 10. Top and oblique 3D view of the initial paleobathymetry used as a base for the stratigraphic model construction. The surface was sliced out of the northern part of the reconstructed O/M horizon, fitting with the size of the study area and elevated to paleosea level.

The resulting initial bathymetric surface spanned the entire width of the Maldives carbonate platform and ocean floor from 72° 23' E to 73°44' °E and most of the present central Maldives atolls from *2* ° N to *6* ° N (figure 9). This large domain required a grid cell size of 2000 m x 2000 m to be able to run a simulation, which is too large to represent progradation trends over a few kilometers. Therefore, an E-W slice of the large domain was selected as study area between 4°39' N to 5°01'N (figure 10), similar to the study area in figure 4 (Betzler *et al.*, 2018). This study area was chosen to contain most of the seismic profiles and wells, so the initial bathymetry would be constrained as best as possible. The size of the model domain was subdivided in 300 x 80 grid cells, each 500 m x 500 m in size. The initial bathymetry was assumed to be a well constrained, certain parameter and remained constant for all simulations.

4.1.1.2 Basement subsidence

The tectonic regime of the Maldives is remarkably stable since the latest Oligocene, with no recent faulting, nor signs of differential subsidence (Belopolsky and Droxler, 2004a; Betzler *et al.*, 2013, 2018). The region can be considered as a far-field site, regarding ice load of continental margins, making the impact of glacio-isostatic effects negligible (Fürstenau *et al.*, 2010). Purdy and Bertram (1993) presented a single back-stripped subsidence curve for well NMA-1, based on bulk density calculations from the log (figure 10). The loaded subsidence curve shows a gradually increasing subsidence under an increasing sedimentary load. The unloaded subsidence curve on the other hand shows three episodes of tectonic stability, interrupted by three shorter phases of accelerated subsidence, which currently are still left unexplained. In any case, a total subsidence of around 500 m can be derived from the loaded curve for the interval from 25.75 Ma to 13 Ma. In addition, a total subsidence of 400 m was estimated by Betzler *et al.* (2013) for the interval of 23- 13 Ma. Other long-term subsidence rates derived from deep core data of wells ODP715 and ARI-1 correspond with respective ranges around 0.043-0.047 mm/yr (Backman *et al.*, 1988) and 0.03–0.04 mm/yr (Lüdmann *et al.*, 2013). Higher Pleistocene rates of 0.15 mm/yr were found in sedimentological evidence from the Rasdhoo atoll (Gischler *et al.*, 2008).

In order to reconstruct the structural evolution of the Maldives carbonate platform for this study, the absence of differential subsidence was assumed. By combining all subsidence data and calibrating the model to a geologically plausible result, an average subsidence rate of 0.0385 mm/yr was used for the interval 25.75 Ma -13 Ma and a higher average rate of 0.087 mm/yr until present times. These values approximate the curve presented by Purdy and Bertram (1993), while respecting the long-term subsidence rates and increased Pleistocene rates (figure 10). Due to these constraints the uncertainties on the subsidence values were relatively small and thus considered as a certain parameter.

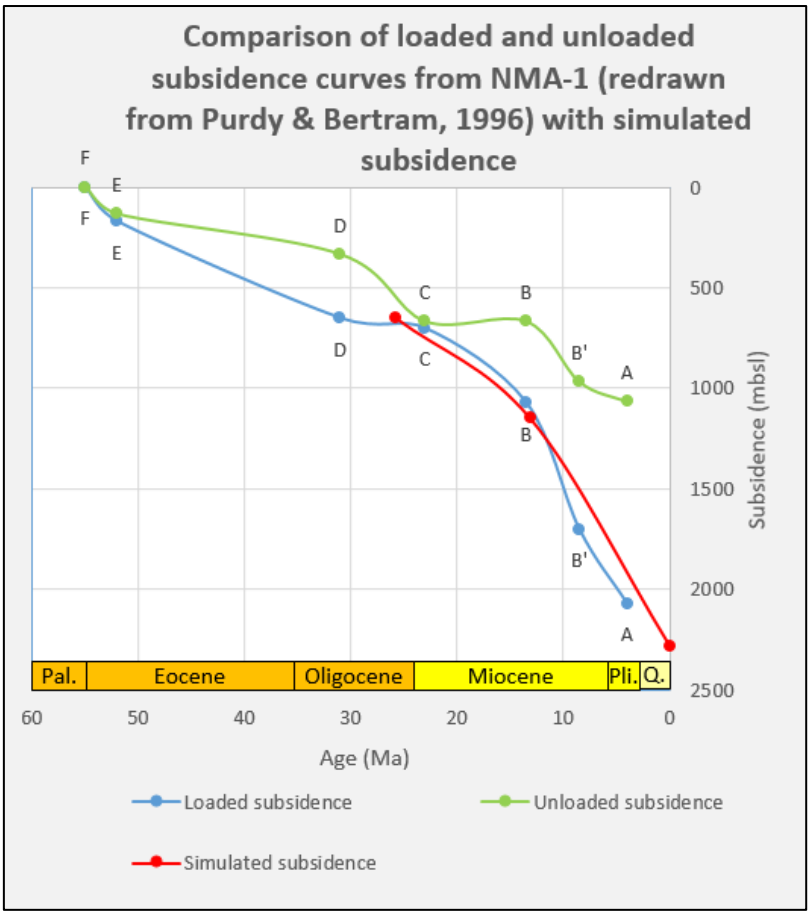

Figure 11. Comparison of simulated subsidence and subsidence curves from well NMA-1. Curvatures between measuring points A-F are redrawn after original curves. Unloaded subsidence curve has only been corrected for sedimentary load and paleobathymetry (redrawn from Purdy and Bertram, 1994).

4.1.1.3 Wave impact

The distribution of wave energy plays two important roles in the definition of the basin conditions: (1) it will determine how sediments are transported by waves as a component of the diffusion equation and (2) it allows to impose ecological restrictions of wave energy to selected sediment classes, to create for example a reef zonation for different wave energy levels (Graus and Macintyre, 1989; Montaggioni, 2005). In this study, waves are simulated along their wave propagation angle (1D) with wave energy decreasing from sea level to a defined wave base.

Until the Oligocene, the Tethys current created dominant westward flowing, circum-global surface circulation crossing the Arabian Sea. Due the convergence of the African and Eurasian plates, the current was gradually reduced and finally cut off by the Early Miocene. This event isolated the Mediterranean from the Indo-Pacific province (Aubert and Droxler, 1996). The collision of the Indian and Eurasian plate invoked the uplift of the Himalaya Massif establishing the SAM system by the Late Miocene (12.9 Ma) (Rea, 1992; Zheng *et al.*, 2004). Before the full enforcement of this new wind system and under reduced Tethys current, a weak proto-monsoon system prevailed between 25 Ma and 12.9 Ma (Betzler *et al.*, 2016). Evidence for this phenomenon, is found in the dominantly eastward progradation of the Maldives carbonate platform and in the eolian dust record in the Inner Sea. Both indicate prevailing summer-monsoon westerly winds for this period, inducing eastward currents. At 12.9 Ma, the proto-monsoon system strengthened to the present SAM system, with vigorous currents hampering the carbonate platform development and generating sediment drift deposits (Betzler *et al.*, 2016, 2018).

The proto-monsoon system was simulated with two constant sets of waves over the study interval from 25.75 Ma to 13 Ma. Both have an average wave base of 20 m (figure 12), which is the average value for shallow-water environments (Coe *et al.*, 2003), but opposite wave propagation angles, namely 90° and 270°. To establish the dominance of the summer monsoon over the study interval, the eastward directed wave was defined by a wave frequency per year of 100%. The minor westward winter monsoon is characterized by a frequency per year of 70%.

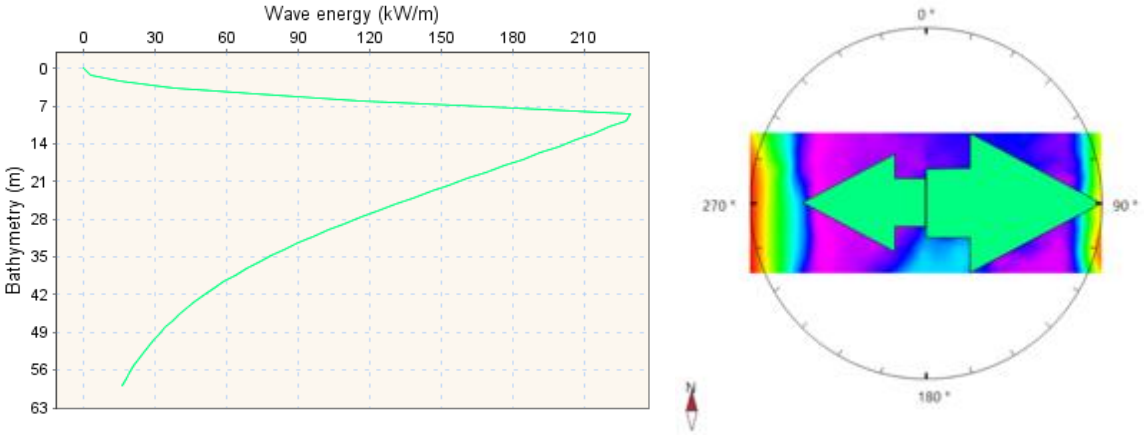

Figure 12. Left: Wave energy distribution in function of bathymetry. Right: Simulated waves orientations over model domain

4.1.1.4 Eustasy

During the DionisosFlow simulation, the available accommodation space is calculated for every time step by sampling a user-defined eustasy curve and calculating the subsidence or uplift (Seard *et al.*, 2013). However, when the model time step surpasses the interval at which the curve was constructed, two major consequences influence the modelling approach, namely: (1) eustasy curve data points will be inevitably lost and (2) depositional sequences might not be gradually stacked within a single sea-level rise/fall. The first issue goes hand in hand with the simplifications that are involved in every model construction. It is nevertheless important that crucial eustatic changes are not displaced in time nor altered in amplitude to produce a geologically relevant stratigraphic model. The second issue depends on the order of sea-level changes, that the model aims to reflect.

Due to its excellent correlation with the depositional stacking patterns of the Maldives carbonate platform (Betzler *et al.*, 2018), this study uses the eustatic sea-level curve by Miller (2005), constructed with an interval of 100 kyrs over the studied section. Due the size of the model, and the available computing power, the lower time step limit was set at 250 kyrs. To tackle the above-mentioned issues, the original sea-level curve was resampled with an interval of 500 kyrs. Using this resampled eustasy curve as an input parameter, allows the software to sample the curve two times for every sea-level rise/fall, producing more gradual sequence stacking patterns. At the same time, the resampled curve honors the expected geometrical evolution of the carbonate platform, associated with the four simulated time intervals (figure 12).

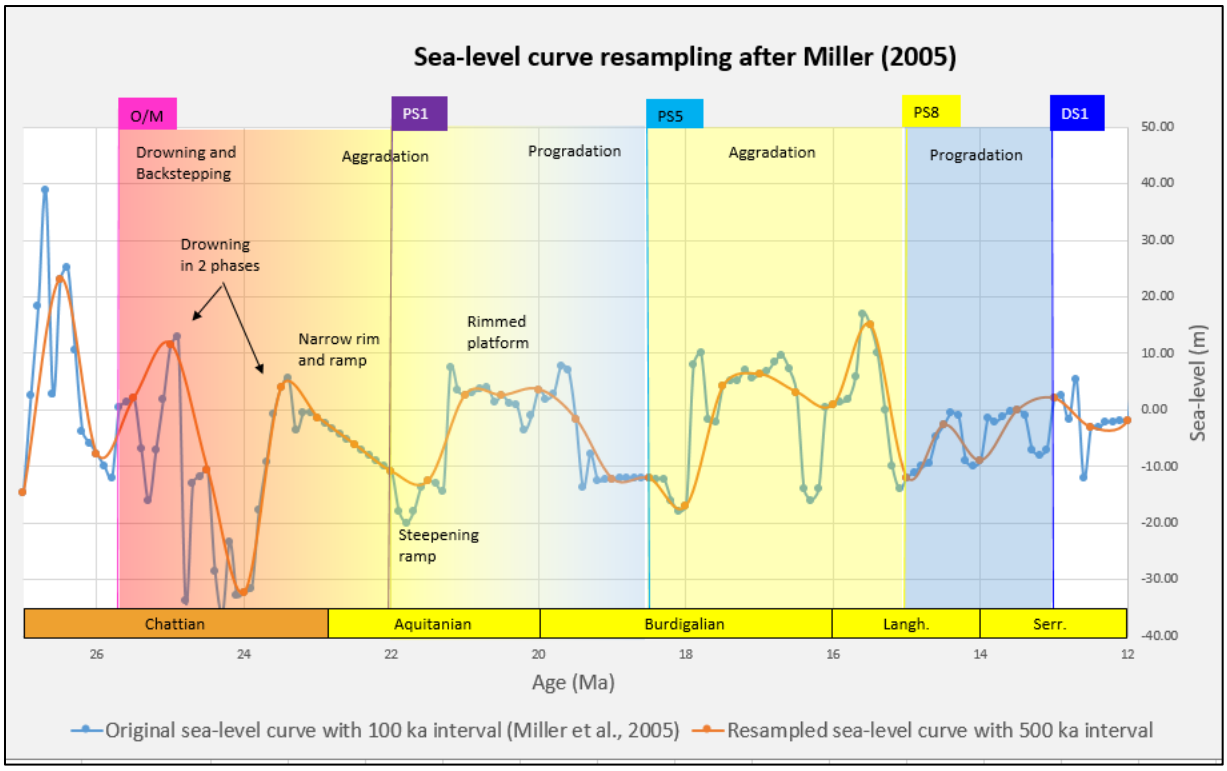

Figure 13. Resampling procedure of the original sea-level curve by Miller (2005). Resampling with a 500 kyrs interval maintains the timing and amplitude of crucial changes but preserves the expected depositional geometries. Stratigraphic turning points 1-5 are indicated with their respective sequence boundary. Expected platform geometries are represented across the time intervals in color code: drowning and backstepping (red), aggradation (yellow) and progradation (blue)

4.1.2 Sediment classes and properties

The selection of the sediment classes is one of the most defining steps in the parametrization of the depositional system. The main idea is to define the sediments by a set of common characteristics, related to its production/supply and transport parameters. The choice of classes embodies how to conceptualize the depositional dynamics of the simulated target system. In carbonate systems, the aim is to simplify the carbonate factory by lumping several production processes into classes. Consequently, conceptual production laws are assigned to each class, representing the combined effect of all its incorporated processes. Lastly, the available calibration data plays a role in the class selection. A class differentiation on grain sizes can be useful, when well logs with grain-size distributions are available. Conversely, a classification based on ecological restrictions is preferable, when only interpreted depositional facies logs are on hand.

Depending on the spatial and temporal scale of the model, several approaches to the sediment class definition exist. Regional stratigraphic models with grid cell sizes of several kilometers, require a greater degree of simplification. These exploration- and reservoir-scale models often differentiate classes based on grain size, to fit them with a different diffusivity. Due to high uncertainties within the equally large time steps, the generalized production laws are assumed to remain constant over time (Hawie *et al.*, 2015; Al-Salmi *et al.*, 2019). Smaller-scale models use a wide range of approaches, that are commonly more fit to the specifics of the depositional system. Classes can be constrained to ecologic requirements of individual biotic communities, like corals, benthic foraminifera, red and green algae. A study on the last deglacial drowning of the Tahiti reefs used different classes for distinct coral assemblages with each their own production rates and depth profiles (Seard *et al.*, 2013). A stratigraphic model of the Quaternary evolution of the western Great Bahama Bank differentiated classes based on the degree of diffusivity. The diffusivity was linked to early cementation processes,

specific to each depositional environment (Busson *et al.*, 2019). A third example, from a case study on a mixed platform from the Messinian of the Sorbas Basin, used wave energy restrictions to constrain each sediment type to a depositional environment (Kolodka *et al.*, 2016).

This study proposes a new sediment classification, fit to the depositional mechanisms that governed many Miocene carbonate platforms around the world. The selection is based on the concepts of carbonate sediment production, outlined in the chapter 1. As many of the adopted ideas were defined by Luis Pomar on Miocene carbonate platforms of the Mediterranean (Pomar, 2001a, 2001b; Pomar and Hallock, 2008; Pomar *et al.*, 2012; Pomar and Haq, 2016), they suit the purpose of this stratigraphic model particularly well.

4.1.2.1 Sediment class definition

Distant from any terrigenous input during the Neogene, all siliciclastic sediment classes can be excluded from our model (Purdy and Bertram, 1993; Aubert and Droxler, 1996). Since the latest Oligocene the Maldives carbonate platform was located in its present equatorial position (Aubert and Droxler, 1996). A regional tropical carbonate factory can thus be assumed to have produced the bulk of the carbonate sediment. Deeper in the water column, the tropical system passes into a cool-water system below the thermocline. This transition between T- and C-factory fluctuates in areas with upwelling of cooler, nutrient-rich waters (Schlager, 2005). Also the latitudinal transition between tropical factories and cool-water factories is known to be very gradual (Betzler *et al.*, 1997). Furthermore, the composition of the carbonate factory has changed over time due to biological evolution under changing environmental conditions.

An extensive overview of the evolution of carbonate-producing organisms through the Mesozoic and Cenozoic is given by Pomar and Hallock (2008). During Paleogene, the marginal seas of the Tethyan Ocean were dominated by Large Benthic Foraminifera (LBF) assemblages. These LBF made up massive carbonate ramps, while often living in symbiosis with light-dependent algae. They would remain an important component of the carbonate factory throughout the Neogene although less abundant than in the Eocene. While many other groups declined during the Paleogene, scleractinian corals increased in diversity since the Eocene. The expansion of these corals contributed to an increased reef-building capacity. Around the Oligocene-Miocene transition, the main reef builder function transferred from these scleractinians corals to coralline red algae. These encrusting organisms diversified strongly in the Oligocene, until they became the dominant carbonate producers in the Early- and Middle Miocene. Halfar and Mutti (2005) argue that the red algae abundance peak from the Burdigalian to the Tortonian was caused by elevated nutrient levels, due to enhanced global productivity. Coralline red algae tend to flourish compared to other reef builders under eutrophic conditions (Halfar *et al.*, 2004). Towards the Late Miocene the competition between coralline red algae and scleractinians corals continued, while the carbonate reef environment expanded towards the shallow euphotic zone. In these shallow environments the zooxanthellate coral species gained the upper hand as dominant reef builders, thanks to their symbiosis with photosynthesizing algae (Pomar and Hallock, 2008). The exact mechanism behind the expansion of reef environments at the Oligocene-Miocene transition and in the Late Miocene of this shallowing reef environment remains a topic of debate. Aguirre *et al.* (2000) argues that the expansion can be attributed to the increasing abundance of scleractinians, which provided habitat for red algae. Conversely, the argument can be made that these same red algae stabilized the coral framework, allowing the scleractinians to expand to higher energy environments (Pomar and Hallock, 2008).

Taking these nuances on the carbonate factory composition into account, several carbonate-producing processes were identified in the Neogene formation of the Maldives carbonate platform (figure 13). As illustrated above scleractinian corals and coralline red algae play an important role in the reef building mechanisms. Coral fragments of massive, platy and branching species were found in well sections from the shallow-water reefs, together with green algae (e.g. *Halimeda*) and large benthic foraminifera (Betzler *et al.*, 2017, 2018). These light-dependent organisms produce sediments within the photic zone, which are lumped together as euphotic bioconstructions (first sediment class). Red algae are also found in the shallow-water reefs and the platform slope, with ahermatypic coral fragments and LBF (Betzler *et al.*, 2017, 2018). Together they make up for the production of oligophotic bioconstructions (second sediment class), because they are able to survive under reduced light conditions (Pomar, 2001b). Photo-independent, heterotrophic organisms, typical for the C-factory, produce loose sand-sized skeletal particles, rather than rigid frameworks (Schlager, 2005). Examples of these organisms in the lithological well descriptions are bryozoans, mollusks and echinoids (Betzler *et al.*, 2017, 2018). Pelagic organisms are not necessarily photo-independent, but their skeletal remains can be found at all water depths across the platform. Therefore, their carbonate production is clustered with photo-independent biotic production and bioconstruction erosion into one sediment class, namely carbonate grains (third sediment class). Lastly, the fourth sediment class is produced by reworking and erosion of the previous classes, resulting in fine-grained carbonate mud. The choice of these four sediment classes, is founded on the common properties for each class, which will be highlighted in the following sections.

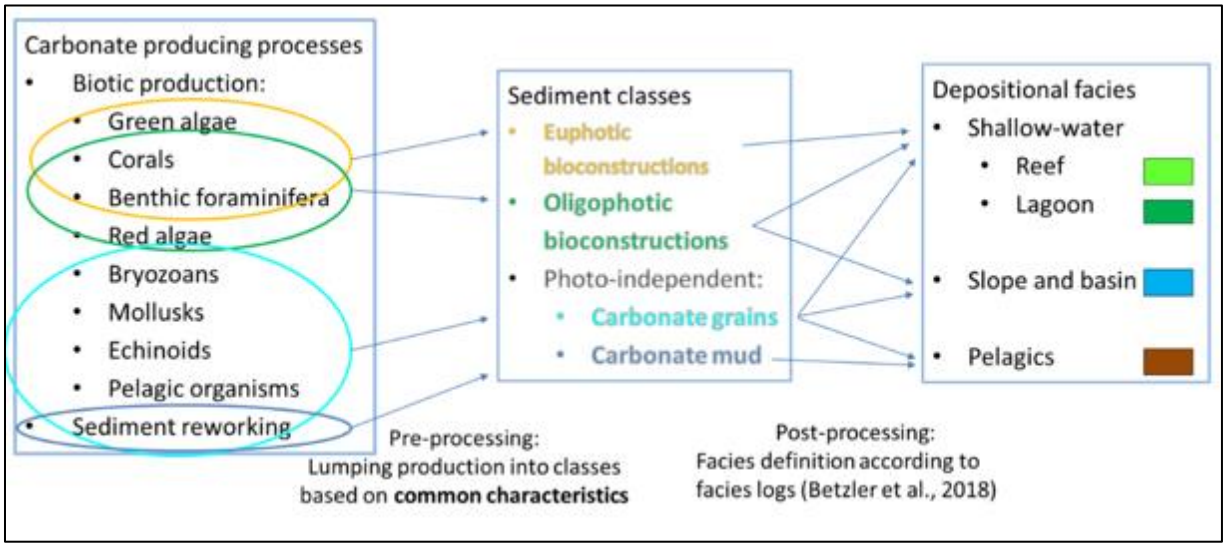

Figure 14. Sediment class definition for reference model based on dominant carbonate-producing processes and available facies logs for calibration

4.1.2.2 Carbonate production depth profiles

The first and most obvious characteristic of each sediment class is its carbonate production as a function of water depth. As this parameter is difficult to assess on fossil species, this study uses modern species ranges as analogues. Each sediment class is fit with a common production efficiency in function of water depth, as a fraction of its maximum production potential (figure 14). As light dependency is undoubtedly the most influential parameters on this carbonate production profile, it forms an excellent differentiation parameter (Pomar, 2001b). The influence of light intensity on reef growth can be represented by an equation, presented by Bosscher and Schlager (1992):

$$G(z) = G_{max} \times \tanh(I_0 \times e^{-kz}/I_k)$$

with G is the reef growth rate (m/kyr), z is the water depth (m), I_0 is the surface light intensity (µE/m^{2}s), k is the extinction coefficient of light (m^{-1}) and I_k is the light intensity at the base of the saturated zone (µE/m^{2}s). Due to the high light dependency of the euphotic sediment producers, their production profile was approached with this formula, with k = 2, I_0/I_k = 50. A relatively high extinction coefficient is justified by the enhanced global productivity during the Early and Middle Miocene (Halfar and Mutti, 2005). This results in a maximum production between 0 and 15 m water depth, with a rapid decline in production towards 20 m, fitting with Holocene coral growths from the Maldives (Gischler *et al.*, 2008) and the Indo-Pacific (Montaggioni, 2005).

Modern coralline red algae and associated encrusters are either found in protected muddy environment, less than 10 m deep or more commonly in deep fore-reef crests and slopes at more than 20 m (Montaggioni, 2005). Their low light requirements make them thrive in water depths between 30 and 80 m, where competition with euphotic biota is absent (figure 15) (Pomar, 2001b). Photo-independent biota can occur all over the water column, but are dependent on a nutrient supply. They live often in symbiosis with light-dependent organisms, leading to an increased abundance within the photic zone (Pomar, 2001b; Schlager, 2005). Nevertheless, a small fraction of photo-independent carbonate production is maintained up until 350 m of water depth for this simulation experiment. This fraction is attributed to pelagic production and reworking of sediment grains. Both the carbonate mud and carbonate grains are characterized by the same photo-independent depth production profile.

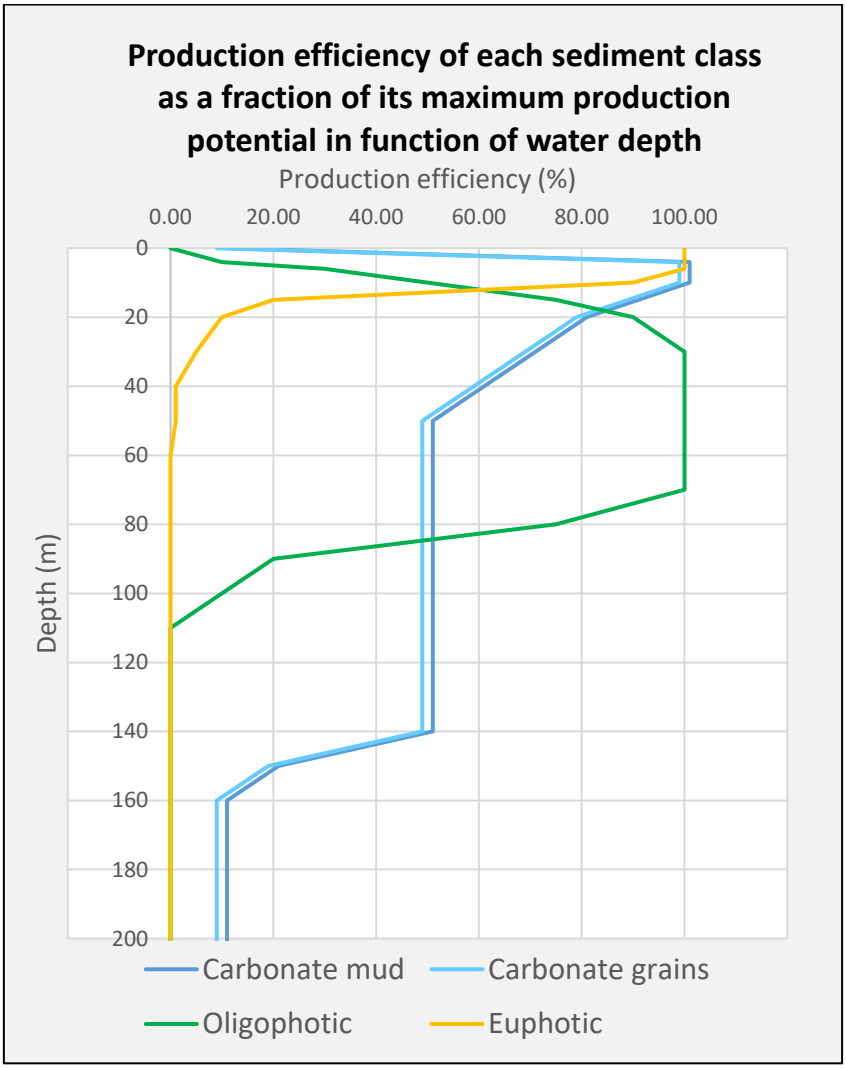

Figure 15. Carbonate production depth profiles of each sediment class

4.1.2.3 Carbonate production over time

As illustrated in the introduction, carbonate production rates from the geological past are difficult to estimate. At best, their lower limit can be calculated from accumulation rates, simply by dividing the sequence thickness by its depositional time interval (Bosscher and Schlager, 1993). This technique is sometimes applied in stratigraphic forward modelling, but works best on rigid reef models during recent time intervals (Seard *et al.*, 2013; Camoin and Webster, 2015). In rigid reef frameworks the carbonate export is minimal due to sediment baffling, which reduces the difference between accumulation and production rates. An overview of calculated accretion rates from Indo-Pacific cores of Holocene reefs provides values for framework-dominated reefs of between 1 to 30 mm/yr with a modal rate of 6-7 mm/yr. Coralline algae achieve lower growth rates, up to a maximum of 3 mm/yr (Montaggioni, 2005). Similar values were calculated from cores of Quaternary reefs in the central Maldives. By dating these cores, Gischler *et al.* (2008) found marginal reefs accreting with rates of 15 mm/yr and lower lagoonal rates around 4 mm/yr.

Modern reef growth rates can be obtained by adding standing crops and growth rates of its composing organisms or by measuring the reduction in alkalinity of sea water by passing over the reef (Bosence and Waltham, 1990). Both techniques result in reef growth rates around 4000-4500 m/Ma. These values are often used in stratigraphic forward models, when lacking quantified data for the paleo-growth rate (Bosence *et al.*, 1994; Warrlich *et al.*, 2008; Williams *et al.*, 2011). As illustrated by Sadler (1981) and Schlager (1999), sedimentation rates on carbonate platforms decrease with a scaling trend over an increasing interval of observation. These authors show how modern analogues have sedimentation rates that are an order of magnitude higher than in reefs from the Miocene. Their results indicate values for Neogene accumulation rates around 100-1000 m/Ma.

With the above-mentioned reference values in mind, several scenarios of carbonate production were tested over time. Due to the low constraints of the carbonate production values this trial and error procedure involved more than 300 simulations to acquire a model fitting with all available calibration data. Two major trends were taken into account during the strenuous calibration of this production curve: (1) the possible hypotheses on the cause for platform drowning around the Oligocene-Miocene boundary (Belopolsky and Droxler, 2004a; Betzler *et al.*, 2018), and (2) the evolving relationship between coralline red algae and scleractinian corals throughout the Miocene (Halfar and Mutti, 2005; Pomar and Hallock, 2008). Every simulation was matched with the morphological evolution of the platform, focusing on the four phases with distinct geometries outlined by Betzler *et al.* (2018) (figure 12). During this calibration process, modelled horizons were compared to sequence boundaries in the interpreted seismic sections (Betzler *et al.*, 2013, 2018) and simulated thicknesses tied to the well markers (Betzler *et al.*, 2017). The final best fitting production curve is shown in figure 15.

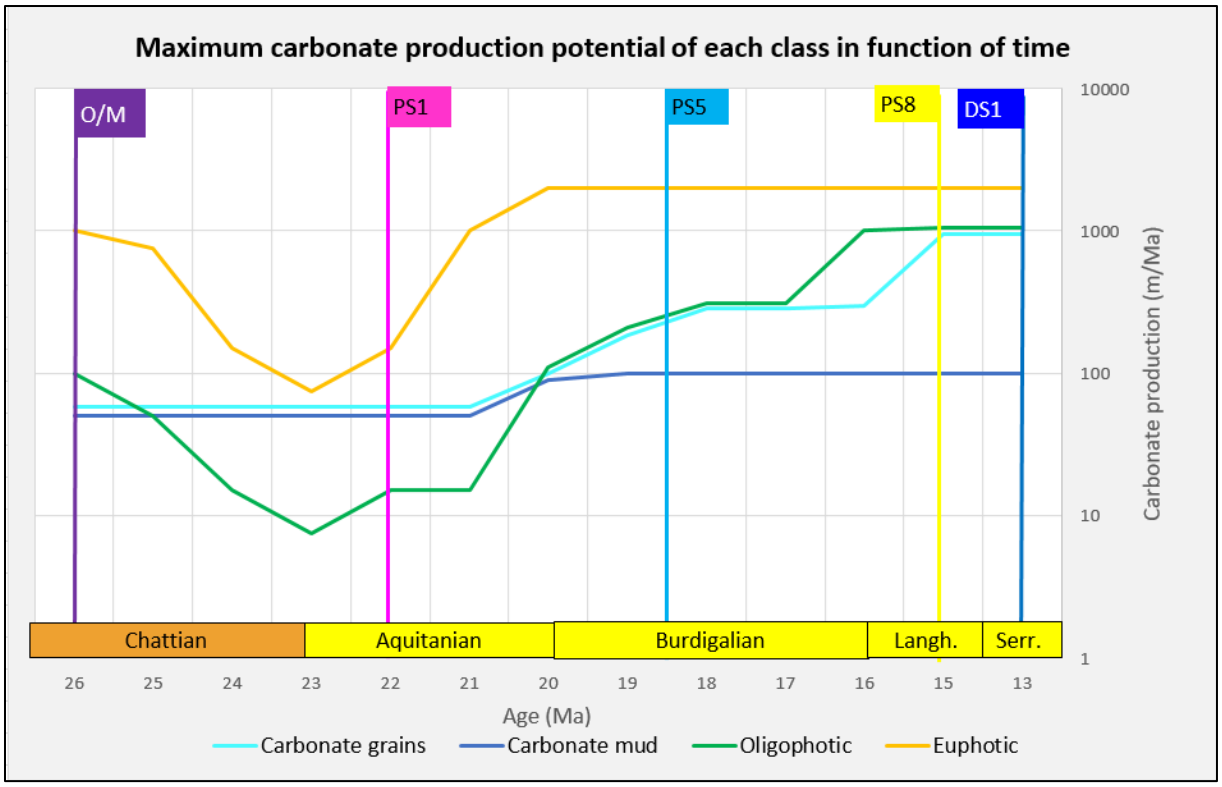

Figure 16. Best fit for carbonate production values in function of time. Note that the scale of y-axis is logarithmic. The most notable features are a dip in light-dependent production between 24 and 22 Ma and a gradual catch up of oligophotic production rates with euphotic rates since the latest Aquitanian.

4.1.2.4 Ecological restrictions

A final constraint on the carbonate production can be imposed in DionisosFlow by ecological requirements for each producing mechanism. As such, the occurrence of certain sediment classes can be restricted to specified environmental conditions, based on salinity, temperature, substrate, wave- and drift energy. This study uses only wave energy to differentiate high- and low-energy environments.

Depending on the species, hermatypic corals inhabit moderate- to high-energy environments, diagnostic of windward margins (Gischler *et al.*, 2008). Coralline red algae on the other hand, occur rather in low-energy environments, either in protected, muddy lagoons or in deeper fore-reef zones below wave base (Montaggioni, 2005). By evaluating the simulated wave energy distribution over time, a boundary of 50 W/m^2 was picked to differentiate between high- and moderate-energy environments on one side, and low-energy environments on the other. Euphotic sediment production was restricted to the former and oligophotic production to the latter.

4.1.2.5 Transport Properties

Transport of sediment particles in DionisosFlow is calculated for each cell through a diffusion equation (section 3.2). Due to the size of the model and the time step, only long-term diffusion processes are simulated in this study. Consequently, the diffusivity of each sediment class is defined by three diffusion coefficients, each linked to a different transport process. The three processes, responsible for sediment transport on a basin scale are gravity, water flux and wave action, with their respective diffusion coefficients $K_{gravity}$, K_{water} and K_{wave}. Each diffusion coefficient has to be estimated by the model user with respect to the grain size of each sediment class and depositional environment, continental or marine (Granjeon and Joseph, 1999; Seard *et al.*, 2013; Hawie *et al.*, 2015). As a rule of thumb, diffusion coefficients for sand-sized particles are often 10 to 5 times lower than for mud (Williams *et al.*, 2011; Hawie *et al.*, 2015). Early depositional cementation or microbial binding can also weigh in on the estimation of diffusion coefficients, when the sediment classes envelop specific lithological or biotic associations (Busson *et al.*, 2019). Lastly, each sediment class also has an angle of repose, based on its grain size, which determines the slope stability (Granjeon, 2014).

Diffusion coefficient are ill constrained by real-world examples, especially in shallow-marine and carbonate systems. Estimates in natural systems range from 560 km^2/ky in the Mississippi delta (Kenyon and Turcotte, 1985) to 7 x 10^{-6} km^2/kyr in pelagic environments, near the Galapagos spreading center (Mitchell, 1996). In shallow carbonate platforms the values are estimated to range within 0 to 50 km^2/kyr (Williams *et al.*, 2011). This poorly-constrained interval makes this input parameter another calibration challenge.

After testing several diffusion coefficients in more than 300 simulations, a best fit was calibrated with the available data, in a similar way as for the production rates. The values associated with this model are given in table 1. All diffusion coefficients are defined within the marine realm, as no significant emersion takes place during the simulation. Diffusion coefficients for carbonate mud and grains differ one order of magnitude as proposed by Williams *et al.* (2011). Diffusion coefficients for euphotic bioconstructions are minimized to represent their rigid reef framework properties. Oligophotic diffusion coefficients are fit to represent the solidifying effect of coralline red algae and other encrusters on the fore-reef slope.

Diffusion coefficients in marine environment	Carbonate mud	Carbonate grains	Oligophotic	Euphotic
$K_{Gravity}(km^2/kyr)$	0.0800	0.0080	0.0003	0.0001
$K_{Water}(km^2/kyr)$	0.7000	0.0700	0.0003	0.0001
$K_{Wave}(km^2/kyr)$	0.7000	0.0700	0.0003	0.0001

Table 1: Diffusion coefficients of each sediment class in marine environment for the best case scenario. Each set of diffusion coefficient represents the three main sediment transport processes, namely by gravity, water flux and wave action.

4.2 Post-processing: Facies definition

The calibration of uncertain parameters, like some sediment properties in this study, is executed through a deterministic "trial-and-error" process (section 3.1). Validation of the input parameters, and of the model by extent, requires ground-truth reference data. This calibration data was constructed from literature by Betzler *et al.* (2013, 2017, 2018). Sequence boundaries, reported as well markers, were used to directly calibrate simulated sequence thicknesses (Betzler *et al.*, 2017). This study validates the simulated lithology of each sequence, by matching it with interpreted depositional facies, hence the choice of sediment classes (figure 13). The lithological descriptions of each IODP 359 well, were interpreted into five depositional facies (Betzler *et al.*, 2018): (1) shallow-water, (2) slope and basin, (3) pelagics, (4) drift fans and (5) sheeted drifts and submarine dunes (appendix B). As the latter two, only occur outside of the study interval, they are irrelevant to the calibration of this model. Based on the remaining three facies, a classification scheme was developed for the stratigraphic model (table 2). The aim is to classify each grid cell into one depositional facies, according to its simulated properties. The boundary between shallow- and deep-water environments was placed at 40 m of water depth at the time of deposition. To gain a deeper insight in the model dynamics and its capacity to simulated conceptual ideas, the shallow-water depositional facies was differentiated into shallow-water reef and –lagoon based on the simulated wave energy and fraction of euphotic bioconstructions. Deep-water facies consists of pelagics and slope and basin and are discriminated by their mud content.

Model parameters	Pelagics	Slope and basin	Shallow-water	
			Reef	Lagoon
Bathymetry (m)	40 - max	40 - max	min – 40	min – 40
Carbonate mud (%)	50 - max	min – 50	-	-
Euphotic (%)	-	-	-	min – 50
Wave energy (kW/m)	-	-	-	min – 50
Classification priority	1	4	3	2

Table 2: Depositional facies definition in function of simulated model properties for model calibration

.

Chapter 5: Model Results

5.1 Reference model

By calibrating the stratigraphic model with the seismic profiles and tying it to the well data, a best-case scenario for the western margin of the Maldives carbonate Platform was developed. The resulting reference model consists of a 3D grid of cells, each 500 x 500 m in base surface size, and with a variable height, depending on the deposited sediment volume over a time step of 0.25 Myr. Each cell is characterized by several syndepositional properties, like bathymetry, wave energy, slope and its composing sediment class fractions. These properties will be used in this chapter to analyze and validate the reference model output.

Firstly, the simulated sequence geometries and slopes are compared with morphologies derived from the seismic interpretation. This comparison focuses in particular on the sequence stratigraphic interpretation which subdivides the platform evolution into four episodes, as proposed by Betzler *et al.* (2018) (figure 6 and 12). Each episode is associated with a distinct platform geometry: (I) The Oligocene platform partially drowns and a carbonate ramp develops on the drowned interior, (II) The steepening carbonate ramp progrades and evolves into a rimmed platform, (III) The aggrading rimmed platform develops a steep internal slope, and (IV) The bank edge progrades further inwards, enclosing the Inner Sea. To illustrate these four phases within the reference model, two cross sections through the stratigraphic grid are presented, crosscutting the wells from the IODP expedition 359 (figure 16). Cross section 1 and 2 envelop respectively, seismic lines 1 and 2 presented in Betzler *et al.* (2018) (appendix A). Furthermore, cross section 1 corresponds to seismic line NEOMA-P65 (Betzler *et al.*, 2013) and its interpretation into stratigraphic turning points: i.e. O/M, PS1, PS5, PS8 and DS1 (figure 6) (Betzler *et al.*, 2018). Each turning point forms a synchronous sequence boundary in the seismic interpretation. Based on their age, these simulated key sequence boundaries are highlighted in all cross sections (figures 17-20). Each cross section is composed of four property views, showing the fraction of each sediment class.

Secondly, the well data is compared with simulated properties in synthetic points of control. The lithologies are checked indirectly through a depositional facies definition of each cell, based on its depositional properties. The defined depositional facies terminology matches with the facies from the well data (Betzler *et al.*, 2018) to facilitate comparison of real and synthetic well logs. Lastly, the thicknesses of the simulated sequences are validated by comparing the depth of the well markers with the scaled position of the simulated sequence boundaries.

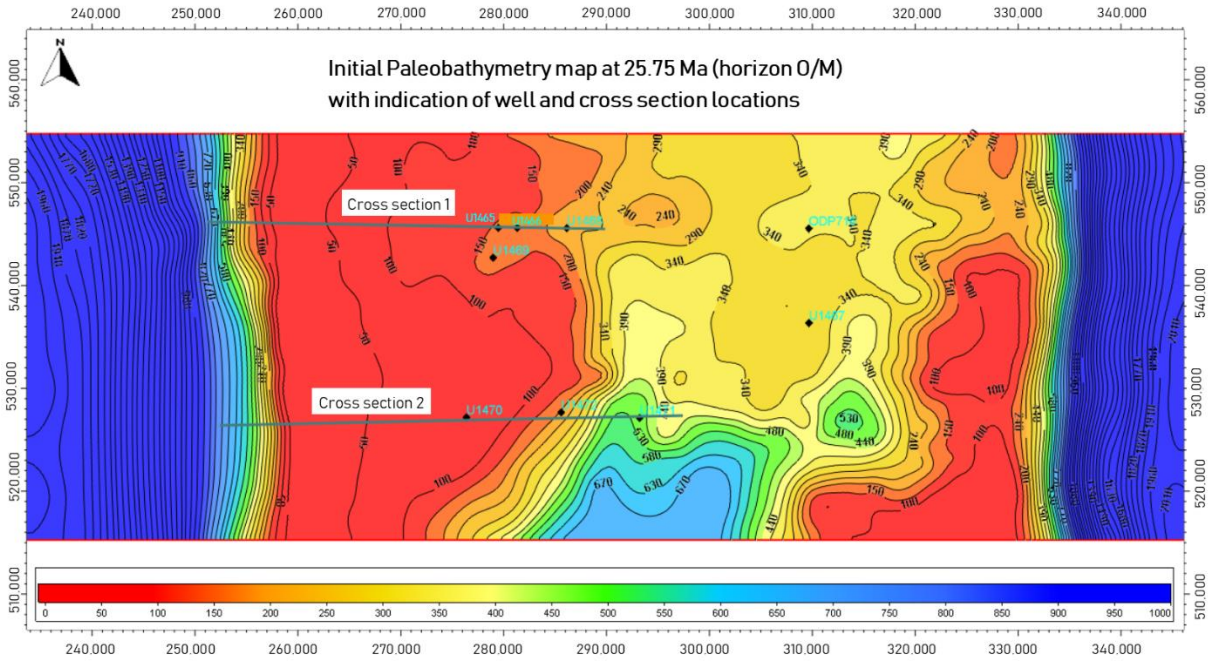

Figure 17. Map of model domain with location of cross sections and well sites, discussed in the text. Color scale and isolines represent the initial bathymetry at the onset of the simulation (25.75 Ma)

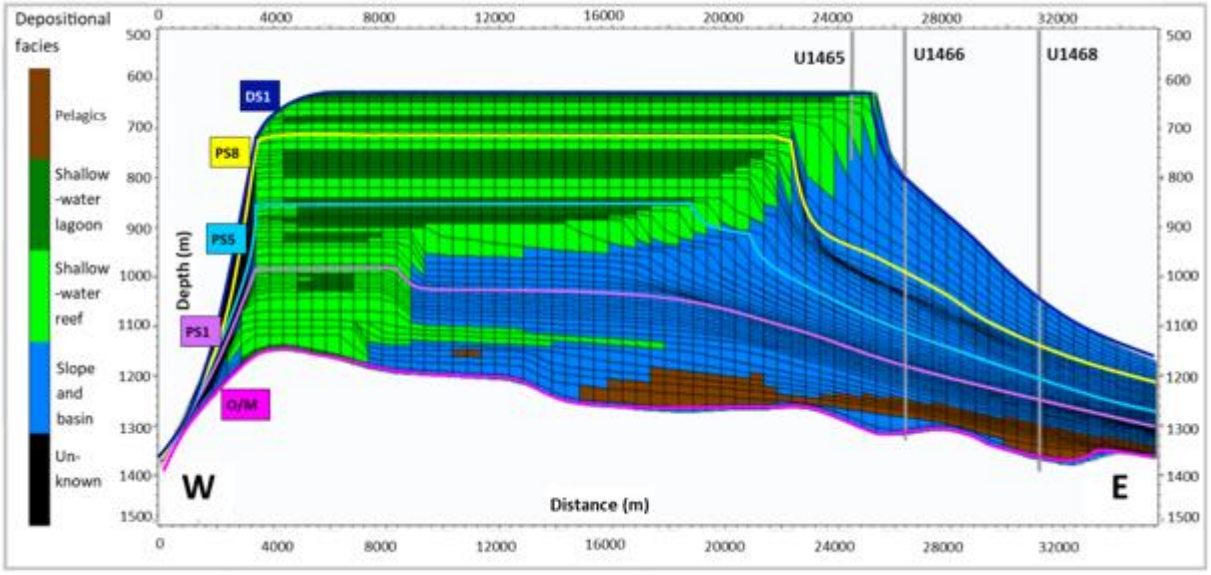

Figure 18. Cross section 1 through the stratigraphic model grid after complete simulation. Colors represent classification of grid cells into depositional facies. Stratigraphic turning points are indicated as sequence boundaries in their respective colors. Indicated wells are located along the cross section. Note that the vertical scale exaggeration is 15x.

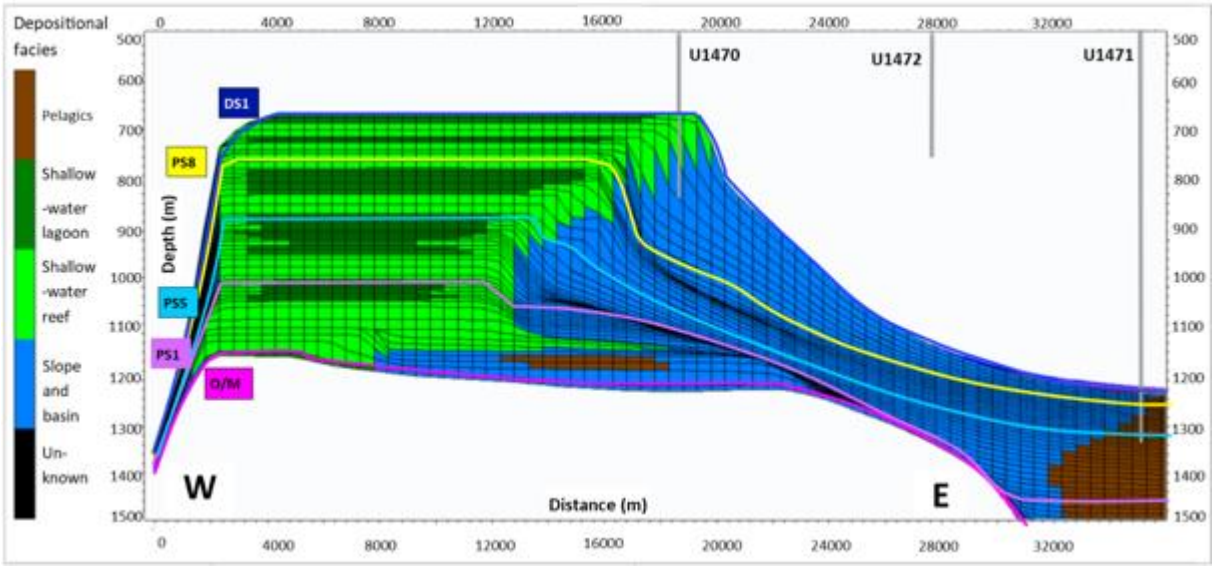

Figure 19. Cross section 2 through the stratigraphic model grid after complete simulation. Colors represent classification of grid cells into depositional facies. Stratigraphic turning points are indicated as sequence boundaries in their respective colors. Indicated wells are located along the cross section. Note that the vertical scale exaggeration is 15x.

5.1.1 Evolution of simulated stratigraphy in four phases with distinct platform geometry

I. Drowning of Oligocene platform and development of carbonate ramp depositional profile (turning point 1-2)

The model is founded upon an initial bathymetry, constructed to reflect the Oligocene drowning unconformity, which forms a marked reflector on the seismic profiles (section 4.1.1.1). Above this O/M horizon, set at age 25.75 Ma, both section 1 and 2 contain a mud-rich sequence (figures 19.c, 20.c), matching with a deepening, fining-upward trend, detected in all deep wells across the platform. The carbonate mud occurs in the interior bank edge slope, increasing in fraction towards the deeper internal basin. Next to mud these slope deposits are composed of carbonate grains, increasing in abundancy towards the platform rim (figures 19.d, 20.d). The slope angle steepens locally when encrusted by oligophotic bioconstructions (figures 19.b, 20.b). The occurrence of these oligophotic mounds is determined by the initial topography of the O/M surface, hence the different morphologies in section 1 and 2. The area behind these elevated structures is filled with flat sequences of slope sediment that transitions into a narrow reef rim, composed mainly of euphotic bioconstructions (figures 19.a, 20.a).

The first phase of the western bank evolution is characterized by the continuation of the drowning event, followed by the establishment of a new carbonate factory on top of the drowned edifice in the form of a carbonate ramp. The resampled eustasy curve, used in the model, contains two high-amplitude sea-level fluctuations that contribute to the drowning (figure 12). The combination of these fluctuations and decreased photic production values restrict the shallow reef to a narrow marginal rim, facing the open ocean. In section 1, the euphotic reef recovers and expands shortly due to a sea-level drop between 23 and 24 Ma, but subsequently drowns again due to a fast, high-amplitude sea-level rise (figure 19.a). In section 2 on the other hand, the reef maintains its width after its recovery thanks to the solidified fore-slope, encrusted by oligophotic organisms (figure 20.a-b). In both sections the following gradual eustatic sea-level lowering prevents the euphotic system from drowning completely. Under the combined effect of the eustasy fall, the continuous subsidence and the recovering production rates, the reef transitions from a backstepping to an aggradation pattern (figures 19.a,

20.a). The culmination of this slow eustatic sea-level drop into a lowstand reduces the wave energy in the narrow reef interior, preventing euphotic framework growth and replacing it with loose carbonate grains and mud. These protected low-energy areas are defined as shallow-water lagoons within the depositional facies classification (figures 17, 18).

While euphotic production survives the drowning event, the oligophotic producers partially disappear after the second sea-level rise at 24 Ma. Their absence results in a greater fraction of loose carbonate grains in the slope sediments (figures 19.d, 20.d), causing the depositional profile to flatten into a carbonate ramp. The slow sea-level lowering from 25 to 22 Ma allows the oligophotic producers to gradually restore their position as slope encrusters, but their abundance remains relatively low due to their reduced production rates. Finally, the depositional profile at turning point 2 (22 Ma) consists of a narrow reef rim connected to a low angle carbonate ramp. Comparing both sections, the relative sizes of the reef rim and the ramp appear to be controlled by the abundance of the oligophotic buildups in the early parts of phase I.

II. Evolution from carbonate ramp to rimmed shelf geometry with first aggradation and progradation phase (turning point 2-3)

The second phase exhibits a change in platform morphology of the internal western bank from a carbonate ramp to a reef rimmed platform. Firstly, the euphotic reef, reduced to a marginal rim during phase I keeps aggrading until 20 Ma. At this point the bank at section 1 suddenly progrades strongly (figure 19.a). Along with the marginal euphotic crests, the low-energy lagoon extends (figure 17), composed of carbonate grains and mud. The reason for this sudden euphotic reef expansion lies with the revival of the oligophotic producers. Since their demise in phase I, these encrusters increase in abundancy throughout phase II, replacing carbonate grain and mud fractions within the internal slope (figure 19.b). Because the oligophotic sediment class possesses a lower diffusivity than the carbonate grains and mud, this replacement causes the simulated depositional profile to steepen over time. Moreover, the sediments lying behind the rigid oligophotic rim are sheltered from incoming waves. They remain in place and form a solid base over which the euphotic reef rim is able to prograde. Once the encrusted base has accumulated enough sediment to reach the euphotic production depth, a strong and abrupt progradation phase is triggered around 20 Ma. In only 0.5 Myrs (two model steps) the western bank expands almost 5 km eastwards. After this explosive expansion, the progradation continues more gradually, due to the stepwise interaction between prograding slope and reef sequences. Similar as for the oligophotic bioconstructions, the low-diffusive euphotic components, are not transported down-slope and prevent carbonate grains and mud in the back-reef from being redistributed (figure 19.c-d).

Opposed to section 1, the western bank barely progrades at section 2 during this second phase. The abundant encrusters are not able to provide a base for reef progradation. Instead they steepen the short slope, increasing down-slope sediment transport to the deeper basin (figure 20.b). The deep seaway in front of the slope functions as a large sink for all exported sediment. Without a flattened progradation base, the shallow-water reefs keep aggrading and form extensive internal lagoons (figure 18). Similar as for section 1, the bank develops a clearly defined edge transitioning into an angular slope. As such, the depositional profile in contact with the Inner Sea evolves into a reef rimmed platform with a steep slope and a flat back-reef area.

III. Second aggradation phase with development of steep platform slopes (turning point 3-4)

In the last two phases (III and IV) the evolutionary trends between section 1 and 2 remain similar. At the third turning point, horizon PS5 (18.5 Ma), accommodation space is increased under a eustatic sea-level rise and the rimmed platform is flooded with high energy waves. This results in an interruption of the low-energy, lagoon deposits and high-energy, shallow-reef deposits populating the entire bank surface (figures 17,18). Under these elevated sea levels, the internal slope reaches its maximum angle, inhibiting further progradation. Most of the carbonate grains are transported downslope, removing the progradation base for oligophotic and euphotic bioconstructions. In the restricted remaining zone for reef building, both producers compete to keep up with rising sea level. The euphotic producers gain the upper hand, thanks to their relatively higher production rates (figure 15) and shallower optimal production depth (figure 14). Due to the sea-level rise and the competition with the euphotic producers, the oligophotic encrusters are driven to below their optimal growth depth and gradually drown (figures 19.b, 20.b). As the marginal euphotic reef crests further keep up with the sea-level rise, the platform interior turns into extensive low-energy lagoons, composed of carbonate grains and mud (figures 19.c-d, 20.c-d). In all, the high eustatic sea levels from 18 to 15.1 Ma, shaped the western rim into a more symmetrical and continuous bank, bounded by steep edges facing both the open ocean and the Inner Sea. Furthermore, it placed the platform in a precarious position, where it was no longer able to accumulate interior fore-slope sediments and put the oligophotic producers on the brink of drowning.

IV. Second progradation phase (turning point 4-5)

The fourth phase is characterized again by progradation, although less substantial and abrupt than in the phase II. The onset of phase IV is marked by a eustatic sea-level drop (figure 12), placing the fourth turning point (PS8) around 15.1 Ma. Due to the model time step of 0.25 Ma, the age of this turning point and its associated sequence boundary was rounded to 15 Ma. The lowered sea level and increased carbonate production rates of oligophotic bioconstructions and carbonate grains allow for the deposition of clinoform sequences. These sequences reflect the prograding character of this phase and maintain a similar slope gradient. While the platform exterior progrades under relatively low sea levels compared to the third phase, minor sea-level fluctuations are reflected in the platform interior. Alternating beds of euphotic bioconstructions indicate minor sea-level highstands (figure 19.a, 20.a), while beds with carbonate grains and mud indicate lowstands (figures 19.c-d, 20.c-d). The simulation ends abruptly at 13 Ma, sequence boundary DS1, where platform growth is inhibited by the onset of sediment drift deposition.

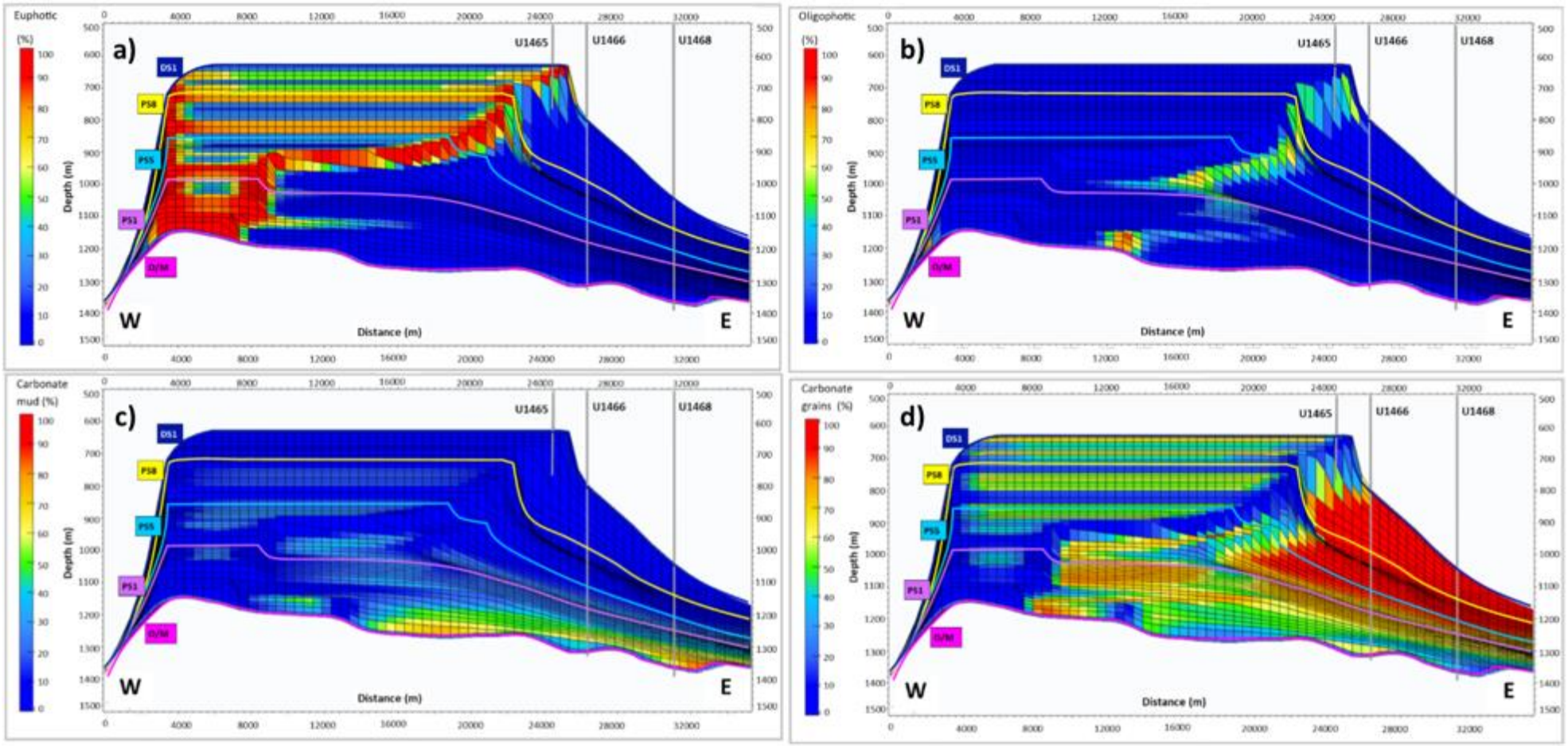

Figure 19. Cross section 1 through the stratigraphic grid of the reference model after complete simulation. Color scale represents a different grid property in every subsection, respectively the fraction of (a) euphotic bioconstructions, (b) oligophotic bioconstructions, (c) carbonate mud and (d) carbonate grains. Stratigraphic turning points are indicated as sequence boundaries in their respective colors. Indicated wells are located along the cross section. Note that the vertical scale exaggeration is 15x.

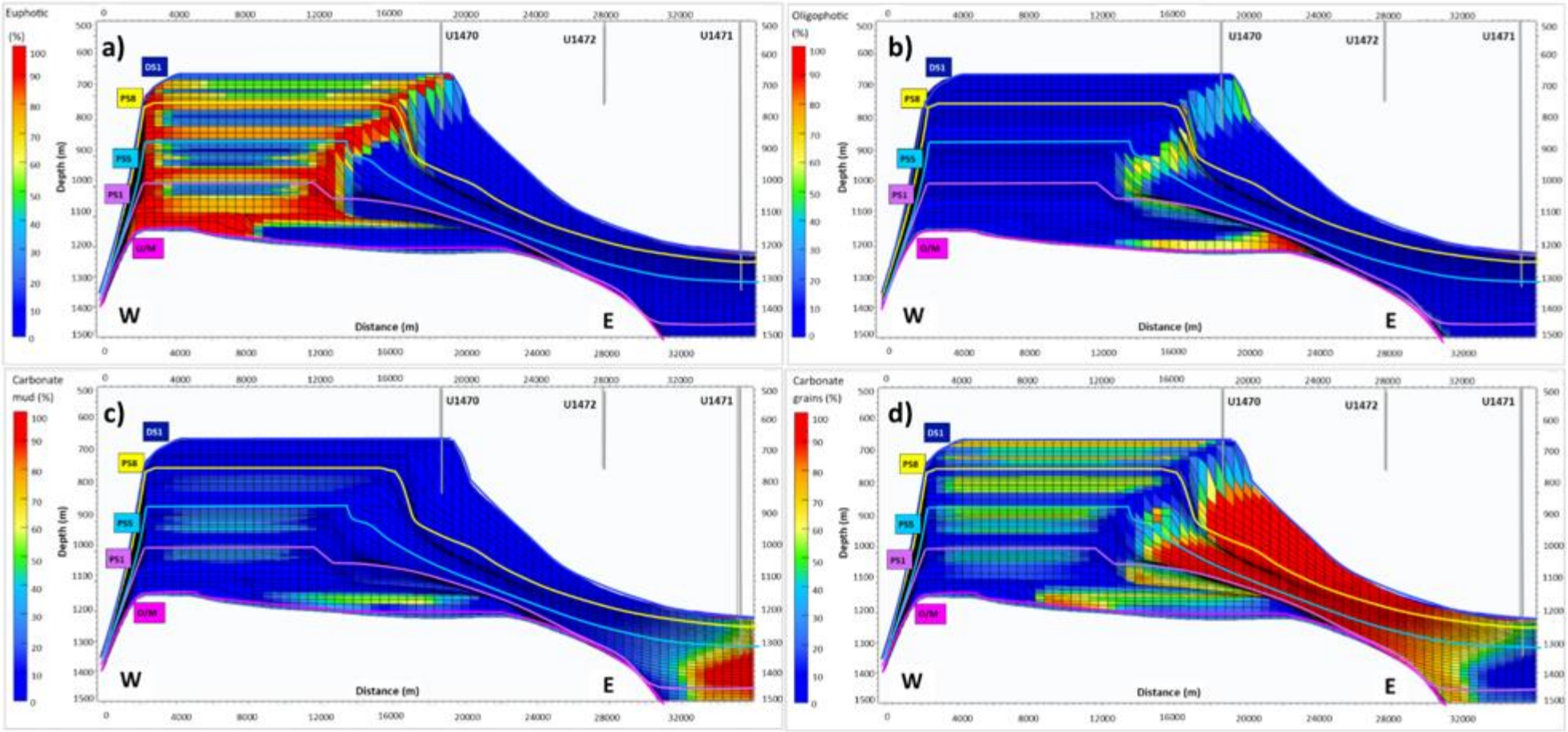

Figure 20. Cross section 2 through the stratigraphic grid of the reference model after complete simulation. Color scale represents a different grid property in every subsection, respectively the fraction of (a) euphotic bioconstructions, (b) oligophotic bioconstructions, (c) carbonate mud and (d) carbonate grains. Stratigraphic turning points are indicated as sequence boundaries in their respective colors. Indicated wells are located along the cross section. Note that the vertical scale exaggeration is 15x.

5.1.2 Depositional facies validation

Seismic profiles only provide exact subsurface stratigraphy, when converted from the time to the depth domain. As this was not the case for the seismic lines in the study area, the only available ground-truth data are wells. The data of eight wells from the IODP expedition 359 are published in its proceedings (Betzler *et al.*, 2017). Based on the cores, five depositional facies were defined by Betzler *et al.* (2018): (1) shallow-water, (2) slope and basin, (3) pelagics, (4) drift fans and (5) sheeted drifts and submarine dunes (appendix B). These facies will be used to calibrate and indirectly check the simulated lithological properties of the reference model. Well U1465, U1466 and U1468 are crossed by section 1 (figure 17, 19) or seismic line 1 (appendix A)(Betzler *et al.*, 2018), and wells U1470, U1471 and U1472 by section 2 (figure 18, 20) or seismic line 2 (appendix A)(Betzler *et al.*, 2018).

The comparison of the well facies logs and the simulated facies logs of the reference model for these six wells is presented in figure 21 and 22. Focusing on the carbonate platform growth, the study interval ends at 13 Ma without modelling the onset of drift deposition. However, to provide a clear sedimentary boundary within the log comparison, artificial drift sediment was added to the simulated logs on top of sequence boundary DS1. In other words, the depositional facies “Drift fans” and “Sheeted drifts and submarine dunes”, used in the real facies logs, equal the “Drift”-facies in the synthetic wells.

The wells in section 1 provide an excellent calibration dataset as they are adequately distributed over the bank, covering the reef edge, proximal and distal slope. The deep penetration of wells U1466 and U1468 offer insight in the thickness and lithology of the different slope sequences up to the initial bathymetric surface. This includes the thickness of the pelagic sequence at the base of the wells, associated with the Oligocene drowning. Well 1465, penetrating the shallow reef, illustrates how far the internal margin must have prograded from its original position. The match between the real and the simulated logs from the reference model is particularly good. A minor deviation occurs in well U1465 where the bottom of the synthetic log is classified as “slope and basin” instead of “shallow water”. Other small deviations (< 50 m) occur in the thickness of the “slope and basin” deposits in wells U1466 and U1468.

The three wells crossed by section 2 contain less extensive data that can be used for reference model validation. Well U1470 provides again a reference point for the extent of the prograded western bank. The upper boundary between the real and simulated “shallow water” package do not match. This can be explained by the abrupt ending of the simulated platform growth and its artificial replacement by “Drift”-facies. In reality, the platform drowned gradually and diachronously after 13 Ma. The “shallow water” facies in the well facies log at site U1470 is thereby also present above sequence boundary DS1. At first sight, well U1472 seems to be of no use to this study as it does not contain any carbonate platform facies. The absence of “shallow water” facies, proves however that the bank progradation did not reach this point. Thus, the absence of simulated platform facies can be interpreted as a match. Lastly, well U1471 contains a large section through the drift deposits, abruptly shifting to “shallow water” facies. Although the lower boundary of drift deposits concurs in both the simulated and real well data, the underlying facies does not match. In contrast to the U1471 well data, the lowest part of the synthetic well contains pelagic sediments, deposited in a deeper seaway. The origin of this seaway at this point is associated with the initial surface topography, based on deep seismic data from Belopolsky and Droxler (2004a). The presence of “shallow water” facies in this deep seaways cannot be explained by the dynamics of this stratigraphic model, even with different production scenarios. A solution for this issue might be found by converting the seismic sections to the depth domain, possibly revealing erroneous estimations for the initial bathymetry.

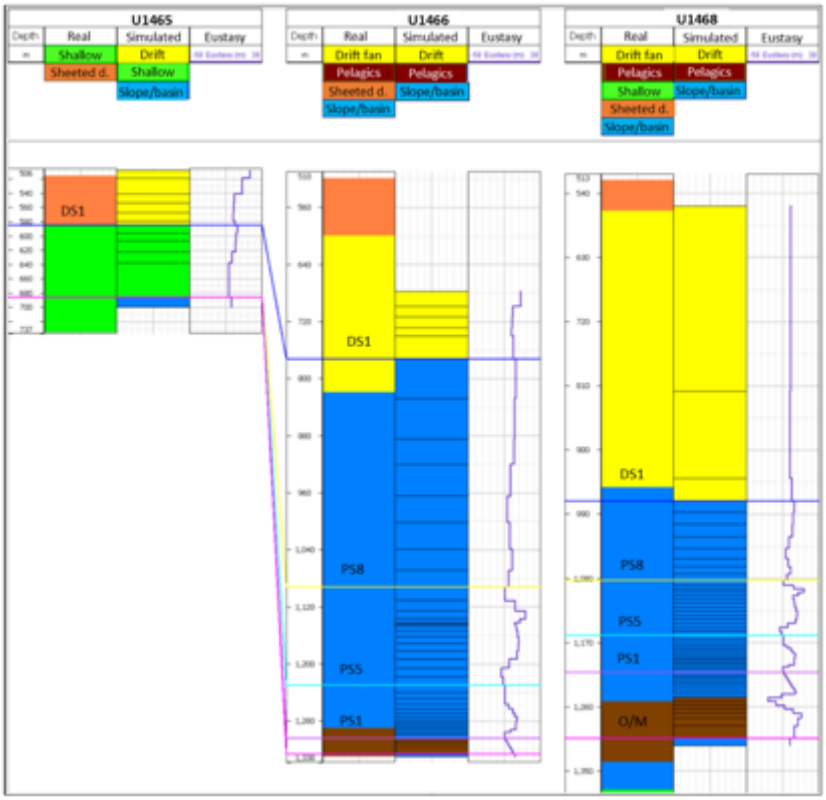

Figure 22. Comparison of depositional facies in real and simulated wells along cross section 1 through the reference model. The positions of the simulated stratigraphic turning points are indicated along the wells.

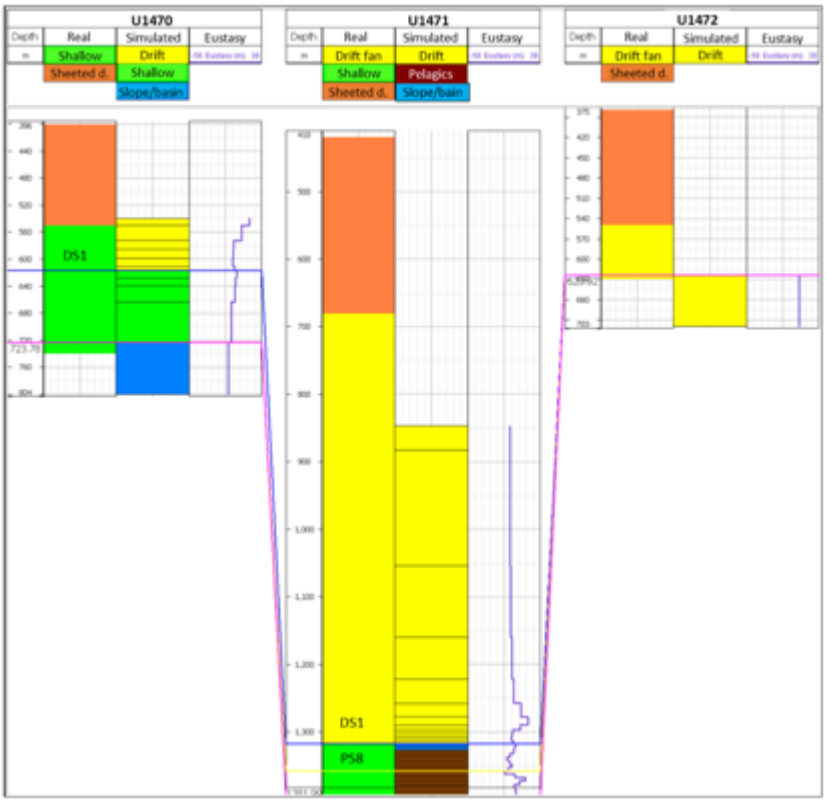

Figure 23. Comparison of depositional facies in real and simulated wells along cross section 2 through the reference model. The positions of the simulated stratigraphic turning points are indicated along the wells.

5.1.3 Sequence thickness validation

To validate the thickness and geometry of each simulated stratigraphic sequence, sequence boundaries described in the well logs (Betzler *et al.*, 2017) are compared to the depth of simulated ones in synthetic logs. Figure 23 displays a segment of cross section 1 containing wells U1465, U1466 and U1468 and visualizes the calibration quality. On each well path, the depth markers of several platform and drift sequence boundaries are positioned to scale. Based on the average age determination of each depth marker (Betzler *et al.*, 2018), simulated sequence boundaries are selected by their approximate depositional age. Each of these sequence boundaries is represented in a different color, matching those of the original seismic interpretation (appendix A). Sequence boundary PS11 is not visualized in the section as its average age coincides with the age of PS10. The wells along cross section 2 are not discussed, as they do not provide many sequence boundaries for calibration.

Well 1465 provides only two relevant markers for this study interval, namely DS1 and PS11. Their equivalent simulated sequence boundaries are respectively 30 m below and 25 m above their marker depth. This suggests that the upper sequences are not thick enough. Unfortunately, this trend appears also in the upper sequences of wells U1466 and U1468, where simulated horizons PS7 to DS1 consistently lie below their respective markers. This accumulating effect is particularly visible in well 1468 where the cumulative offset for DS1 amounts to almost 100 m. Conversely, horizons PS1, PS5, PS6 in well 1466 and O/M, PS2 and PS5 in well 1468 are located above their ground-truth position, suggesting that simulated sequences are too thick in the lower part of the stratigraphic model. Overall, however, the individual difference between the depth of each marker and its simulated sequence boundary is never more than 50 m. Therefore, this reference model and its input parameters provide a solid best-case scenario for further modelling experiments, such as the testing of different hypotheses and assessment of the impact of individual input parameters.

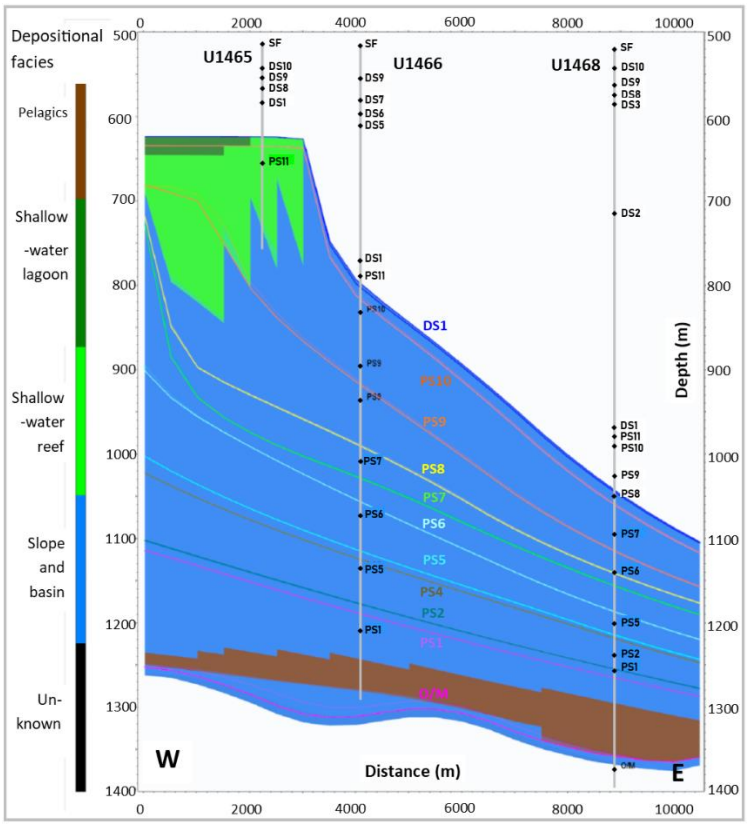

Figure 24. Segment of cross section 1 across the reference model, comprising the wells along the transect. Well markers of sequence boundaries are positioned to scale on the well path. Equivalent simulated sequence boundaries are represented in colors matching the seismic interpretation (appendix A). Background colors represent the depositional facies classification.

5.4 Alternative scenarios

Several alternative scenarios were tested in this study by varying one of the major uncertainties in the input parameter set, namely the carbonate production rates of each sediment class. Two of these scenarios are of particular interest to the evolution of the Maldives, as they highlight two debated biotic changes: (1) a simulation without a dip in photo-dependent carbonate production, and (2) a simulation with a constant oligophotic/euphotic carbonate production ratio. The respective model results are presented in the following sections, but could not provide a match with the given calibration data. The link between each of these scenarios and the proposed hypotheses are clarified in the discussion chapter.

To allow a visual comparison between the different model outputs, a new facies classification of the reference model is presented in figure 24. This classification was merely developed to visualize the distribution of the different facies classes in a single property view, instead of four. Each cell is classified as specific sediment class facies when it contains more than 50 % of this particular sediment. The remaining cells are classified as mixed facies (table 3).

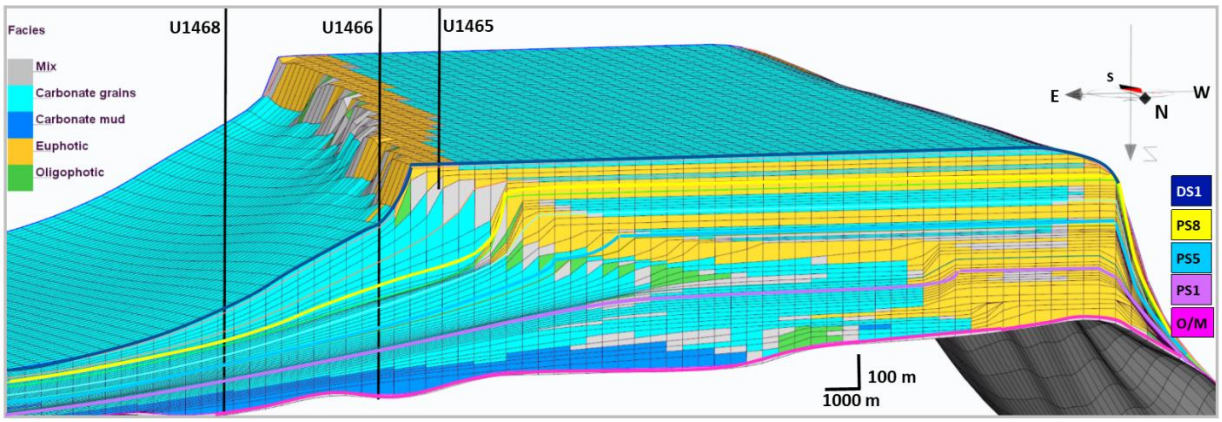

Figure 25. Oblique view on reference model result. The 3D stratigraphic grid is cut off along cross section 1 for comparison. The colors represent a facies classification, based on the dominant sediment fraction (table 3). The location of wells and stratigraphic turning points are indicated along the cross section. Note that the vertical scale exaggeration is 10x.

Model parameters	Oligophotic	Euphotic	Carbonate mud	Carbonate grains	Mix
Oligophotic (%)	50 - max	-	-	-	-
Euphotic (%)	-	50 - max	-	-	-
Carbonate mud (%)	-	-	50 - max	-	-
Carbonate grains (%)	-	-	-	50 - max	-
Classification priority	1	2	3	4	5

Table 3: Facies classification for visualization purposes. Each facies class represents a dominant sediment class fraction. The remaining cells are classified as mixed facies, due to the classification priority.

5.4.1 Simulation without dip in photo-dependent carbonate production

To evaluate the impact of a reduction in photo-dependent carbonate production during phase I (figure 15), a model without this particular dip was executed. Instead, carbonate production rates were kept constant throughout the expected drowning phase of the platform (figure 25). The resulting 3D model (figure 26) differs fundamentally in internal and external morphology from the reference model (figure 24).

During phase I, the euphotic bioconstructions are able to keep up with the sea-level rises and produce aggrading instead of retrograding sequence geometries. Additionally, the euphotic reef is able to expand strongly during the punctuating sea-level fall around 24 Ma. This 10-15 km wide rim maintains its dimensions until the end of phase I. The internal platform slope at this first turning point (PS1) is relatively small compared to the broad flat-topped reef, and composed of carbonate grains and oligophotic bioconstructions. In contrast to the reference model, the oligophotic producers survived throughout phase I. Their abundance severely steepens the short slope, leading to the development of a well-defined internal bank edge at PS1 rather than the expected ramp depositional profile from the reference model.

The steep internal bank at 22 Ma sheds most of the accumulated carbonate grains and mud downslope, limiting the platform progradation during phase II. The inability to accumulate sediment in the fore-slope will dominate the remainder of the simulation until 13 Ma, resulting in thin slope sequences and limited progradation of the reef. At 13 Ma, the total width of the western bank at section 1 only amounts to 18 km instead of the 20 km, prescribed by the calibration data.

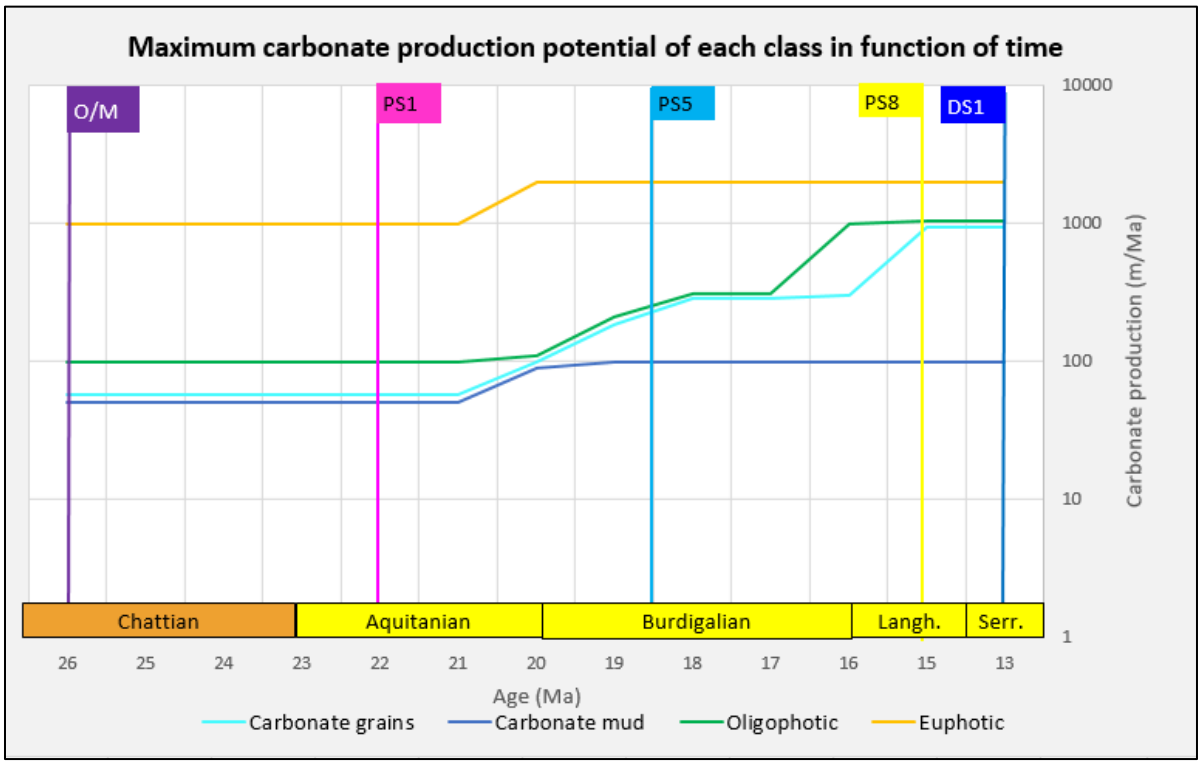

Figure 26. Carbonate production rates for simulation without dip in photo-dependent production during phase I.

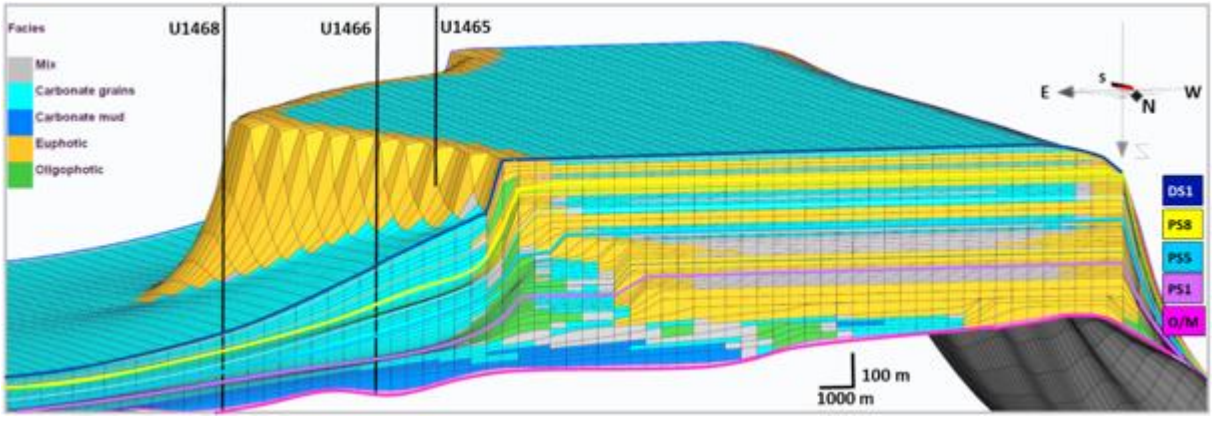

Figure 27. Oblique view on stratigraphic model without a dip in photo-dependent production during phase I (figure 26). The 3D stratigraphic grid is cut off along cross section 1 for comparison. The colors represent a facies classification, based on the dominant sediment fraction (table 3). The location of wells and stratigraphic turning points are indicated along the cross section. Note that the vertical scale exaggeration is 10x.

5.4.2 Simulation with constant ratio between oligophotic and euphotic production

The second carbonate production scenario assumes a constant relationship between oligophotic and euphotic production rates (figure 27). While the production curve for the euphotic production is taken from the reference model, the oligophotic production values are an order of magnitude lower over the entire simulated time interval. In order not to overestimate the contribution of carbonate grains in the slope, their maximum production rate was limited to the oligophotic curve since the Burdigalian.

The resulting stratigraphic model (figure 28) is similar to the reference model up to sequence boundary PS5, as the production curves up to the corresponding point in time are identical. Subsequently, the slope platform aggrades vertically in phase III, developing a steep slope. The same aggrading trend occurs synchronously in the reference model, although slightly inclined and tending a little more toward progradation. As such the platform slope at 15 Ma (PS8) is more gentle in the reference model than in the simulation with a constant euphotic/oligophotic ratio. The effect of the constant production ratio is clearly exposed in phase IV, where the platform progradation is completely halted. Due to the steep angle of the slope the loose carbonate sediment are no longer accumulated and the oligophotic producers no longer have a substrate within their growth depth range to encrust. The shallow euphotic bioconstructions can only aggrade when new accommodation is created by relative sea-level changes. The missing progradation during phase IV, prevents the western bank margin from reaching well U1465 and does not provide a match with its depositional facies log.

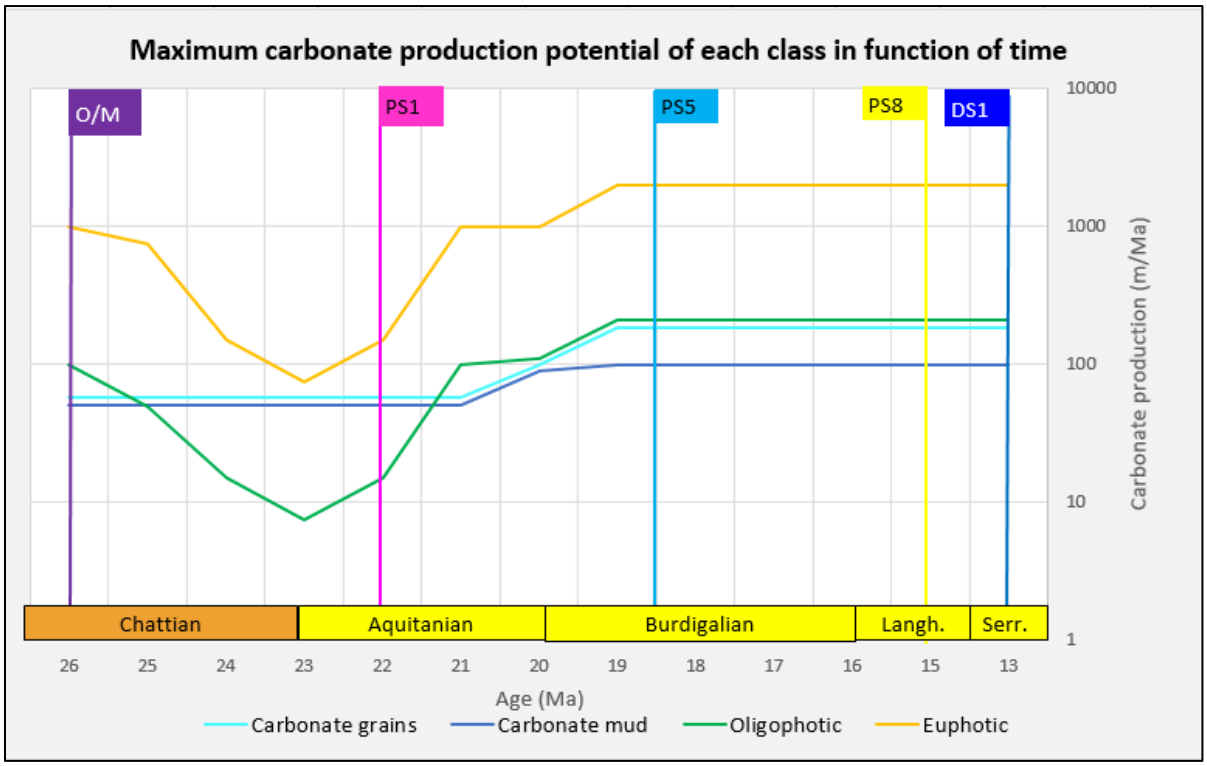

Figure 28.Carbonate production rates for stratigraphic model with a continuous ratio between euphotic and oligophotic carbonate production rates over the entire simulation.

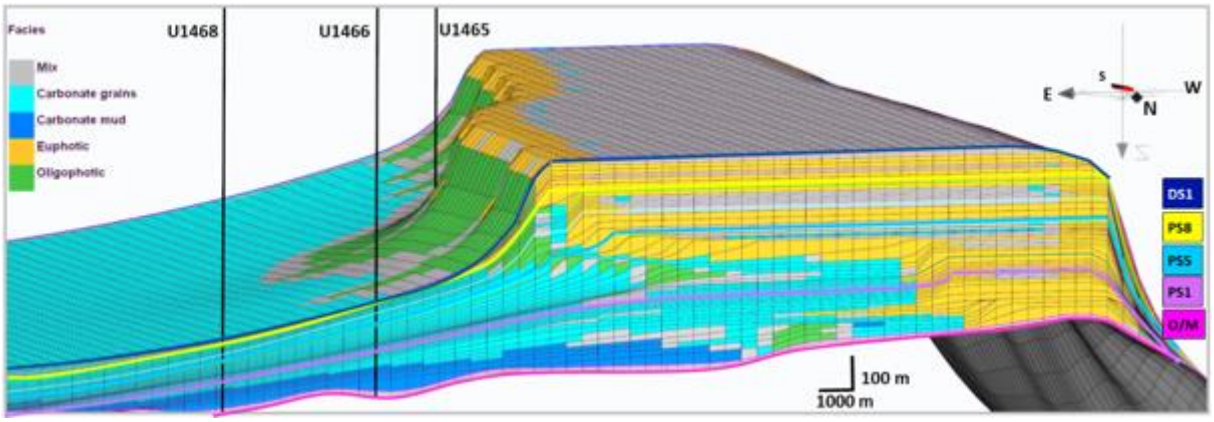

Figure 29. Oblique view on stratigraphic model with a continuous ratio between euphotic and oligophotic carbonate production rates (figure 28). The 3D stratigraphic grid is cut off along cross section 1 for comparison. The colors represent a facies classification, based on the dominant sediment fraction (table 3). The location of wells and stratigraphic turning points are indicated along the cross section. Note that the vertical scale exaggeration is 10x.

Chapter 6: Discussion

The impact of individual controlling parameters on the stratigraphy of a sedimentary body is difficult to assess, as all these factors interact in a complex web (figure 3). Stratigraphic forward modelling allows to simulate different depositional processes, involved in the formation of the sediment body. The impact of each process, can be assessed by varying a single parameter and comparing the new model output to a reference model, representative of the sedimentary body architecture. This study will use the above described reference model to test the impact of several uncertain input parameters.

6.1 Testing carbonate production rates in function of conceptual scenarios

Production rates of carbonate factories in the geological past remain ill-quantified for stratigraphic model applications. Many studies thereby use either growth rates from modern analogue settings (Bosence *et al.*, 1994; Warrlich *et al.*, 2008) or derive accumulation rates from the geological record. Though accumulation rates only provide a lower limit to the production rate (section 1.1), variations can be calculated through time from age-depth plots, by assuming constant values between measuring points (Bosscher and Schlager, 1993; Camoin and Webster, 2015). Alternatively, accumulation rates from similar settings and ages are used in SFM, and kept constant over time (Al-Salmi *et al.*, 2019). Another approach is to acknowledge and assess the uncertainties on the production rate values and calibrate the model with several plausible scenarios (Kolodka *et al.*, 2016). The latter approach is followed in this study, while other input parameters are quantified by available data or assumptions. To link the production-rate uncertainties to existing theoretical hypotheses, two debates on the carbonate production rates are tested: (1) the cause for the drowning of the Oligocene Maldives platform and (2) the interaction and competition between euphotic and oligophotic carbonate-producing organisms throughout the Miocene.

6.1.1 The partial drowning of the Oligocene carbonate platform

The carbonate platform of the Maldives can be subdivided in three stages of carbonate platform growth, namely during the Paleogene, Neogene and Quaternary (section 2.3.2). The three stage are divided by two drowning events lasting respectively from the latest Oligocene to the earliest Miocene (~ 25.7 to 22 Ma), and from the latest Middle Miocene to the latest Pliocene (~ 13 to 3.8 Ma). The cause for the extensive second drowning episode has been proven to be the abrupt onset and continuation of the South Asia Monsoon (SAM) system, inducing strong currents that inhibit further platform growth (Betzler *et al.*, 2009, 2016, 2018). Though, the cause for the first drowning event remains a matter of debate.

Belopolsky and Droxler (2004a) interpreted the O/M drowning unconformity in function of the depositional geometries, derived from the seismic interpretation. The restriction of the backstepping reefs to a narrow 5 km wide rim at the platform margins, and the drowned patch reefs in the platform interior describe a platform type referred to as “empty bucket”. Such an “empty bucket” morphology is typically conceived due to different biotic growth potentials of platform interior and margins (Kendall and Schlager, 1981; Schlager, 1993). Following this rationale, it is suggested that the Maldives endured a substantial relative sea-level rise, causing the platform interior to drown and the reduced margins to aggrade and keep up with sea level (Belopolsky and Droxler, 2004a). This theory is substantiated by the presence of organic-rich pelagic limestones above the O/M horizon in well ARI-1. These very fine grained sediments were interpreted to indicate an abrupt deepening facies trend.

Contradictorily, a fast- and high-amplitude sea-level rise is not supported by eustatic, nor tectonic changes. The eustatic sea-level curve by Miller *et al.* (2005) suggests a sea-level rise of merely 50 m around the Oligocene-Miocene transition. Additionally, the subsidence curve from well NMA-1 indicates no tectonically induced subsidence for the lower Miocene (figure 10) (Purdy and Bertram, 1993). Differential subsidence is implausible as all faults from seismic interpretations seem to terminate at the O/M horizon (e.g. figure 5). Furthermore, the pelagic sequence above this surface is detected in several wells across the platform and relatable to similar depths, which contradicts differential subsidence (Aubert and Droxler, 1996; Betzler *et al.*, 2013, 2018).

Therefore, Betzler *et al.* (2018) argue that a total relative sea-level rise of 50 m seems insufficient to drown the carbonate producers across the entire platform interior and induce pelagic sedimentation instead. These authors proposed an alternative cause, relating both events to an influx of nutrients and associated enhanced primary productivity. These processes can occur as equatorial upwelling, induced over topographic highs on the seafloor by ocean currents. Nutrient upwelling could be responsible for enhanced organic matter production, explaining the presence of organic-rich, sapropel-like layers found above the O/M horizon in wells U1466 and U1468 (Betzler *et al.*, 2018). Additionally, enhanced nutrification and primary productivity are known to increase turbidity, reducing carbonate production potential of light-dependent organisms (Hallock and Schlager, 1986). This phenomenon also explains the presence of organic-rich deposits on top of a drowned platform interior. Most recently, a third mechanism was proposed for the origin of these sapropel layers, namely the occurrence of cyclic anoxic conditions in the Inner Sea (Swart *et al.*, 2019). Eustatic sea-level fluctuations could temporarily restrict the exchange with the Indian Ocean leading to periodical stable water mass stratification and sapropel formation.

To investigate the interacting mechanisms behind the drowning of the platform, several depositional scenarios were tested in a stratigraphic model and calibrated with its sequence- and lithostratigraphy. All simulated scenarios were nevertheless constrained by certain input parameters and a few assumptions in the model design (chapter 4). As carbonate production rates were ill-constrained over time, multiple curves for each sediment class were tested by 'trial-and-error'.

The input parameter set of the final reference model indicates a dip in carbonate production, between 24 and 22 Ma, similar to the hypothesis proposed by Betzler *et al.* (2018). Inducing platform drowning during phase I (turning points 1-2) was namely impossible without reducing the carbonate production rates. Compensation of the low eustatic sea-level rise with increased subsidence is not validated by the subsidence data. Alternatively, using continuous low production values would drown the bank permanently, while inducing constant high production values results in no drowning geometries at all. The latter scenario is illustrated in section 5.4.1. The essential carbonate production drop affects only photo-dependent organisms, which fits the effect of a nutrient influx, described by Hallock and Schlager (1986).

The executed modelling experiment substantiates the hypothesis that the Oligocene platform was not only drowned by relative sea-level changes. The input parameters of the reference model suggest that the carbonate production was hampered during the drowning interval by an internal or external stress. A nutrient influx or cyclic anoxic events are valid propositions for such an environmental stress. A more detailed and comprehensive simulation would be required to shed light on the cause of the dip in carbonate production. The experiment nevertheless exhibits how continuous production rates should be used with precaution in stratigraphic model designs. Production rates over longer time scales can fluctuate significantly under environmental changes affecting different components of the carbonate factory.

6.1.2 The evolving relationship between oligophotic coralline red algae and euphotic scleractinian corals throughout the Miocene

The Miocene is in particular a period of biotic change under different environmental stresses. During the Oligocene, the LBF assemblages were gradually replaced by coralline red algae and scleractinian corals in shallow-, warm waters (Pomar and Hallock, 2008). These two carbonate producers would compete with one another to become the dominant reef builders throughout the Miocene. Strengthening of the thermodynamic circulation and thermal gradients impose environmental changes, affecting the biotic competition. Halfar and Mutti (2005) suggest that enhanced upwelling and increased run-off induced enhanced surface-water productivity. This augmented nutrient availability favored the growth of coralline red algae over scleractinian corals, resulting in a global abundancy peak from the Burdigalian to early Tortonian. Halfar *et al.* (2004) illustrated how modern red algae communities can thrive under a broader range of temperatures and nutrient levels than corals, hence dominating reefs under eutrophic conditions.

This study proposes a stratigraphic model design for the Lower and Middle Miocene of the Maldives, that allows to test the evolving relationship between oligophotic and euphotic assemblages. Lithological descriptions of the system, indicate that these sediment classes are respectively dominated by encrusting red algae and ahermatypic corals (section 4.1.2). By calibrating a reference model with varying carbonate production rates, the abundancy and distribution of each group can be tested in time and space.

As illustrated in the experiment above (section 6.1.1), it might be necessary to fluctuate the production rates over time, in order to obtain a calibrated and geologically realistic stratigraphic model. This deviation from modern-day production rates raises the question of whether the modern-day ratio between different sediment classes should be maintained throughout the model. With modern growth rates ranging between 1 and 30 mm/yr for corals and between 0.1 and 3 mm/yr for coralline red algae (Montaggioni, 2005), both growth rates were initially estimated to differ one order of magnitude in the geological past (figure 27). This assumption did however not provide a suitable model result, fitting with the calibration data. Figure 28 illustrates how the simulated western bank, under a constant euphotic/oligophotic production ratio of 10, matches with the reference model only until 18.5 Ma (PS5). To induce a final progradation phase, similar to the expected geometry from phase IV (figure 6), the ratio oligophotic/euphotic production needs to be gradually increased from PS5 onwards. The necessary increase can be explained by an enhancement of oligophotic producer efficiency under changing environmental conditions. Furthermore, this gradual increase from 18.5 Ma, matches the global peak in rhodalgal lithofacies abundancy, starting in the Burdigalian (Halfar and Mutti, 2005). The exact cause of the biotic change, cannot be determined with this conceptual model design, but increased nutrient availability could be a plausible scenario. A more extensive set of input parameters, incorporating various nutrient sources and associated ecological restrictions for each biotic assemblage, would be required to exclude other scenarios.

As both of the experiments illustrate, production rates, derived from modern-day settings, do not always generate realistic results when modelling processes from the geological past. Assuming continuous values over an entire simulation, neglects the impact of environmental changes on the carbonate production. When several biotic communities are simulated, the ratio between their respective production rates in time and space will reproduce their dominance in the stratigraphic model. These ratios change, according to the evolving biotic requirements under changing environmental conditions. Treating production rates as calibration variables, allows to analyze possible biotic and environmental changes during the evolution of the depositional system.

6.2 Impact of other uncertain parameters and assumptions

6.2.1 Initial bathymetry

In previous studies, the initial bathymetry has been proven to be an input parameter with a significant impact on the model output (Warrlich *et al.*, 2002; Seard *et al.*, 2013; Al-Salmi *et al.*, 2019). The topography controls the location and production rate of each sediment class, the wave-energy distribution, the transport and deposition of sediments. As such, it determines the morphology of the first sequence, which in turn determines the bathymetry for the next. Due to this chain-effect certain geometries can be inherited from the initial surface across the entire simulation (Al-Salmi *et al.*, 2019).

In this study the impact of the depositional geometry was not tested for different surfaces. Instead, a best-case scenario was constructed, based on the model response and constraints, imposed by well and seismic data (section 4.1.1.1). Yet, the effect of the initial bathymetry can be observed, by comparing different sections through the 3D stratigraphic reference model.

Cross section 1 (figure 17 and 19) and cross section 2 (figure 18 and 20) through the reference model exemplify how small topographic differences in the initial bathymetry can determine the outcome of the completed simulation. The initial bathymetry at cross section 1 contains several relief irregularities but has an average homoclinal slope. During phase I, these topographic highs are located within the optimal oligophotic production depth and determine the distribution of these bioconstructions (figure 19.b). The isolated structures, shield areas from incoming waves that are filled up with carbonate grains and sand (figure 19.c-d). The gradual drowning of the oligophotic patch reefs leaves the loose grains and mud prone to redistribution along the slope. The resulting depositional profile at 22 Ma consists of a narrow, 5 km wide rim followed by a broad slope. The bathymetry at cross section 2 on the other hand, is relatively flat until it reaches the slope break, where it transitions into a deeper seaway. The flat fore-slope allows deposition of extensive oligophotic banks holding large amount of carbonate grains and mud (figure 20.b-d). This solidified base prevents the reef from backstepping under a second sea-level pulse at 24 Ma. Consequently, the reef rim remains relatively broad until, compared to cross section 1, while the internal slope is strongly reduced. This illustrates how the slope gradient and topography of the initial model surface, have a strong impact on the internal model heterogeneity and lateral facies variability.

6.2.2 Diffusion coefficients

Alongside the production rates, also the diffusion coefficients are ill-constrained input parameters. The values used in the reference model (table 1) were determined based on multiple calibration runs while respecting a few rules of thumb (section 4.1.2.5). The lack of theoretical scenarios and hypotheses, yields a great number of possible combinations. To gain proper insight in the impact of each diffusion coefficient on the model outcome, an automated sensitivity analysis is required (Hawie *et al.*, 2015). Such a workflow generates multiple valid realizations by sampling a range of values for each parameter and quantifying the match of the model outcome with a reference model. Then, a final selection of scenarios is made based on their geological plausibility. As such, multiple reference models with diffent diffusion coefficient combinations can be developed for a single calibration dataset. Furthermore, the impact of each coefficient can be quantified by a sensitivity analysis of the different model outcomes. Such an extensive study of the model output falls outside of the scope of this project, but sounds promising for future research.

6.3 Advantages and limitations of the model design

The proposed model design is founded on several concepts in carbonate sedimentology and stratigraphy, developed by Luis Pomar on outcrops from the Miocene around the Mediterranean Sea (Pomar, 2001b, 2001a; Pomar and Hallock, 2008; Pomar and Kendall, 2008; Pomar *et al.*, 2012; Pomar and Haq, 2016). Many of these concepts are valid for contemporaneous carbonate depositional systems across the globe. The proposed model design could therefore function as a reference setup for future modelling efforts on Miocene carbonate platforms.

6.3.1 Interacting sediment classes

The proposed set of sediment classes differentiates based on (1) diffusivity and (2) carbonate production. The differentiation based on diffusivity, allows the model to produce textural gradients and lithological variations that resemble real physical processes. Similar to reality, unconsolidated sediments are brought into suspension by wave energy and transported downslope by water flow and gravitational processes. Framework-building and encrusting biota produce more rigid structures, able to defy the expected hydrodynamic thresholds, associated with clastic systems. Characterized by their diffusion coefficients, the model design simulates the transport behavior of each class. When these transport characteristics are properly calibrated, each sediment class fulfills an essential role in the total evolution of the carbonate platform.

Carbonate grains and mud are exported away from the rigid bioconstructions and redeposited deep in the basin. Due to their diffusivity difference, carbonate grains make up an angular platform slope, while carbonate mud gradually fills the deeper internal basin as pelagic deposits. During this process, the deep internal seaways, originating from the *en échelon* grabens, are gradually filled. The rigid bioconstructions create protected low-energy zones that prevent the export of loose sediments. These sediment accumulations will occur in the fore-reef as solidified slope parts, and in the back-reef as flat-topped lagoon deposits. Thus, the depositional profile is altered from the shelf equilibrium profile, which determines the surface topography for the next simulated sequence.

The distribution of the bioconstructions is determined by the carbonate production laws, defined in time and depth, and restricted by wave-energy. By differentiating between euphotic and oligophotic production, two major reef components of the Miocene can be reproduced, namely ahermatypic corals and coralline red algae. The interaction between these two classes characterizes the progradation mechanism of the western carbonate bank. As the oligophotic organisms encrust the carbonate grains of the slope, it allows the accumulation of fore-slope sediment. When the thickness of this solidified fore-slope reaches the optimal production depth of euphotic producers, the euphotic reef rim is able to expand. This stepwise progradation mechanism is similar to the interaction between chlorozoan and rhodalgal factories, reconstructed from outcrop data of the Upper-Miocene Llucmajor Platform (Pomar and Ward, 1994, 1999) and the upper Tortonian to lower Messinian Reef Complex of Menorca (Pomar *et al.*, 2012). It also shows how both groups collaborate on the reef expansion. The wave-energy restrictions create a clear vertical differentiation between oligophotic and euphotic bioconstructions. In addition, the restriction of euphotic frameworks to high-energy zones also creates a horizontal differentiation between reef crest and back-reef. The low-energy back-reef area is infilled by *in situ* produced carbonate grains and mud. Followed by a facies classification (table 2), this setup illustrates how lagoon environments can be simulated, without the need for a separate lagoon-restricted sediment class (figure 17 and 18). As fewer classes involve fewer model uncertainties, this greatly facilitates the calibration procedure while creating a whole-system model with depositional environments from source to sink.

6.3.2 Spatial and temporal scale

The complete model domain covers a well-studied E-W section of the Maldives carbonate platform of 150 x 40 km (section 4.1.1.1). This model domain envelops a complete source-to-sink model that contains all depositional environments, from the shallow lagoons to the bathyal ocean floor. In order to adequately represent the progradation movements of the western bank in several steps, a minimum spatial scale of 500 x 500 m was chosen for each cell surface. Unlike many other basin scale models (Granjeon and Joseph, 1999; Hawie *et al.*, 2015; Al-Salmi *et al.*, 2019), this study uses a very age- and basin-specific model design. The model design focuses on simulating different biotic assemblages, to provide a depositional facies distribution and gain insight in the biotic changes during platform evolution.

During the simulated time interval of 12.75 Myrs, an almost 1 km thick platform was generated, composed of multiple sequences. Each sequence varies in thickness, representing 0.25 Myrs of deposited sediments. This time step was picked to capture the essential lithological variations in the platform and sample the eustatic sea-level curve in way that results in gradual sequence stacking pattern (section 4.1.1.4). Ideally, the model time step could have been reduced to 0.125 Myrs, in order to sample the sea-level at least four times per sea-level rise/fall. However, the total amount of time steps needed to be balanced with the grid resolution, to maintain an appropriate computation speed.

A consequence of the large time step, used for each simulated sequence, is the alternation of shallow-lagoon and shallow-reef layers in the back-reef (figure 17 and 18). Due to the modelling step, the eustatic sea-level curve is only sampled twice for each sea-level rise/fall. This results in considerable fluctuations that episodically flood the entire platform. During the flood, wave energy is high across the entire platform surface, generating extensive euphotic bioconstruction layers. In reality, the sea-level would rise gradually, allowing the reef crest to keep up and maintain a low-energy back-reef environment. The resulting lagoon facies would be deposited continuous throughout the simulation and follow sea-level fluctuations by increasing and decreasing in size. A smaller simulation time step was, however, not achievable due to computational limits. This oversimplified result, however, validates the approach to consciously resample the eustatic sea-level curve before application in a stratigraphic forward model.

6.4 Perspectives on stratigraphic forward modelling

Even when the reference model provides a solid match with the calibration data, the possibility of another scenario with an equally good match exists. To tackle this issue, recent developments in industrial applications of stratigraphic forward modelling use automated multiple realizations to quantify the match between simulated and reference data (Warrlich *et al.*, 2008; Hawie *et al.*, 2015). With an experimental design several simulations can be executed by varying a single parameter over a range of values, associated with the uncertainty on the parameter value. The results of several parameters are then analyzed using Response Surface Modelling to quantify the impact of each parameter on the model output. This sensitivity analysis allows to screen for the most influential parameters. Developing such insight in the model is particularly useful when a high number of uncertain parameters are involved in the calibration of the model. This way, the most plausible and geologically realistic scenarios are easily extracted for a more detailed comparison.

A calibrated and geologically validated stratigraphic model can be used to estimate subsurface properties away from point of control. As such, it can complement geostatistical techniques in the construction of a static geological model. As illustrated by Amour *et al.* (2013) several geostatistical methods are often required to cover different reservoir heterogeneity scales. Stratigraphic forward modelling does not suffer from scale-dependent uncertainties, thanks to its internal mathematical consistency. Although, the resolution of the model (spatial and temporal) is dependent on its total size and the available computation power (section 6.3.2). So far, industrial applications have mostly focused on the prediction of depositional facies at an exploration (Al-Salmi *et al.*, 2019) and reservoir scale (Hawie *et al.*, 2015). More research should, however, be conducted on the accuracy of stratigraphic modeling for different scales.

Depositional facies distributions, predicted by stratigraphic forward models, are being introduced bit-by-bit into reservoir characterization and dynamic flow models, both in hydrocarbon exploration (Whitaker *et al.*, 2014) and geothermal applications (Willems *et al.*, 2017). Whitaker *et al*. (2014) illustrates how the predicted depositional facies can be coupled with early diagenetic processes. By coupling petrophysical parameters to different diagenetic facies, these authors conducted flow experiments for several diagenetic scenarios. The development of process-based workflows for diagenetic and depositional models are still actively researched by industry and academics (Agar and Hampson, 2014). Though, many novel model approaches still require validation on well-studied datasets or outcrops.

Chapter 7: Conclusions

A 3D stratigraphic model was developed in DionisosFlow on an extensively studied section of the Maldives carbonate platform. This study focuses on the evolution of the western bank of the platform from the late Oligocene to the Middle Miocene (25.7 – 13 Ma). During this tectonically stable period, the bank strongly prograded under eustatic fluctuations and enclosed the internal basin. The stratigraphic model tests a conceptual model proposed by Betzler *et al.* (2018) for the platform evolution. Accordingly, four distinct phases of platform growth are simulated, characterized by distinct morphological changes, and separated by stratigraphic turning points. A best-case scenario was calibrated with seismic profiles and well data, acquired across the platform. The design of the resulting reference model was founded on general principles and concepts in carbonate sedimentology that were originally developed for Miocene carbonate platforms in the Mediterranean. Even with a coarse spatial and temporal resolution, the model design was constructed to respect the biotic nature of the carbonate platform and the depositional processes involved. The selected sediment classes interact with one another, in way that captures the driving mechanisms behind the platform evolution. The proposed basin-specific design can thus be altered to fit other carbonate platform models, similar in age and composition.

The calibration of the reference model was executed primarily by varying the production rates of the different sediment classes, and quantifying other input parameters by available data or assumptions. This approach allowed to gain insight in biotic changes under changing environmental conditions within the simulated time interval. Consequently, two hypotheses linked to variations in carbonate production were substantiated. Firstly, the Oligocene platform drowned under reduced carbonate production conditions, possibly induced by an external stress. Secondly, the ratio between euphotic and oligophotic production dropped beneath present-day values during the Middle Miocene. The exact cause of both production fluctuations requires a modelling experiment, that involves more environmental conditions in the model design. The reference model calibration indicates nevertheless the importance of carbonate production fluctuations in stratigraphic forward modelling. This aspect is often neglected by using continuous values, derived from modern growth rates. As these values do not necessarily yield geologically plausible scenarios, carbonate production rates should rather be treated as uncertain calibration parameters.

Finally, the calibrated reference model forms a mathematically robust predictive tool for the carbonate platform architecture away from point of control. Its stratigraphic framework can be used to predict sequence boundary terminations and associated stratigraphic hydrocarbon traps. The regional-scale depositional facies prediction can be fitted with petrophysical properties to predict the distribution of potential reservoir rocks. Nevertheless, a more comprehensive sensitivity analysis of the model output to its uncertain input parameters should be executed with automated multiple realizations. Additional research on the quantification of the uncertainty of the model output is needed before the technique can be incorporated in a streamlined workflow for exploration purposes.

References

Agar, S. M. and Hampson, G. J. (2014) 'Fundamental controls on flow in carbonates: an introduction', *Petroleum Geoscience*, 20, pp. 3–5.

Aguirre, J., Riding, R. and Braga, J. C. (2000) 'Diversity of coralline red algae: origination and extinction patterns from the Early Cretaceous to the Pleistocene', *Paleobiology*, 26, pp. 651–667.

Al-Salmi, M., John, C. M. and Hawie, N. (2019) 'Quantitative controls on the regional geometries and heterogeneities of the Rayda to Shu'aiba formations (Northern Oman) using forward stratigraphic modelling', *Marine and Petroleum Geology*, 99, pp. 45–60.

Amour, F., Mutti, M., Christ, N., Immenhauser, A., Benson, G. S., Agar, S. M., Tomás, S. and Kabiri, L. (2013) 'Outcrop analog for an oolitic carbonate ramp reservoir : A scale-dependent geologic modeling approach based on stratigraphic hierarchy', *AAPG Bulletin*, 97(5), pp. 845–871.

Aubert, O. and Droxler, A. W. (1996) 'Seismic stratigraphy and depositional signatures of the Maldive carbonate system (Indian Ocean)', *Marine and Petroleum Geology*, 13(5), pp. 503–536.

Backman, J., Duncan, R. A. and Peterson, L. (1988) *Proceedings of the Ocean Drilling Program, Initial Reports*, *Ocean Drilling Program*. College Station, Texas.

Belopolsky, A. (2000) *Tectonic and eustatic controls on the evolution of the maldive carbonate platform*. PhD thesis, Rice University, Houston.

Belopolsky, A. and Droxler, A. (2003) 'Imaging Tertiary carbonate system---the Maldives, Indian Ocean: Insights into carbonate sequence interpretation', *The Leading Edge*, (July), pp. 646–652.

Belopolsky, A. and Droxler, A. (2004a) *Seismic Expressions and Interpretation of Carbonate Sequences: The Maldives Platform, Equatorial Indian Ocean*, *AAPG Studies in Geology*. Edited by J. C. Lorenz and E. A. Mancini. Tulsa, Oklahoma, U.S.A.: The American Association of Petroleum Geologists.

Belopolsky, A. and Droxler, A. (2004b) 'Seismic Expressions of Prograding Carbonate Bank Margins: Middle Miocene, Maldives, Indian Ocean', in Eberli, G. P., Masaferro, J. L., and Sarg, J. F. (eds) *Seismic Imaging of Carbonate Reservoirs*. AAPG Memoir 81, pp. 267–290.

Betzler, C., Hübscher, C., Lindhorst, S., Reijmer, J. J. G., Römer, M., Droxler, A. W., Fürstenau, J. and Lüdmann, T. (2009) 'Monsoon-induced partial carbonate platform drowning (Maldives, Indian Ocean)', *Geology*, 37(10), pp. 867–870.

Betzler, C., Fürstenau, J., Lüdmann, T., Hübscher, C., Lindhorst, S., Paul, A., Reijmer, J. J.G. and Droxler, A. W. (2013) 'Sea-level and ocean-current control on carbonate-platform growth, Maldives, Indian Ocean', *Basin Research*, 25, pp. 172–196.

Betzler, C., Eberli, G. P., Kroon, D., Wright, J.D., Swart, P. K., Nath, B. N., Alvarez-Zarikian, C. A., Alonso-Garciá, M., Bialik, O. M., Blättler, C. L., Guo, J. A., Haffen, S., Horozal, S., Inoue, M., Jovane, L., Lanci, L., Laya, J. C., Mee, A. L. H., Lüdmann, T., Nakakuni, M., Niino, K., Petruny, L. M., Pratiwi, S. D., Reijmer, J. J.G., Reolid, J., Slagle, A. L., Sloss, C. R., Su, X., Yao, Z. and Young, J. R. (2016) 'The abrupt onset of the modern South Asian Monsoon winds', *Scientific Reports*, 6, pp. 1–10.

Betzler, C., Eberli, G.P., Alvarez-Zarikian, C.A. and the Expedition 359 Scientists (2017) *Maldives Monsoon and Sea Level. Proceedings of the International Ocean Discovery Program, vol 359*. College Station, TX, U.S.A.: International Ocean Discovery Program.

Betzler, C., Eberli, G. P., Lüdmann, T., Reolid, J., Kroon, D., Reijmer, J. J.G., Swart, P. K., Wright, J.,

Young, J. R., Alvarez-Zarikian, C. A., Alonso-García, M., Bialik, O. M., Blättler, C. L., Guo, J. A., Haffen, S., Horozal, S., Inoue, M., Jovane, L., Lanci, L., Laya, J. C., Hui Mee, A. L., Nakakuni, M., Nath, B. N., Niino, K., Petruny, L. M., Pratiwi, S. D., Slagle, A. L., Sloss, C. R., Su, X. and Yao, Z. (2018) 'Refinement of Miocene sea level and monsoon events from the sedimentary archive of the Maldives (Indian Ocean)', *Progress in Earth and Planetary Science*, 5(5), pp. 1–18.

Betzler, C., Brachert, T. C. and Nebelsick, J. (1997) 'The warm temperate carbonate province a review of the facies, zonations, and delimitations', *Courier Forschungs-Institut Senckenberg*, 201, pp. 83–99.

Bosence, D. W. J. and Waltham, D. A. (1990) 'Computer modeling the internal architecture of carbonate platforms', *Geology*, 18, pp. 26–30.

Bosence, D. W. J., Waltham, D. A. and Lankester, T. H. G. (1994) 'Computer modeling a Miocene carbonate Computer Modeling a Miocene Carbonate Platform , Mallorca, Spain', *AAPG Bulletin*, 78(2), pp. 247–266.

Bosscher, H. and Schlager, W. (1992) 'Computer simulation of reef growth', *Sedimentology*, 39, pp. 503–512.

Bosscher, H. and Schlager, W. (1993) 'Accumulation Rates of Carbonate Platforms', *Journal of Geology*, 101(3), pp. 345–355.

Braithwaite, C. J. R., Rizzi, G. and Darke, G. (2004) *The Geometry and Petrogenesis of Dolomite Hydrocarbon Reservoirs*, *Geological Society, Special Publications*. Edited by C. J. R. Braithwaite, G. Rizzi, and G. Darke. London, UK: Geological Society, Special Publication.

Burchette, T. P. and Wright, V. P. (1992) 'Carbonate ramp depositional systems', *Sedimentary Geology*, 79, pp. 3–57.

Burgess, P. M. (2012) 'A brief review of developments in stratigraphic forward modelling, 2000–2009', in Bally, A. W. and Roberts, D. G. (eds) *Regional Geology and Tectonics: Principles of Geologic Analysis*. 1st edn. Amsterdam, The Netherlands: Elsevier, pp. 379–404.

Busson, J., Joseph, P., Mulder, T., Teles, V., Borgomano, J., Granjeon, D., Betzler, C., Poli, E. and Wunsch, M. (2019) 'High-resolution stratigraphic forward modeling of a Quaternary carbonate margin: Controls and dynamic of the progradation', *Sedimentary Geology*. Elsevier B.V., 379, pp. 77–96.

Camoin, G. F. and Webster, J. M. (2015) 'Coral reef response to Quaternary sea-level and environmental changes: State of the science', *Sedimentology*, 62, pp. 401–428.

Catuneanu, O. (2002) 'Sequence stratigraphy of clastic systems: Concepts, merits, and pitfalls', *Journal of African Earth Sciences,* 35 (1), pp. 1–43.

Clift, P. D., Hodges, K. V., Heslop, D., Hannigan, R., Van Long, H. and Calves, G. (2008) 'Correlation of Himalayan exhumation rates and Asian monsoon intensity', *Nature Geoscience*, 1, pp. 875–880.

Coe, A. L., Bosence, D. W. J., Church, K. D., Flint, S. S., Howell, J. A. and Wilson, R. C. L. (2003) *The Sedimentary Record of Sea-level Change*, *Geosciences Journal*. Edited by A. L. Coe. Cambridge, UK: Cambridge University Press and the Open University.

Cojan, I., Fouche, O., Lopez, S. and Rivoirard, J. (2005) 'Process-based aquifer modelling in the example meandering channel', in Leuangthong, O. and Deutsch, C. V. (eds) *Geostatistics Banff 2004*. Dordrecht: Springer, pp. 611–619.

Csato, I., Catuneanu, O. and Granjeon, D. (2014) 'Millennial-Scale Sequence Stratigraphy: Numerical Simulation With Dionisos', *Journal of Sedimentary Research*, 84, pp. 394–406.

Duncan, R. A. and Hargraves, R. B. (1990) 'Ar / 39 Ar Geochronology of basement rocks from the Mascarene Plateau, the Chagos Bank, and the Maldives Ridge', in Duncan, R.A., Backman, J., and Peterson, L. C. (eds) *Proceedings of the Ocean Drilling Program, Scientific Results*. College Station, TX, U.S.A., pp. 43–51.

Fürstenau, J., Lindhorst, S., Betzler, C. and Hübscher, C. (2010) 'Submerged reef terraces of the Maldives (Indian Ocean)', *Geo-Marine Letters*, 30, pp. 511–515.

Gischler, E., Hudson, J. H. and Pisera, A. (2008) 'Late Quaternary reef growth and sea level in the Maldives (Indian Ocean)', *Marine Geology*, 250, pp. 104–113.

Granjeon, D. (2014) '3D forward modelling of the impact of sediment transport and base level cycles on continental margins and incised valleys', *International Association of Sedimentololologists Special Publications*, 46, pp. 453–472.

Granjeon, D. and Joseph, P. (1999) 'Concepts and applications of a 3-D multiple lithology , diffusive model in stratigraphic modeling', *SEPM Special Publications*, 62, pp. 197–210.

Graus, R. R. and Macintyre, I. G. (1989) 'The zonation patterns of Caribbean coral reefs as controlled by wave and light energy input, bathymetric setting and reef morphology: computer simulation experiments', *Coral Reefs*, 8, pp. 9–18.

Gupta, A. K., Yuvaraja, A., Prakasam, M., Clemens, S. C. and Velu, A. (2015) 'Evolution of the South Asian monsoon wind system since the late Middle Miocene', *Palaeogeography, Palaeoclimatology, Palaeoecology*, 438, pp. 160–167.

Halfar, J., Godinez-Orta, L., Mutti, M., Valdez-Holguín, J. E. and Borges, J. M. (2004) 'Nutrient and temperature controls on modern carbonate production: An example from the Gulf of California, Mexico', *Geology*, 32, pp. 213–216.

Halfar, J. and Mutti, M. (2005) 'Global dominance of coralline red-algal facies: A response to Miocene oceanographic events', *Geology*, 33(6), pp. 481–484.

Hallock, P. and Schlager, W. (1986) 'Nutrient Excess and and the Demise of Coral Reefs Carbonate Platforms', *PALAIOS*, 1(4), pp. 389–398.

Handford, C. R. and Loucks, R. G. (1993) 'Carbonate depositional sequences and systems tract - Responses of carbonate platforms to relative sea-level changes', in Handford, C. R. and Loucks, R. G. (eds) *Carbonate sequence stratigraphy. Recent developments and applications.* AAPG Memoir 57, pp. 3–41.

Hawie, N., Barrois, A., Marfisi, E., Murat, B. and Hall, J. (2015) 'Forward Stratigraphic Modelling , Deterministic Approach to Improve Carbonate Heterogeneity Prediction ; Lower Cretaceous , Abu Dhabi', in *Abu Dhabi International Petroleum Exhibition and Conference*.

Holbourn, A., Kuhnt, W., Schulz, M. and Erlenkeuser, H. (2005) 'Impacts of orbital forcing and atmospheric carbon dioxide on Miocene ice-sheet expansion', *Nature, 438, pp. 483–487*.

Holbourn, A., Kuhnt, W., Kochhann, K. G. D., Andersen, N. and Sebastian-Meier, K. J. (2015) 'Global perturbation of the carbon cycle at the onset of the Miocene Climatic Optimum', *Geology, 43(2), pp. 123-126*.

Jervey, M. T. (1988) 'Quantitative Geological Modeling of Siliciclastic Rock Sequences and Their Seismic Expression', in *Sea-Level Changes*, pp. 47–69.

Kendall, C. G. S. C. and Schlager, W. (1981) 'Carbonates and relative changes in sea level', *Marine Geology*, 44(1–2), pp. 181–212.

Kenyon, P. M. and Turcotte, D. L. (1985) 'Morphology of a delta prograding by bulk sediment transport.', *Geological Society of America Bulletin*, 96, pp. 1457–1465.

Kolodka, C., Vennin, E., Bourillot, R., Granjeon, D. and Desaubliaux, G. (2016) 'Stratigraphic modelling of platform architecture and carbonate production: a Messinian case study (Sorbas Basin, SE Spain)', *Basin Research*, 28(5), pp. 658–684.

Kroon, D., Steens, T. N. F. and Troelstra, S. R. (1991) 'Onset of Monsoonal Related Upwelling in the Western Arabian Sea as Revealed by Planktonic Foraminifers', in *Proceedings of the Ocean Drilling Program, 117 Scientific Results*.

Lucia, F. J. and Fogg, G. E. (1990) 'Geological/Stochastic Mapping of Heterogeneity in a Carbonate Reservoir', *Journal of Petroleum Technology*, 42, pp. 1298–1303.

Lüdmann, T. *et al.* (2013) 'The Maldives, a giant isolated carbonate platform dominated by bottom currents', *Marine and Petroleum Geology*. Elsevier Ltd, 43, pp. 326–340.

Marzouk, I., Takezaki, H. and Miwa, M. (1995) 'Geologic Controls on Wettability of Carbonate Reservoirs, Abu Dhabi, U.A.E.', in *Society of Petroleum Engineers Middle East Oil Show*, pp. 449–460.

Mazzullo, S. J. (2004) 'Overview of Porosity Evolution in Carbonate Reservoirs', *Kansas Geological Society Bulletin*, 79(3), pp. 243–255.

Miller, K. G., Kominz, M. A., Browning, J. V., Wright, J. D., Mountain, G. S., Katz, M. E., Sugarman, P. J., Cramer, B. S., Christie-Blick, N. and Pekar, S. F. (2005) 'The phanerozoic record of global sea-level change', *Science, 310, pp. 1293-1298*.

Mitchell, N. C. (1996) 'Creep in pelagic sediments and potential for morphologic dating of marine fault scarps', *Geophysical Research Letters*, 23, pp. 483–486.

Montaggioni, L. F. (2005) 'History of Indo-Pacific coral reef systems since the last glaciation: Development patterns and controlling factors', *Earth-Science Reviews*, 71(1–2), pp. 1–75.

Nurmi, R., Charara, M., Waterhouse, M. and Park, R. (1990) 'Heterogeneities in carbonate reservoirs: detection and analysis using borehole electrical imagery', *Geological Society, London, Special Publications*, 48(1), pp. 95–111.

Pomar, L. (2001a) 'Ecological control of sedimentary accommodation: Evolution from a carbonate ramp to rimmed shelf, Upper Miocene, Balearic Islands', *Palaeogeography, Palaeoclimatology, Palaeoecology*, 175(July), pp. 249–272.

Pomar, L. (2001b) 'Types of carbonate platforms : A genetic approach Types of carbonate platforms : a genetic approach', *Basin Research*, 13(April), pp. 313–334.

Pomar, L., Bassant, P., Brandano, M., Ruchonnet, C. and Janson, X. (2012) 'Impact of carbonate producing biota on platform architecture: Insights from Miocene examples of the Mediterranean region', *Earth-Science Reviews*, 113(3–4), pp. 186–211.

Pomar, L. and Hallock, P. (2008) 'Carbonate factories: A conundrum in sedimentary geology', *Earth-Science Reviews*, 87(3–4), pp. 134–169.

Pomar, L. and Haq, B. U. (2016) 'Decoding depositional sequences in carbonate systems: Concepts vs experience', *Global and Planetary Change*, 146, pp. 190–225.

Pomar, L. and Kendall, C. G. S. C. (2008) 'Architecture of Carbonate Platforms: A Response to Hydrodynamics and Evolving Ecology', *SEPM Special Publication*, 89, pp. 187–216.

Pomar, L. and Ward, W. C. (1994) 'Response of a late Miocene Mediterranean reef platform to high-

frequency eustasy', *Geology*, 22, pp. 131–134.

Pomar, L. and Ward, W. C. (1999) 'Reservoir-scale heterogeneity in depositional packages and diagenetic patterns on a reef-rimmed platform, upper Miocene, Mallorca, Spain', *AAPG Bulletin*, 83(11), pp. 1759–1773.

Posamentier, H. W. and Allen, G. P. (1999) *Siliciclastic Sequence Stratigraphy*, *SEPM Concepts in Sedimentology and Paleontology no. 7*.

Purdy, E. G. and Bertram, G. T. (1993) 'Carbonate concepts from the Maldives, Indian Ocean', *American Association of Petroleum Geologists, Studies in Geology*.

Rea, D. K. (1992) 'Delivery of Himalayan Sediment to the Northern Indian Ocean and Its Relation to Global Climate, Sea Level, Uplift, and Seawater Strontium', in Duncan, R. A. (ed.) *Synthesis of results from scientific drilling in the Indian Ocean*. American Geophysical Union Geophysical Monograph, pp. 387–402.

Sadler, P. M. (1981) 'Sediment Accumulation Rates and the Completeness of Stratigraphic Sections', *The Journal of Geology*, 89(5), pp. 569–584.

Schlager, W. (1993) 'Accommodation and supply-a dual control on stratigraphic sequences', *Sedimentary Geology*, 86(1–2), pp. 111–136.

Schlager, W. (1999) 'Scaling of sedimentation rates and drowning of reefs and carbonate platforms', *Geology*, 27(2), pp. 183–186.

Schlager, W. (2000) 'Sedimentation rates and growth potential of tropical, cool-water and mud-mound carbonate systems', *Geological Society, London, Special Publications*, 178(1), pp. 217–227.

Schlager, W. (2005) *Carbonate Sedimentology and Sequence Stratigraphy*. Edited by W. Schlager. Tulsa, Oklahoma, U.S.A.: SEPM, Concepts in Sedimentology and Paleontology, 8.

Seard, C., Borgomano, J., Granjeon, D. and Camoin, G. (2013) 'Impact of environmental parameters on coral reef development and drowning: Forward modelling of the last deglacial reefs from Tahiti (French Polynesia; IODP Expedition #310)', *Sedimentology*, 60, pp. 1357–1388.

Shafie, K. R. K. and Madon, M. (2008) 'A review of stratigraphic simulation techniques and their applications in sequence stratigraphy and basin analysis', *Bulletin of the Geological Society of Malaysia*, 54(November), pp. 81–89.

Swart, P. K., Blättler, C. L., Nakakuni, M., Mackenzie, G. J., Betzler, C., Eberli, G. P., Reolid, J., Alonso-García, M., Slagle, A. L., Wright, J. D., Kroon, D., Reijmer, J. J. G., Hui Mee, A. L., Young, J. R., Alvarez-Zarikian, C. A., Bialik, O. M., Guo, J. A., Haffen, S., Horozal, S., Inoue, M., Jovane, L., Lanci, L., Laya, J. C., Lüdmann, T., Nagender Nath, B., Niino, K., Petruny, L. M., Pratiwi, S. D., Su, X., Sloss, C. R. and Yao, Z. (2019) 'Cyclic anoxia and organic rich carbonate sediments within a drowned carbonate platform linked to Antarctic ice volume changes: Late Oligocene-early Miocene Maldives', *Earth and Planetary Science Letters*, 521(January), pp. 1–13.

Swift, D. J. P. and Thorne, J. A. (1991) 'Sedimentation on Continental Margins, I: A General Model for Shelf Sedimentation', in *Shelf Sand and Sandstone Bodies. Geometry, Facies and Sequence Stratigraphy*, pp. 3–31.

Tomczak, M. and Godfrey, J. S. (2001) *Regional Oceanography*, *Regional Oceanography: An Introduction*. Edited by M. Tomczak and J. S. Godfrey. Oxford: Elsevier.

Vail, P. R., Mitchum, R. M., Todd, R. G., Widmier, J. M., Thompson III, S., Sangree, J. B., Bubb, J. N. and Hatlelid, W. G. (1977) 'Seismic stratigraphy and global changes of sea-level', in Payton, C. E. (ed.) *Seismic Stratigraphy - Applications to Hydrocarbon Exploration*. AAPG Memoir 26, pp. 49–212.

Warrlich, G. M. D., Bosence, D. W. J., Waltham, D. A., Wood, C., Boylan, A. and Badenas, B. (2008) '3D stratigraphic forward modelling for analysis and prediction of carbonate platform stratigraphies in exploration and production', *Marine and Petroleum Geology*, 25, pp. 35–58.

Warrlich, G. M. D., Waltham, D. A. and Bosence, D. W. J. (2002) 'Quantifying the sequence stratigraphy and drowning mechanisms of atolls using a new 3-D forward stratigraphic modelling program (CARBONATE 3D)', *Basin Research*, 14, pp. 379–400.

Watney, W. L., Rankey, E. C. and Harbaugh, J. (1999) 'Perspectives on stratigraphic simulation models: current approaches and future opportunities', in *Numerical Experiments in Stratigraphy*.

Whitaker, F. F., Felce, G. P., Benson, G.S., Amour, F., Mutti, M. and Smart, P. L. (2014) 'Simulating flow through forward sediment model stratigraphies: insights into climatic control of reservoir quality in isolated carbonate platforms', *Petroleum Geoscience*, 20(1), pp. 27–40.

Willems, C. J. L., Nick, H. M., Goense, T. and Bruhn, D. F. (2017) 'Geothermics The impact of reduction of doublet well spacing on the Net Present Value and the life time of fluvial Hot Sedimentary Aquifer doublets', *Geothermics*, 68, pp. 54–66.

Williams, H. D., Burgess, P. M., Wright, V. P., Della Porta, G., Granjeon, D. (2011) 'Investigating Carbonate Platform Types: Multiple Controls and a Continuum of Geometries', *Journal of Sedimentary Research*, 81(1), pp. 18–37.

Zachos, J., Pagani, H., Sloan, L., Thomas, E. and Billups, K. (2001) 'Trends, rhythms, and aberrations in global climate 65 Ma to present', *Science,* 292 , pp. 686–693.

Zheng, H., Powell, C. M. A., Rea, D. K., Wang, J. and Wang, P. (2004) 'Late Miocene and mid-Pliocene enhancement of the East Asian monsoon as viewed from the land and sea', *Global and Planetary Change*, 41, pp. 147–155.

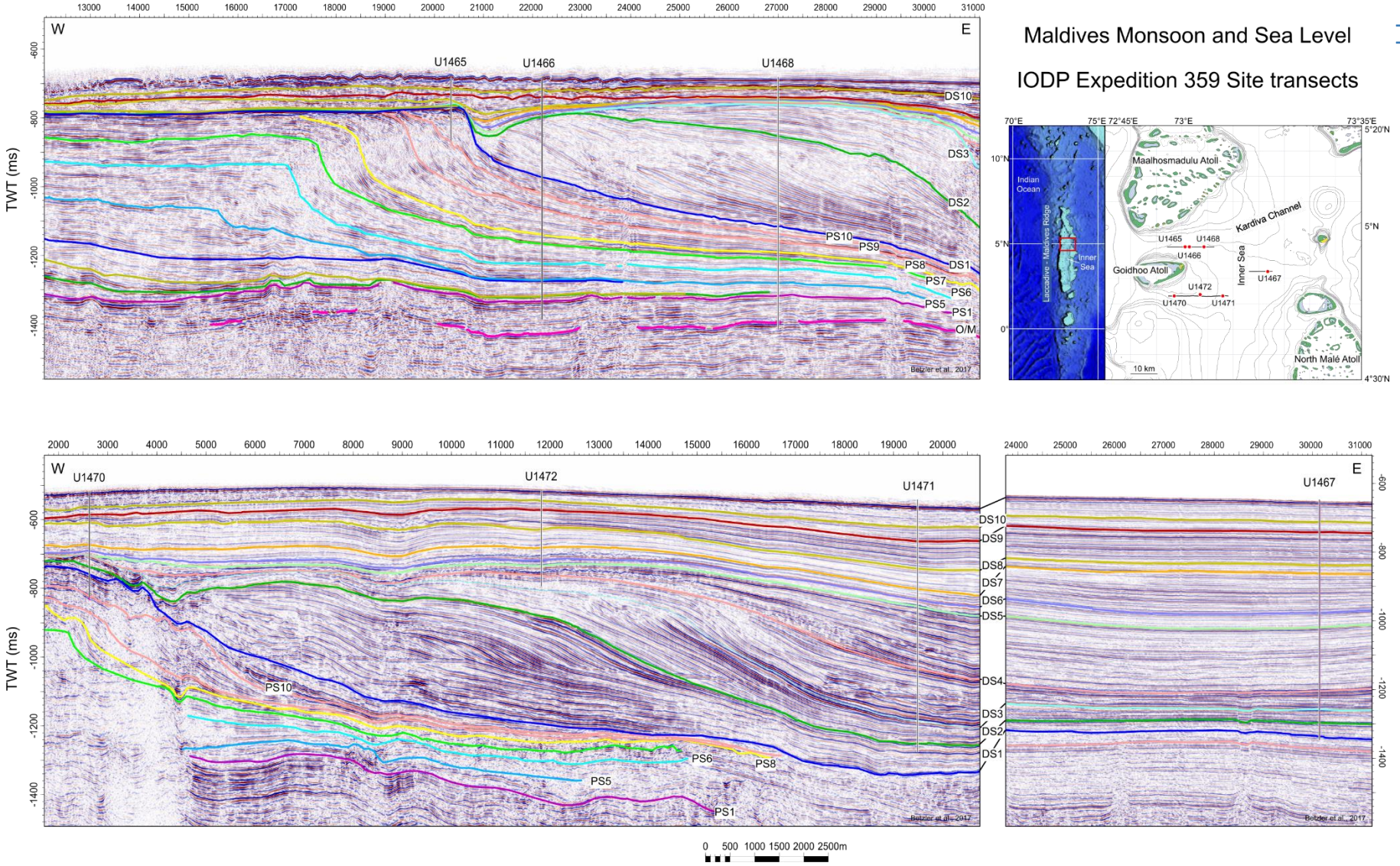

Appendix A. Seismic lines with locations of IODP Exp. 359 sites and identification of platform sequence (PS) and drift sequence (DS) boundaries.(Betzler et al., 2018)

Appendix B

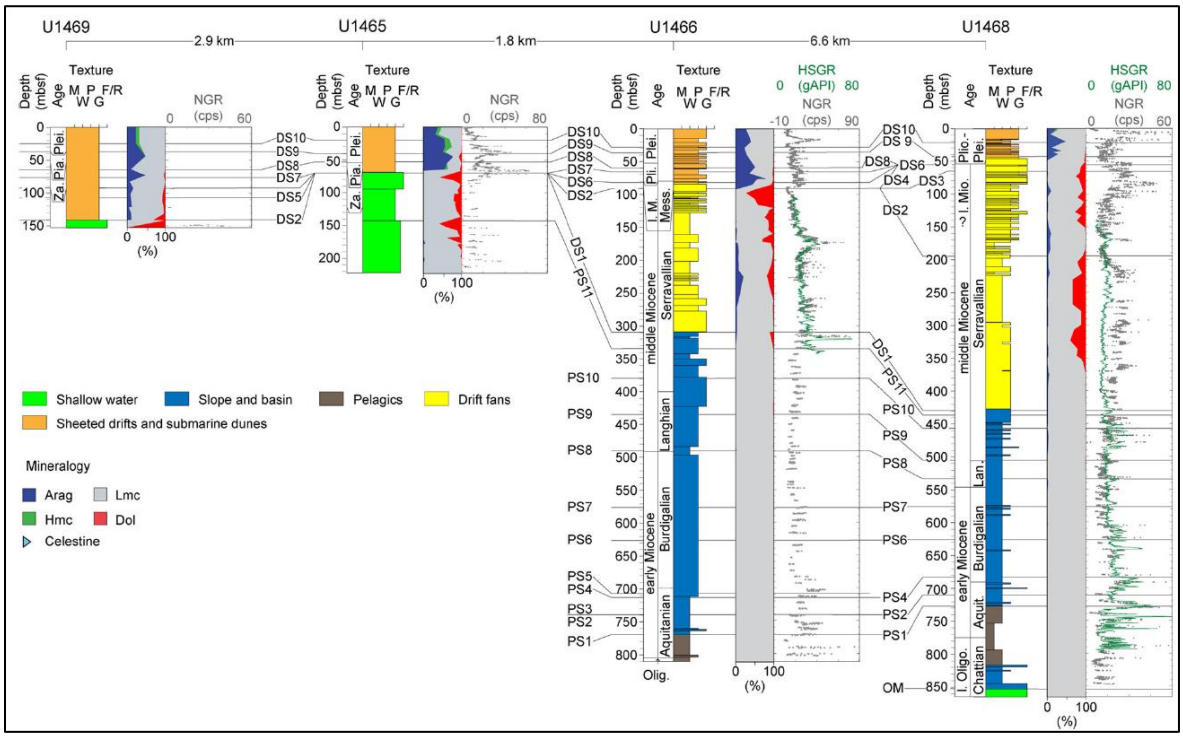

Sequence stratigraphic correlation of IODP Expedition 359 sites along the northern transect of wells in the Maldives HSGR: downhole gamma ray log; NGR: gamma ray counts on wholeround cores. M mudstone, W wackestone, P packstone, G grainstone, F/R floatstone/rudstone. (Betzler et al., 2018)

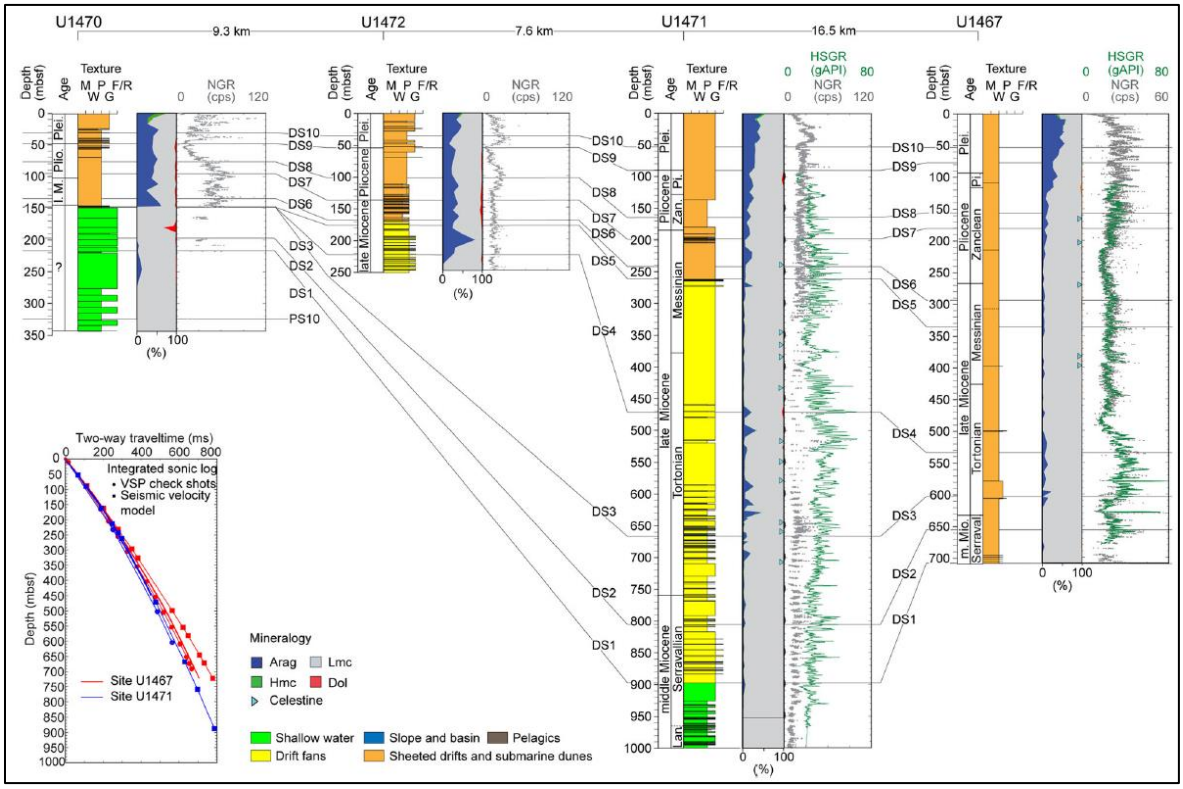

Sequence stratigraphic correlation of IODP 359 sites along the southern transect of wells in the Maldives. HSGR: downhole gamma ray log; NGR: gamma ray counts on whole cores. Inset to the left shows the time-depth curves for Sites U1467 and U1471. M mudstone, W wackestone, P packstone, G grainstone, F/R floatstone/rudstone. (Betzler et al., 2018)